Performance-Based Structural-Fire Engineering Analysis Approaches for Highway Bridges

Principal Investigator: Spencer Quiel, Ph.D., P.E. (Lehigh University)

Project Team: Saidong Ma, M.S. (Lehigh University)
Zheda Zhu, Ph.D. (Lehigh University)
Thomas Murphy, Ph.D., P.E. (Modjeski & Masters, Inc.)
Maria Lopez, Ph.D., P.E. (Modjeski & Masters, Inc.)
Frank Artmont, Ph.D., P.E. (Modjeski & Masters, Inc.)

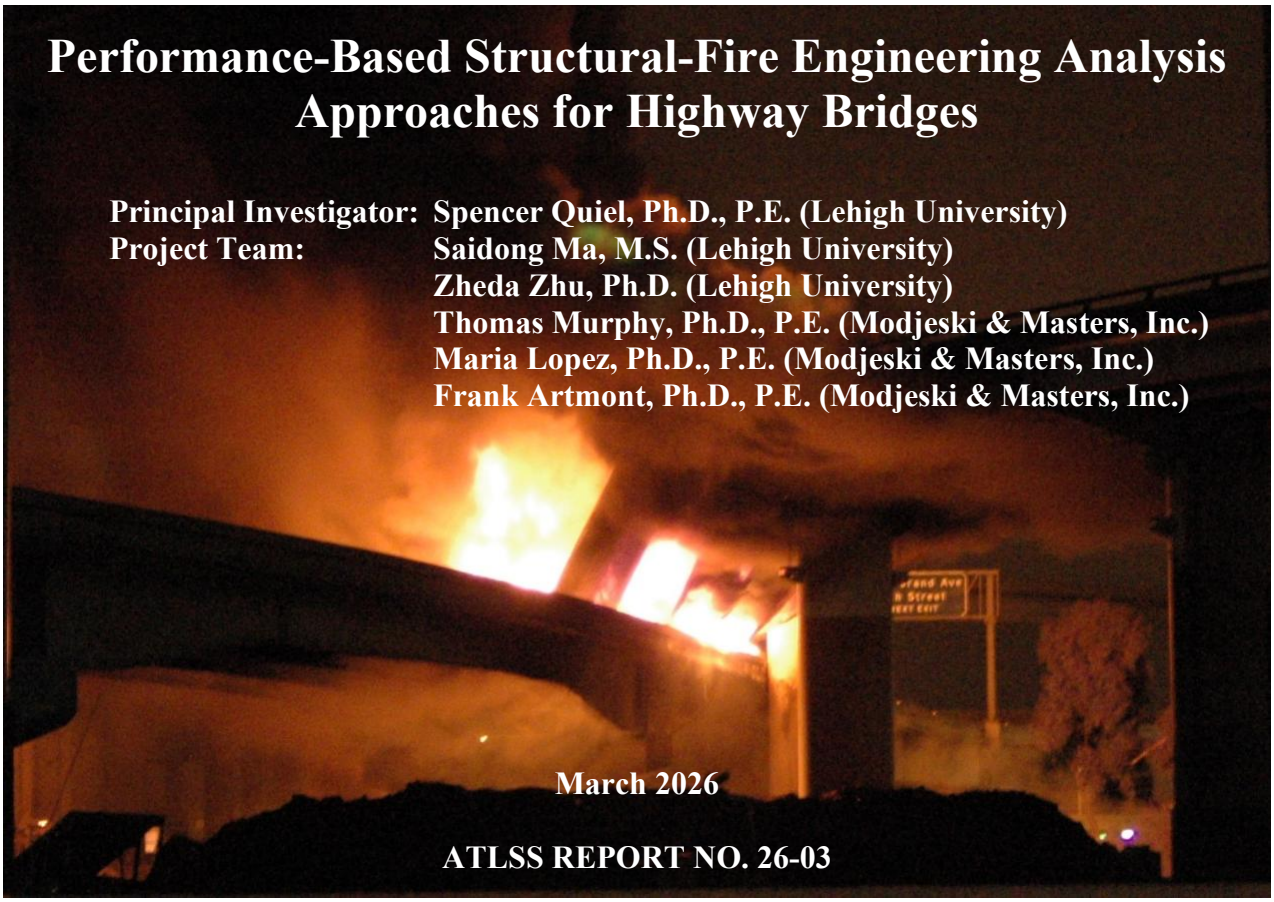

March 2026

ATLSS REPORT NO. 26-03

ATLSS is a National Center for Engineering Research on

Advanced Technology for Large Structural Systems

117 ATLSS Drive

Bethlehem, PA 18015-4729

Phone: (610)-758-3525
Fax: (610)-758-5902

www.atlss.lehigh.edu
Email: inatl@lehigh.edu

Cover photo by Philip Liborio Gangi (https://liboriogangi.tripod.com; used with permission)

Technical Report Documentation Page

1. Report No. ATLSS 26-03	**2. Gov't Accession No**. N/A	**3. Recipient's Catalog No.** N/A
4. Title and Subtitle Performance-Based Structural-Fire Engineering Analysis Approaches for Highway Bridges		**5. Report Date** 3/27/2026 **6. Performing Org. Code** N/A
7. Author(s) Spencer Quiel, Ph.D., P.E. (Principal Investigator, Lehigh Univ., ORCID ID: 0000-0002-1316-7059) Saidong Ma, M.S. (Lehigh Univ.) Zheda Zhu, Ph.D. (Lehigh Univ.) Thomas Murphy, Ph.D., P.E. (Modjeski and Masters, Inc.) Maria Lopez, Ph.D., P.E. (Modjeski and Masters, Inc.) Frank Artmont, Ph.D., P.E. (Modjeski and Masters, Inc.)		**8. Performing Org. Report No.** N/A
9. Performing Organization Name and Address Lehigh University 117 ATLSS Drive Bethlehem, PA 18015 Modjeski and Masters, Inc. 100 Sterling Parkway, Suite 302 Mechanicsburg, PA 17050		**10. Work Unit No.** N/A **11. Contract or Grant No.** 693JJ321C000035 Phase II
12. Sponsoring Agency Name and Address Federal Highway Administration 1200 New Jersey Avenue, SE Washington, DC 20590		**13. Type of Report and Period** Final Report, Phase II **14. Sponsoring Agency Code** HIBS
15. Supplementary Notes None		

16. Abstract

This report is the second part of a two-phase study to assemble performance-based design guidance for the evaluation and mitigation of severe fire hazards for highway bridges. The following are addressed: (1) summarize design-basis tools that can be used for "engineering analysis" per NFPA 502 Chapter 6 to calculate the thermo-structural impact of design-basis fires on a particular bridge; (2) summarize approaches for evaluating common thermo-structural limit states of steel and prestressed girders as well as other common structural elements in bridge structures under fire; and (3) review fire mitigation strategies and recommend needs for future research. Thermal and structural finite element (FE) analysis is demonstrated as an effective tool for evaluating both steel and concrete bridge elements under fire exposure. Simpler lumped mass methods of thermal analysis are appropriate for steel materials, which have relatively high thermal conductivity and can therefore be approximated as having a relatively uniform temperature increase over their cross-section, which has a large ratio of exposed area to thermal mass. For other materials with lower thermal conductivity like concrete, a significant internal thermal gradient will develop under fire exposure, thus making lumped mass methods ineffective. More research is needed to develop simplified calculation tools to evaluate concrete bridge elements under fire.

17. Key Words Highway bridges, performance-based structural-fire assessment, passive fire protection	**18. Distribution Statement** No restrictions.		
19. Security Classification (of this report): Unclassified	**20. Security Classification (of this page):** Unclassified	**21. No. of Pages:** 60	**22. Price** N/A

Form DOT F 1700.7 (8-72) Reproduction of completed page authorized.

SI* (MODERN METRIC) CONVERSION FACTORS

APPROXIMATE CONVERSIONS TO SI UNITS

Symbol	When You Know	Multiply By	To Find	Symbol
		LENGTH		
in	inches	25.4	millimeters	mm
ft	feet	0.305	meters	m
yd	yards	0.914	meters	m
mi	miles	1.61	kilometers	km
		AREA		
in^2	square inches	645.2	square millimeters	mm^2
ft^2	square feet	0.093	square meters	m^2
yd^2	square yard	0.836	square meters	m^2
ac	acres	0.405	hectares	ha
mi^2	square miles	2.59	square kilometers	km^2
		VOLUME		
fl oz	fluid ounces	29.57	milliliters	mL
gal	gallons	3.785	liters	L
ft^3	cubic feet	0.028	cubic meters	m^3
yd^3	cubic yards	0.765	cubic meters	m^3
		NOTE: volumes greater than 1000 L shall be shown in m^3		
		MASS		
oz	ounces	28.35	grams	g
lb	pounds	0.454	kilograms	kg
T	short tons (2000 lb)	0.907	megagrams (or "metric ton")	Mg (or "t")
		TEMPERATURE (exact degrees)		
°F	Fahrenheit	5 (F-32)/9 or (F-32)/1.8	Celsius	°C
		ILLUMINATION		
fc	foot-candles	10.76	lux	lx
fl	foot-Lamberts	3.426	$candela/m^2$	cd/m^2
		FORCE and PRESSURE or STRESS		
lbf	poundforce	4.45	newtons	N
lbf/in^2	poundforce per square inch	6.89	kilopascals	kPa

APPROXIMATE CONVERSIONS FROM SI UNITS

Symbol	When You Know	Multiply By	To Find	Symbol
		LENGTH		
mm	millimeters	0.039	inches	in
m	meters	3.28	feet	ft
m	meters	1.09	yards	yd
km	kilometers	0.621	miles	mi
		AREA		
mm^2	square millimeters	0.0016	square inches	in^2
m^2	square meters	10.764	square feet	ft^2
m^2	square meters	1.195	square yards	yd^2
ha	hectares	2.47	acres	ac
km^2	square kilometers	0.386	square miles	mi^2
		VOLUME		
mL	milliliters	0.034	fluid ounces	fl oz
L	liters	0.264	gallons	gal
m^3	cubic meters	35.314	cubic feet	ft^3
m^3	cubic meters	1.307	cubic yards	yd^3
		MASS		
g	grams	0.035	ounces	oz
kg	kilograms	2.202	pounds	lb
Mg (or "t")	megagrams (or "metric ton")	1.103	short tons (2000 lb)	T
		TEMPERATURE (exact degrees)		
°C	Celsius	1.8C+32	Fahrenheit	°F
		ILLUMINATION		
lx	lux	0.0929	foot-candles	fc
cd/m^2	$candela/m^2$	0.2919	foot-Lamberts	fl
		FORCE and PRESSURE or STRESS		
N	newtons	0.225	poundforce	lbf
kPa	kilopascals	0.145	poundforce per square inch	lbf/in^2

TABLE OF CONTENTS

LIST OF FIGURES

LIST OF TABLES

LIST OF ABBREVIATIONS

1LM	one-lumped-mass
AADT	average annual daily traffic
AASHTO	American Association of State Highway and Transportation Officials
AHJ	authority having jurisdiction
AISC	American Institute of Steel Construction
ASCE	American Society of Civil Engineers
AST	adiabatic surface temperature
ASTM	American Society for Testing and Materials
BS	British Standard
DFT	dry film thickness
DL	dead load
DOT	Department of Transportation
ECCS	European Commission for Constructional Steelwork
FDS	Fire Dynamics Simulator
FE	finite element
FEM	finite element method
FFFS	fixed firefighting systems
HDPE	high-density polyethylene
HGV	heavy goods vehicles
HRR	heat release rate
ICs	intumescent coatings
ISO	International Organization for Standardization
LHS	Latin hypercube sampling
LL	live load
LWC	lightweight concrete
MCS	Monte Carlo simulation
NFPA	National Fire Protection Association
NWC	normal-weight concrete
PCI	Precast Concrete Institute
PennDOT	Pennsylvania Department of Transportation
PFP	passive fire protection
PP	polypropylene fiber
SFPE	Society of Fire Protection Engineers
SFRM	spray-applied fire-resistive material
TTP	truck traffic percentage
TVRA	threat, vulnerability, and risk assessment

LIST OF NOTATIONS

A_i	cross-sectional area of the insulating material (m^2)
Bi	Biot number
b_{tf}	width of top flange (mm)
c_i	specific heat of insulation (J/kg·K)
$c_{i,t-1}$	specific heat of insulation (J/kg·K) at time $t-1$
c_s	specific heat of steel (J/kg·K)
$c_{s,t-1}$	specific heat of steel (J/kg·K) at time $t-1$
d	distance between the extreme compression fiber and the extreme tension fiber of the critical section (m)
d_i	thickness of insulation (m)
F	surface area of unit length of the member (m^2)
F_c	contact area unit length between top flange and slab (m^2)
F_f	surface area of unit length of the member exposed to fire (m^2)
F_a	surface area of unit length of the member exposed to ambient conditions (m^2)
f_c'	specified compressive strength of concrete (MPa)
f_{pk}	characteristic tensile strength (MPa) of prestressing steel in Eurocode 2 Part 1-2
h	heat transfer coefficient (W/(m^2·K))
h_c	convective heat transfer coefficient (W/(m^2·K))
k	thermal conductivity (W/m·K)
k_i	thermal conductivity of insulation (W/m·K)
$k_{i,t-1}$	thermal conductivity of insulation (W/m·K) at time $t-1$
$k_{y,T}$	probabilistic reduction factor of the yield strength of hot-rolled steel at temperature T
$k_{y,EN,T}$	reduction factor of nominal yield strength according to Eurocode 3 Part 1-2
L	clear span (m)
L_c	member length (m)
M_{mid}	moment capacity at the midspan section (N·m)
$M_{n,20℃}$	nominal flexural capacity of the section at ambient temperature (20°C) (N·m)
$\dot{q}_a''$	heat flux lost to the ambient environment (W/m^2)
$\dot{q}_{a,t}''$	heat flux lost the to the ambient environment (W/m^2) at time t
$\dot{q}_c''$	heat flux to concrete slab (W/m^2)
$\dot{q}_{c,t}''$	heat flux to concrete slab (W/m^2) at time t
$\dot{q}_f''$	heat flux from the fire source (W/m^2)
$\dot{q}_{f,t}''$	heat flux from the fire source (W/m^2) at time t
r_{logit}	logit transformation of the Eurocode reduction Factor $k_{y,EN,T}$
T	steel temperature (°C)
T_a	ambient temperature (°C)
T_f	fire temperature (°C)
$T_{f,t-1}$	fire temperature (°C) at time $t-1$
$T_{f,t}$	fire temperature (°C) at time t
T_s	member surface temperature (°C)
$T_{s,t-1}$	steel temperature (°C) at time $t-1$
$T_{s,t}$	steel temperature (°C) at time t
$T_{tf,s}$	top flange temperature (°C)
t	time (s)
V	volume of steel in unit length of the member (m^3)

β	strength reduction factor according to Eurocode 2 Part 1-2
ε	emissivity
ε_e	emissivity of the hot gases
ε_f	resultant emissivity for incoming radiation heat energy
ε_k	standard normal random variable
ε_r	surface emissivity
σ	Stefan-Boltzmann constant (W/(m²·K⁴))
ρ_i	insulation density (kg/m^3)
$\rho_{i,t-1}$	insulation density (kg/m^3) at time $t-1$
ρ_s	steel density (kg/m^3)
$\rho_{s,t-1}$	steel density (kg/m^3) at time $t-1$
ΔT_f	change in fire temperature (K)
ΔT_s	change in steel temperature (K)
Δt	time increment (s)

EXECUTIVE SUMMARY

Recent events have demonstrated that the consideration of vehicular or stationary fire hazards may be justifiable for highway bridges that are shorter than the 1,000-ft (300-m) lower-bound length prescribed by the National Fire Protection Association (NFPA) Standard 502[1] [1] Rather than using the bridge length as the sole parameter in determining the importance of the bridge, the decision to address the impact of fire on a bridge structure can instead be made based on an assessment that considers the likelihood of occurrence for a structurally significant fire near a bridge, the vulnerability of the bridge's structural elements to fire-induced damage or collapse, and the resulting impacts to user life-safety and the transportation network functionality both during and after the fire. When applicable, NFPA 502[1] states that an "engineering analysis," including the consideration of design fire scenarios and their proximity to the structure, is needed to determine whether the collapse of the bridge due to fire would have adverse impacts to life safety or other unacceptable impacts to functionality.

This report is the second part of a two-phase study to assemble performance-based design guidance for the evaluation and mitigation of severe fire hazards for highway bridges. This evaluation can be conducted for a given bridge structure using the approach illustrated in the flowchart in Figure 1-1. The two-phase study has four overall objectives: (1) characterize the size and probability of potential fire hazards; (2) if a significant hazard is identified, model the fire and calculate the resulting thermal exposure to the bridge structure; (3) evaluate the potential for fire-induced structural damage; and (4) establish the most practical mitigation measures based on the needs of the bridge owner. Phase I culminated in a final report [2], which presented the development of a structurally significant design fire exposure as input for the engineering analysis of a bridge based on its vulnerability to various fire scenarios. That report summarized methods for modeling the fire itself ("Fire Model") and calculating its thermal impact on structural elements ("Heat Transfer"). This report (Phase II) is focused on the remaining items ("Thermal Response" and "Structural Response") and addresses the following:

- Summarize design-basis tools that can be used for "engineering analysis" per NFPA 502[1] Chapter 6 to calculate the thermo-structural impact of design-basis fires on a particular bridge.
- Summarize approaches for evaluating common thermo-structural limit states of steel and prestressed girders as well as other common structural elements in bridge structures under fire.
- Review fire mitigation strategies and recommend needs for future research.

Thermal and structural finite element (FE) analysis is demonstrated as an effective tool for evaluating both steel and concrete bridge elements under fire exposure. These exposures can include a "standard" fire temperature time history (which are used to develop fire resistance ratings and continue until a failure condition is reached) or a design-basis "natural" fire temperature time history (which ramps up to a peak intensity and then eventually burns out). Temperature-dependent material properties are needed as the input for these analyses, and available sources for structures made with steel and concrete are summarized.

Simpler lumped mass methods of thermal analysis are appropriate for steel materials, which have relatively high thermal conductivity and can therefore be approximated as having a relatively uniform temperature

[1] Use of NFPA 502, Standard for Road Tunnels, Bridges, and Other Limited Access Highways, is not a Federal requirement.

increase over the cross-section. Calculated changes in steel temperature can then be used to calculate the corresponding decrease in the element's strength and stiffness, as well as its thermal elongation. In this study, a large suite of thermo-structural analyses for composite steel bridge girders identified steel temperature thresholds that correspond to levels of fire-induced flexural performance. Lumped mass methods could then be used to calculate the steel temperature under a given fire hazard exposure, to determine whether those thresholds would be exceeded. For concrete and other materials with lower thermal conductivity, a significant internal thermal gradient will typically develop under fire exposure, thus rendering the lumped mass method ineffective. More research is needed to develop calculation tools that are more simplified than FE analysis to evaluate concrete bridge elements under fire.

1 INTRODUCTION

Over the past 30 years, fire has caused bridge failure in the US at a rate consistent with other hazards that garner significantly more attention and mitigation resources [2–5]. For example, fire causes bridge failures at an annualized rate comparable to, or exceeding that, of earthquakes and construction defects, both of which are addressed much more extensively in current practice via design and inspection. Most of the recent fire-induced bridge failures in the U.S. have been highway overpasses (typically supported by steel girders) that are subjected to the effects of burning tanker trucks, heavy goods vehicles (HGVs), or a platooned combination of vehicles [2,4,6]. These events include but are not limited to the near-collapse of an I-65 overpass near Birmingham, AL in 2002; the collapse of two overpass spans of the MacArthur Maze I-80/I-580/I-880 interchange in Oakland, CA in 2007; and the collapse of an overpass of I-95 at Cottman Avenue in Philadelphia, PA in 2023. Fire hazards due to materials stored underneath bridges have also been highlighted by the total collapse of an I-85 overpass in Atlanta, GA in 2017, where high-density polyethylene (HDPE) conduit stored under the overpass caught fire and caused the collapse of a 100-foot span of the overpass [7]. That overpass was supported by prestressed concrete girders, indicating that fire resistant design is warranted for bridge structures beyond those supported by steel elements.

Fire is not explicitly addressed in the current American Association of State Highway and Transportation Officials (AASHTO) Bridge Design Specifications[2] [8], nor is it addressed in most bridge design manuals that are maintained by state departments of transportation (DOTs). The most significant national provisions for the design of bridges exposed to fire is provided by Chapter 6 of National Fire Protection Association (NFPA) 502[1] [1], which states that the primary structural elements of bridges or elevated highways should be protected to achieve the following functional requirements:

- support firefighter accessibility
- mitigate structural damage and prevent collapse
- minimize economic impact

However, these provisions are stated as being applicable only for bridges that have a length of at least 300 m (1,000 ft.), even though most of the overpasses that have collapsed in the last 30 years have been shorter spans [2]. Long-span bridge projects often include a threat, vulnerability, and risk assessment (TVRA) for fire hazards, but short- and medium-span bridge projects such as common highway overpasses typically receive little-to-no consideration for vulnerability to fire.

When applicable, NFPA 502[1] states that an "engineering analysis," including the consideration of design fire scenarios and their proximity to the structure, is needed to determine whether the collapse of the bridge due to fire would have adverse impacts to life safety or other unacceptable impacts to functionality. However, no guidance is provided regarding the available approaches and performance objectives for such an analysis. NFPA 502[1] Section A.6.3.2 suggests that for bridges spanning a freeway or highway, the design fire scenario typically includes a flammable tanker; for bridges spanning other types of roadways, the design

[2] FHWA approves the use of the AASHTO LRFD Bridge Design Specifications 9th Edition, although the use is not required (see Memorandum dated April 11, 2022 at https://www.fhwa.dot.gov/bridge/structures/04112022.pdf).

fire scenario typically includes an HGV. These threat scenarios represent the upper bound of vehicular fire hazards, as both tankers and HGVs produce significant heat release rate (HRR) when on fire (see Table 1-1). Fire hazards on the bridge deck can also be considered, particularly for bridge elements such as trusses or cables that would be directly exposed to heat transfer from such a fire [9–14].

As mentioned above, most bridge failures due to fire are indeed caused by tanker trucks and HGVs [2]. However, the possibility for considering stationary or stored fuels that are in close proximity to the bridge are not explicitly considered in NFPA 502[1], even though fire events, such as the aforementioned I-85 collapse in Atlanta highlight their importance. Following the I-85 collapse, for example, the Pennsylvania Department of Transportation (PennDOT) commissioned several research studies to investigate the impact of fires due to construction trailers [15] and farm products [16] that are stored underneath highway overpasses. Combustible materials that are often stored underneath[3] or near bridges can pose a structurally significant fire hazard depending on their quantity, combustion properties, and proximity.

Table 1-1: Peak Heat Release Rate (HRR) for vehicular fires per NFPA 502[1]

Vehicle Type	Representative Peak HRR (MW)	Experimental Peak HRR (MW)
Passenger Car	5	5–10
Bus	30	25–34
Heavy Goods Vehicle (HGV)	150	20–200
Fuel Tanker	300	200–300

This report is the second part of a two-phase study to assemble performance-based design guidance for the evaluation and mitigation of severe fire hazards for highway bridges. This evaluation can be conducted for a given bridge structure using the approach illustrated in the flowchart in Figure 1-1. The two-phase study has four overall objectives: (1) characterize the size and probability of potential fire hazards; (2) if a significant hazard is identified, model the fire and calculate the resulting thermal exposure to the bridge structure; (3) evaluate the potential for fire-induced structural damage; and (4) establish the most practical mitigation measures based on the needs of the bridge owner. Phase I culminated in a final report [2], which presented the development of a structurally significant design fire exposure as input for the engineering analysis of a bridge based on its vulnerability to various fire scenarios. That report summarized methods for modeling the fire itself ("Fire Model") and calculating its thermal impact on structural elements ("Heat Transfer"). This report (Phase II) is focused on the remaining items ("Thermal Response" and "Structural Response") in the flowchart in Figure 1-1. Specifically, the following will be addressed in the subsequent sections of this report:

[3] FHWA issued a memo on November 11, 2023 deeming flammable goods stored beneath a bridge to be deemed "critical findings" under the National Bridge Inspection Standards, thus requiring immediate follow-up action by the bridge owner. While this does not condone the practice of the storing flammable goods beneath a bridge, the bridge owner would have to demonstrate (e.g. using fire analysis described in this report) if those goods caught on fire, that bridge safety is maintained.

- Summarize design-basis tools that can be used for "engineering analysis" per Chapter 6 of NFPA 502[1] to calculate the thermo-structural impact of design-basis fires on a particular bridge.
- Summarize approaches for evaluating common thermo-structural limit states of steel and prestressed girders as well as other common structural elements in bridge structures under fire.
- Review fire mitigation strategies and recommend needs for future research.

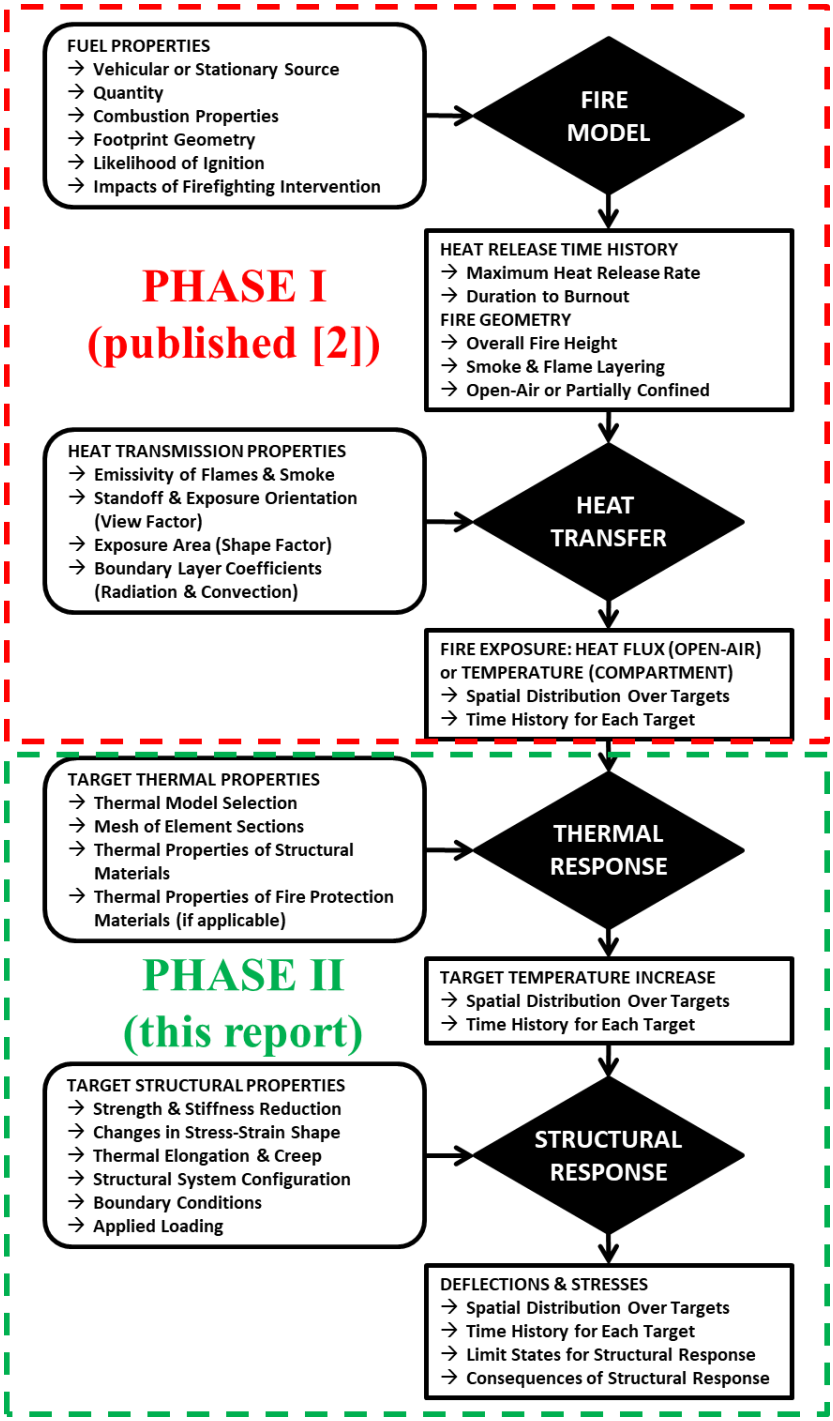

Source: S. Quiel, S. Ma, Lehigh University

Figure 1-1: Illustration. General framework for performance-based structural-fire engineering.

2 THREAT, VULNERABILITY, AND RISK ASSESSMENT FOR BRIDGE FIRES

Recent events have demonstrated that the consideration of vehicular or stationary fire hazards may be justifiable for highway bridges that are shorter than the least 300-m (1,000-ft.) lower-bound length provided by NFPA 502[1]. Rather than using the bridge length as the sole parameter in determining the importance of the bridge, the decision to address the impact of fire on a bridge structure can instead be made based on an assessment that considers the likelihood of occurrence for a structurally significant fire near a bridge, the vulnerability of the bridge's structural elements to fire-induced damage or collapse, and the resulting impacts to user life-safety and the transportation network functionality both during and after the fire. Long-span structures do indeed warrant these considerations because they typically represent a bottleneck in a highway system and are signature (i.e., high-profile) structures – the consequences of a severe fire for these bridges can be significant in the event of failure or in terms of downtime for repair or replacement. These structures often include cable arrays and trusses that are vulnerable to vehicle fires on their deck [9–14], and they can also be impacted by fires from vehicles traveling below [17].

Common overpass bridges (particularly those carrying interstate highways) may also warrant consideration for a fire TVRA due to the high volume of traffic that they carry and their relative proximity to both vehicular fire hazards on roadways below [4,14,18] as well as combustible materials that are located nearby [7,15]. At the very least, the development of a TVRA can make an authority having jurisdiction (AHJ) more aware of the potential impact of fire hazards, particularly the response time needed for firefighting efforts to prevent damage or collapse as well as the standoff or clearance needed to mitigate the impact of the fire. Contingency plans for repair or reconstruction can be proactively developed for a bridge that is determined to be highly vulnerable to fire.

In general, a TVRA for bridge fire exposure can be developed using the following considerations:

- Does the bridge have features below[4] the bridge that can lead to a fire below the deck, or does it have features above[4] the bridge such that a fire on the deck can have consequence to the feature above the bridge?
    - Would the fire resulting from vehicles have sufficient intensity and flame height to adversely impact the bridge's structural elements?
    - Is the frequency of large vehicles (tankers, HGVs, cargo ships, etc.) significant enough to justify the concern about an associated fire?
    - Does the geometry of the passage under the bridge (for roadways: curvature, slope, grade, sightlines, etc.; for waterways: navigable routes, presence of natural or manmade obstacles,

[4] The Specification for the National Bridge Inventory (SNBI) has two coding items to capture this, Items B.F.01 and B.F.02, that work hand-in-hand to identify features carried, above, or below the bridge. Item B.F.01 describes what the feature is, for example "H##" for highway, "R##" for railroad, or "B##" for an urban feature. The "urban feature" coding can capture places that may intentional or unintentionally be storing combustible materials. Item B.F.02 describes the location of the feature, for example "C" if it is carried on bridge, "A" if it is above the bridge, or "B" if it is below the bridge.

operational or logistical challenges, etc.) potentially increase the risk of vehicular allisions or collisions that could result in fire?

- Does the bridge have materials stored (intentionally or unintentionally) underneath or nearby, or are there structures (fuel tanks, pipelines, storage sheds, etc.) underneath or nearby that pose a significant fire hazard?
    - What is the potential for ignition and the potential peak HRR that can be generated by these materials (which can be determined via inventory method analysis [7,15,19], in which the calorific potential of available fuels is summed, and their collective combustion efficiency is used to estimate a total HRR)?
    - Would the fire resulting from these materials have sufficient intensity and flame height to adversely impact the bridge's structural elements?
    - Can those materials be relocated or reconfigured to either increase standoff and clearance, or to shield the bridge elements from the effects of a resulting fire?
- What type of structural system does the bridge use?
    - How susceptible are the materials used for the bridge structure (structural steel, reinforced or prestressed concrete, cables, etc.) or the connections between elements to fire-induced losses of strength and stiffness that could result in permanent damage or loss of functionality?
    - Do any fire-exposed elements include materials that are potentially combustible (such as high-density polyethylene sheathing for stay cables) and could contribute to fire-induced losses of structural capacity for those and nearby elements [14]?
    - Does the structural system have load-path redundancies that could withstand the loss of one or more structural elements due to localized fire exposure?
    - How much fire-induced damage to the structural elements can be sustained before the bridge collapses or is damaged such that it is taken out of service?
    - Does the bridge have structural elements (trusses, cables, thru-girders, etc.) that are vulnerable to a vehicular fire on its deck?
        - How close are those structural elements to the roadway where an on-deck fire could be located?
        - How many structural elements would be affected at the same time by an on-deck fire, depending on its size and intensity?
- What are the consequences associated with the loss of functionality for the bridge in question?
    - Does the bridge's length and traffic configuration pose a direct threat to user life-safety during the fire if the structure were to become damaged or collapse?
    - Are there structures, bystanders, or vehicles underneath the bridge whose life safety may be threatened by debris falling from the fire-affected bridge if it were to partially or totally collapse?
    - What is the average annual daily traffic (AADT) and truck traffic percentage (TTP) carried by the bridge?
    - What is the estimated cost and turn-around time associated with potential repair or replacement following fire-induced damage or collapse?
    - What is the estimated detour length if the bridge were to be out of service?
    - Are there feasible options for erecting a temporary bridge structure to accommodate at least some of the traffic during reconstruction or repair of the original bridge?
    - What would be the socio-economic impact associated with the loss of functionality for this particular bridge?

        - Is the bridge part of a major transportation route, service a shipping corridor, or provide an essential lifeline for a rural community?
    - What is the potential for collateral environmental impacts of the bridge fire event (including contamination of nearby waterways by falling debris or combustion residue, the potential to ignite a wildfire event, etc.)?
- What is the likelihood that firefighting efforts would be able to mitigate the effects of a fire for a particular bridge?
    - What is the response time and firefighting capacity available to address a severe fire?
- Is it possible to introduce fire protection strategies for this bridge?
    - Can passive protection systems (such as surface-applied fire resistive coatings or encasement paneling) be feasibly applied at an acceptable cost-benefit to mitigate the risk of fire-induced damage or collapse?
    - Would active fire protection systems (such as alarms, sensors for detection, or fixed firefighting systems [FFFS], all of which have been used extensively for tunnel structures [20] but are rarely used for bridges) be a feasible consideration to mitigate the risk of fire-induced damage or collapse?

A compilation of these considerations can be used to assess the threat and vulnerability of fire to an individual bridge or to compare the relative risk of a portfolio of bridge assets. Based on these assessments, a decision can be made to proceed with structural-fire engineering analysis to determine in greater detail the nature of the fire hazard, the heat transfer to the structural elements, the thermal response of those elements, and the resulting structural response and associated consequences (as illustrated previously in Figure 1-1).

Several previous studies have used these considerations to develop various metric-based classification ratings systems to determine whether a particular bridge may warrant evaluation for fire hazards [18,21,22]. The weighting and scoring system used to develop these ratings, however, should be closely examined to determine whether they are appropriately applicable to a particular bridge structure or portfolio of bridge structures. In general, the flowchart shown in Figure 2-1 can be used to determine a general level of risk associated with fire-induced damage to a particular bridge. The three levels of risk can be described as follows:

- **LOW RISK**:
    - The bridge is located such that there is a low probability that a severe (i.e., structurally significant) fire would substantively impact its structural elements.
    - By virtue of their materials, design, or construction, the bridge's structural elements have low vulnerability to fire-induced damage or failure.
    - The consequences of closure, repair, or replacement of the bridge due to fire-induced damage are relatively low.
- **MEDIUM RISK**:
    - The bridge has a higher probability of experiencing the effects of a nearby severe fire but may have lower vulnerability to fire-induced damage or failure due to its design, materials, redundancy, etc.
    - The bridge structural has a higher vulnerability to fire-induced damage or failure, but the perceived probability of a nearby structurally significant fire is modest.
    - The consequences of closure or replacement due to fire-induced damage are not insignificant but not critical.

- **HIGH RISK**:
  - The bridge has a high probability of experiencing the effects of a nearby severe fire as well as high vulnerability to fire-induced damage or failure due to its design.
  - The impacts to life-safety and economic consequences of closure or replacement due to fire-induced damage are significant.

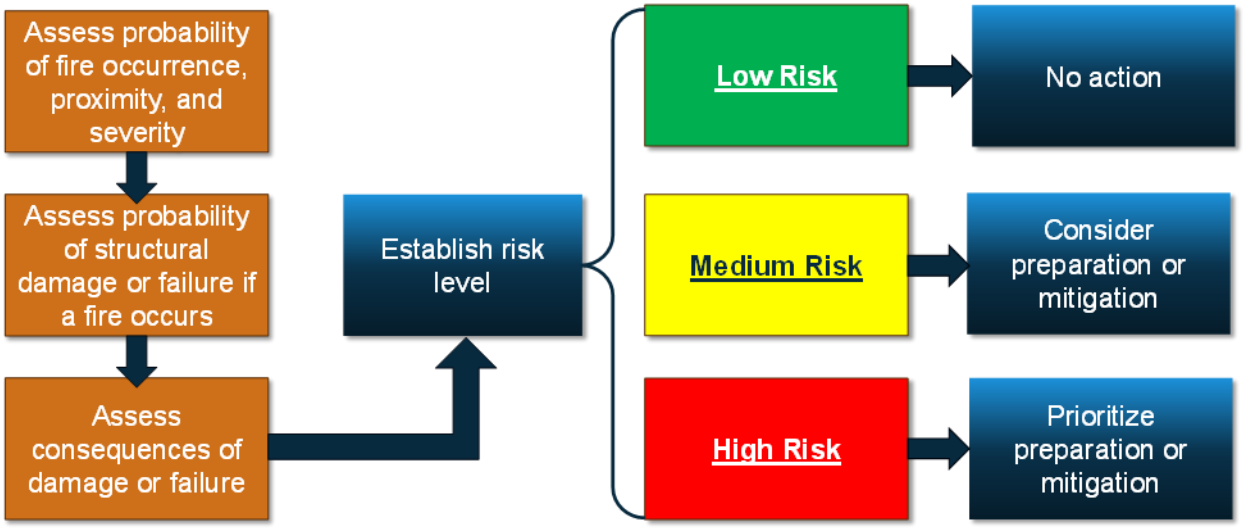

Source: F. Artmont, Modjeski & Masters

Figure 2-1: Illustration. Risk assessment framework for fire-induced damage to bridges.

Previous fire-induced bridge collapse events can be used to identify key considerations in the risk assessment of fire-induced damage. For example, the collapse of northbound overpass at I-95 Cottman Avenue in Philadelphia, PA in 2023 [19] (see Figure 2-2) and the overpass at the I-80/I-580/I-880 MacArthur Maze complex interchange in Oakland, CA in 2007 [23] (see Figure 2-3) were caused by tanker truck fires on the roadway below. In both cases, the overhead bridge and the roadway below had not only high AADT but also significant frequency of large trucks, including tankers. Both had clearances of approximately 15 ft. above the roadway where the fire occurred, and the flames from these large fires would therefore be expected to directly engulf the bridge overhead [19,23]. It is also notable that while the bridge spans directly over each fire collapsed after less than 15 minutes of estimated exposure, none of the adjacent spans collapsed, but instead exhibited a range of fire-induced damage (which ultimately required repair and replacement of multiple structural elements).

A review of these incidents (as well as numerous other similar incidents [2]) supports the statement in NFPA 502[1] Section A.6.3.2 that for bridges spanning a freeway or highway, the design fire scenario would typically include a flammable tanker. Work completed in Phase I of this project [2] also indicated that the design-basis fire hazard for these clearances (based on an applicable reliability index of 3.5 for bridge structural components and the expected frequency of truck traffic for a highway) would correspond to a heat flux that would be expected for engulfment by a hydrocarbon fire. Using the MacArthur Maze incident as a case study, Phase I of this project [2] highlighted multiple spans (including the span that collapsed) with low clearances that could be considered as highly vulnerable to severe fire hazards on the roadways below, based on the estimated design-basis fire load.

Actions to mitigate the risk of fire-induced damage for a particular bridge could include but are not limited to the following:

- Preparation and curation of a plan for rapid reconstruction or repair, including coordination with fabricators, contractors, and consultants
- Coordination with emergency responders to develop a firefighting and egress plan, including standpipe and water source locations, evacuation and detour routes, and response time
- Preparation of engineering assessment tools that correlate the proximity and size of the fire to the time to onset of damage or collapse
- Assessment of the impacts of roadway geometry and traffic features on the probability of fire occurrence or the vulnerability of the structural system to fire effects
- Signage or other visual markings to indicate locations where fire could pose a significant hazard to the bridge's structural elements
- Additional training for truck drivers regarding operational awareness for fire safety, particularly regarding the proximity of their vehicle to a bridge in the event of an onboard fire or accident
- Application of fire resistive coatings, encasement, or paneling on or near structural elements, to mitigate their temperature increase due to potential fire exposure.

(a)

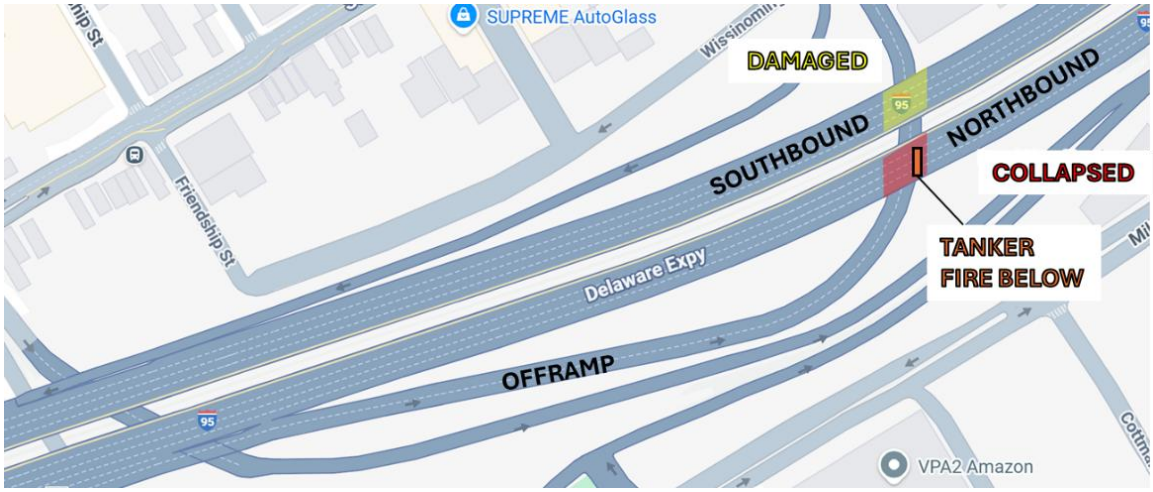

Source: Google Maps, Cottman Ave. and I-95, Philadelphia, PA (with annotation by S. Quiel and S. Ma, Lehigh University)

(b)

Source: Pennsylvania Department of Transportation

Figure 2-2: Illustrations. Images for the June 2023 tanker fire at the Cottman Avenue exit ramp underneath I-95 in Philadelphia, PA: (a) roadway plan view and (b) photo of the aftermath of the fire event [19].

(a)

Source: Google Maps, MacArthur Maze Interchange, Oakland, CA (with annotation by S. Quiel and S. Ma, Lehigh University)

(b)

Source: Philip Liborio Gangi (https://liboriogangi.tripod.com)

Figure 2-3: Illustrations. Images for the April 2007 tanker fire at the MacArthur Maze interchange of I-80/I-580//I-880 in Oakland, CA: (a) roadway plan view and (b) photo of the fire event.

3 METHODS OF ANALYSIS

In the final report for Phase I of this project [2], methods for quantifying fire intensity and heat exposure to a bridge element were summarized. Once the decision is made to pursue "engineering analysis" of the affected bridge, the next essential steps are to determine the temperature evolution of the structural elements during and after a fire event, in order to calculate the structural response and assess whether the structure can withstand the fire and return to service. As shown in Figure 3-1, the first two blocks specify the fire source; their outputs are the time- and space-dependent thermal boundary conditions applied to the structure. The subsequent analysis then uses these boundary conditions, together with heat transfer modes (conduction, convection, and radiation), to compute internal temperature histories. These temperature data are passed to the structural model as inputs to obtain the structural response. Normally the workflow is one-way coupling. However, if the structural response alters the boundary conditions or geometry in a way that affects the fire/heat transfer field (i.e., large deformation changes the clearance between the flames and the structures), then two-way coupling may be required, as indicated by the dashed arrows in Figure 3-1. In a two-way coupled formulation, a staggered iterative scheme is adopted: within each time step, the thermal and structural fields are updated until convergence. If the thermo-structural response leads to appreciable geometric changes, the altered configuration is fed back to update the applied thermal boundary conditions before advancing to the next step [24].

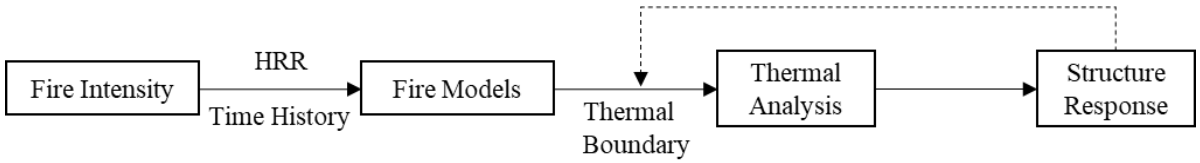

Source: S. Quiel, S. Ma, Lehigh University

Figure 3-1: Illustration. General steps for fire analysis.

Because of the high thermal conductivity, the temperature field within steel members is often assumed to be uniform in many practical fire engineering calculations, especially in the thickness direction (e.g., across the cross section of a steel beam). In-plane temperature variations (e.g., along the longitudinal direction), however, can still be significant. Owing to both the inherent properties of steel and the geometry of steel sections, simplified approaches can be applied to estimate the temperature. Such approaches may involve hand calculations, using simple fire-spread spreadsheets or quick programming routines. For more complex or detailed scenarios, such as when thermal boundary conditions are complicated or when cross-sections involve mostly concrete materials, finite element methods (FEM) or other numerical analyses are generally employed as an alternative.

3.1 Finite element method

Actual structural systems typically consist of assemblies of multiple components and are exposed to complex fire scenarios. In the performance-based approach, it is necessary to capture the temporal and spatial variation of temperatures throughout the structural members. Under these conditions, complex numerical approaches such as FEM may be more appropriate and commonly adopted. The fundamental principles of FEM have been extensively described in textbooks and the published research literature. In engineering practice, several heat transfer FE programs can be used to directly calculate the temperature distribution in components exposed to fire. Examples of software with specific modules for structural fire

FE analysis include SAFIR and OpenSees [25,26]. General FE softwares such as Ansys or Abaqus [27,28], can also be used to simulate transient temperature distributions under fire exposure. For a typical thermal analysis in these programs, the required input generally includes:

(1) geometric information describing the discretization of the structural member into elements and nodes;
(2) thermophysical properties of materials such as steel and concrete (density, specific heat, thermal conductivity, etc.); and
(3) initial and boundary conditions associated with the fire scenario.
(4) numerical parameters such as time history duration, time step values, convergence criteria, output result frequency, etc.

Overall, most programs can accommodate time-dependent boundary conditions and material properties, but for some complicated phenomena like concrete spalling during heating, some assumptions and modeling techniques need to be incrementally updated when performing analysis [7,29]. Attempts to model underlying mechanisms, such as moisture migration and pore-pressure buildup within the concrete [30–32], may require more advanced hygro-thermal models to be captured explicitly.

Thermal FE analysis of a heated structural member is often conducted for its 2D cross-section, while heat conduction along the longitudinal direction of the member is neglected. In the thermal analysis input file, the thermal properties of the materials must be specified. Since the present example uses SAFIR, the required parameters are introduced with reference to this program. In SAFIR, the properties of these commonly used materials are already predefined based on relevant codes and standards. For user-defined materials, temperature-dependent thermal conductivity, specific heat, and dry density need to be provided. In addition, the initial moisture content, the starting and ending temperatures of moisture evaporation, and the reversibility of the thermal properties need to be specified for fire-exposed cementitious materials.

Following thermal analysis, the temperature–time histories of the cross-section are obtained and subsequently used as input for the structural analysis. At this stage, the influence of temperature on structural response is primarily reflected through its effects on the mechanical properties of its materials (including stiffness, strength, and related constitutive parameters) as well as thermal expansion. In SAFIR, some temperature-dependent material models for common construction materials are provided. For user-defined materials, such as steel, it is necessary to explicitly specify the degradation of mechanical properties with increasing temperature, like reduction factors for elastic modulus and yield strength, among others. Parameters governing strain evolution and failure limits should also be defined, which typically include yield strain, thermal strain, and other strain-related quantities that control plastic deformation and ultimate material failure under elevated temperatures and cooling phase.

3.2 Simplified methods of thermal analysis

Lumped mass methods of thermal analysis are generally applicable to materials with relatively high thermal conductivity, such as steel, where the temperature distribution across a given component tends to be relatively uniform. Calculated changes in steel temperature can then be used to calculate the corresponding decrease in the element's strength and stiffness, as well as its thermal elongation.

For concrete and other materials with lower thermal conductivity, a significant internal thermal gradient will typically develop under fire exposure, thus rendering the lumped mass method ineffective. Other simplified approaches [33,34] are available for estimating the one-dimensional heat transfer through a concrete thickness. However, numerical analysis methods such as FEM are generally recommended for structural members whose sections are primarily comprised of materials that have lower thermal conductivity.

3.2.1 Lumped mass method for unprotected steel sections

The "lumped mass" method treats the whole cross-section as a single unit, thereby assuming a uniform temperature and no internal gradient. Heat transfer with the environment is then computed for this single unit. This zero-thickness thermal analysis is suitable for thin steel plated members with high thermal conductivity. Quantitatively, the applicability can be checked using the Biot number, *Bi*, defined as the ratio of the internal conductive thermal resistance to the external convective resistance at the surface. When $Bi < 0.1$, the body's temperature may be assumed uniform.

$$Bi = (L_c/k)/(1/h) = hL_c/k \tag{3-1}$$

In practice, because of the small thickness of the web or flange, the temperature along the thickness is assumed to be equal. For in-plane of the web and flanges, the gradient may be appreciable depending on the boundary conditions. Therefore, the method is particularly suitable when steel sections are heated on all sides. Assuming constant thermal properties, the steel temperature may be obtained directly from analytical formulations.

The principle is that, within a short interval, the steel temperature for a composite bridge girder is increased by absorbing the heat entering from the fire (applied over the fire-exposed surface area, F_f) minus the heat lost to the ambient environment (applied over the surface area exposed to ambient conditions, F_a), and the heat transfer from steel to concrete slab (applied over the contact area between the top flange and the slab, F_c):

$$\left(\dot{q}_f'' F_f - \dot{q}_a'' F_a - \dot{q}_c'' F_c\right)\Delta t = \rho_s c_s V \Delta T_s \tag{3-2}$$

The incident heat flux $\dot{q}_f''$ from the fire can be specified directly via heat transfer from a fire model (see Section 3 of the Phase I report [2]) or calculated as the combination of convection and radiation heat transfer from the fire temperature:

$$\dot{q}_f'' = h_c\left(T_f - T_s\right) + \varepsilon\sigma\left[\left(T_f + 273\right)^4 - (T_s + 273)^4\right] \tag{3-3}$$

Likewise, the heat flux lost to the ambient environment is also calculated as a combination of convection and radiation heat transfer:

$$\dot{q}_a'' = h_c(T_s - T_a) + \varepsilon\sigma[(T_s + 273)^4 - (T_a + 273)^4] \tag{3-4}$$

The term $\dot{q}_c''$ can be estimated using the semi-empirical formulation proposed by Ghojel and Wong [35]:

$$\dot{q}_c'' = a + bT_{tf,s} + cT_{tf,s}^2 + dT_{tf,s}^3 + eT_{tf,s}^4 + fT_{tf,s}^5 + \frac{g}{b_{tf}} + \frac{h}{b_{tf}^2} \quad (3\text{-}5)$$

where a = 7,025.058155, b = 92.10056821, c = −0.325555284, d = 0.000809452, e = −1.02099E-6, f = 4.671E-10, g = −2,786,576.15, h = 240,879,025.7, and flange width b_{tf} in millimeters [35]. Note that $\dot{q}_c''$ is taken as a function of the top flange temperature, $T_{tf,s}$. This equation can instead utilize T_s for a lumped mass approach in which the entire steel section is approximated as having the same steel temperature, T_s.

The temperature evolution of the steel section is computed using a time-discretized form of the lumped heat balance equation. Using a forward finite difference approximation, the steel temperature at time step t is obtained as:

$$T_{s,t} = T_{s,t-1} + \left(\frac{\Delta t}{\rho_{s,t-1} c_{s,t-1} V}\right)\left(\dot{q}_{f,t}'' F_f - \dot{q}_{a,t}'' F_a - \dot{q}_{c,t}'' F_c\right) \quad (3\text{-}6)$$

If the section is fully exposed to fire, then the surface area exposed to ambient conditions, F_a, would be zero. For a girder supporting a slab, the top surface of the girder in contact with the slab will not be exposed to fire or the ambient environment. Rather, that surface could be conservatively assumed to be adiabatic (i.e., the slab is assumed to insulate that surface due to its lower thermal conductivity), or the heat loss to the slab can be calculated [35,36]. For these calculations Eurocode 3[5] Part 1-2 [37] suggests a time step of no more than 30 seconds, while American Institute of Steel Construction (AISC) 360-22[6] Appendix 4 [38] suggests a time step of no more than 5 seconds. Heat transfer coefficients should be taken according to the fire exposure and material. For example, Eurocode 1[7] Part 1-2 [39] states that a hydrocarbon fire can be assumed to have h_c of 50 W/m^2·K while a natural fire exposure (i.e. a cellulosic fire that eventually burns out) would have h_c of 35 W/m^2·K. Per Eurocode 4[8] Part 1-2 [40], the resultant emissivity ε for both steel and concrete surfaces under fire can be taken as 0.7. Thermal material properties for steel are temperature dependent but can be approximated as constant depending on the application [41].

The lumped-mass method can be adapted to practical situations. For example, when a steel beam is heated on three sides, a temperature gradient develops across the depth of the cross-section. In that case, the section can be discretized into several sub-masses, and the temperature within each part is assumed uniform. For an I-section, the cross-section may be divided into the bottom flange, web, and top flange, treating each as a separate lumped mass. The thermal model needs to then account for both (i) external heat transfer to each part and (ii) conduction between the parts within the section [36].

[5] Use of Eurocode 3, Design of steel structures - Part 1-2: General rules - Structural fire design, is not a Federal requirement.

[6] Use of AISC 360-22, Specification for Structural Steel Buildings, is not a Federal requirement.

[7] Use of Eurocode 1, Actions on structures - Part 1-2: General actions - Actions on structures exposed to fire, is not a Federal requirement.

[8] Use of Eurocode 4, Design of composite steel and concrete structures - Part 1-2: General rules - Structural fire design, is not a Federal requirement.

3.2.2 Lumped mass method for protected steel sections

When coated with fire resistive insulation, the steel section underneath is no longer directly exposed to fire but receives heat transfer from the fire via conduction through the insulation thickness. Conversely, the insulation layer also mitigates heat loss to the ambient environment on surfaces that are not exposed to fire, and any such heat loss is commonly neglected for protected steel sections. For simplification, the temperature at the outer surface of the insulation is assumed to be equal to the temperature of the fire exposure. If the fire exposure is specified as a heat flux from a fire model (see Section 3 of the Phase I report [2]), then an equivalent surface temperature at the insulation must be calculated (as demonstrated by Zhu et al. [18] for steel girders under open-air fire exposure).

Two cases can be distinguished depending on whether the heat capacity of the protection is considered. When the heat capacity of the protection is neglected, under equilibrium conditions, heat transferred through the insulation is equal to the heat required to raise the temperature of the steel.

$$k_i F_f \frac{(T_f - T_s)}{d_i} = \rho_s c_s V \frac{\Delta T_s}{\Delta t} \tag{3-7}$$

The temperature distribution within the insulation is assumed to be linear, and the following criterion can be used to determine whether the heat capacity of the insulation can be neglected:

$$\rho_s c_s V > 2\rho_i c_i F_f \tag{3-8}$$

When the heat capacity of the protection must be accounted for, the heat transferred through the insulation is equal to the sum of the heat needed to raise the temperature of the steel and the heat needed to raise the temperature of the protection itself.

$$k_i F_f \frac{T_f - T_s}{d_i} - \dot{q}_c'' F_c = \rho_s c_s V \frac{\Delta T_s}{\Delta t} + \rho_i c_i d_i F_f \frac{\Delta T_s}{2\Delta t} \tag{3-9}$$

By assembling the above heat transfer components and including the heat conduction into the concrete slab, the resulting expression can be written as:

$$\Delta T_s = \frac{k_i F_f (T_f - T_s)/d_i - \dot{q}_c'' F_c}{\rho_s c_s V + (\rho_i c_i d_i F_f)/2} \Delta t \tag{3-10}$$

AISC 360-22[6] Appendix 4 [38] recommends that half of the heat capacity of the insulation be added to the steel heat capacity in order to simplify the expression for computation of steel temperatures. In Eurocode 3[5] Part 1-2 [37], the heat absorption in the insulation is similar but slightly modified to approximately account for realistic nonlinearity in the thermal gradient through the insulation thickness. The resulting expression is given as:

$$\Delta T_s = \frac{k_i F_f (T_f - T_s)/d_i - \dot{q}_{c,t}'' F_c}{\rho_s c_s V + (\rho_i c_i d_i F_f)/3} \Delta t + \left[exp\left(\frac{\rho_i c_i d_i F_f}{10 \rho_s c_s V}\right) - 1 \right] \Delta T_f \tag{3-11}$$

If both formulations are discretized in time using a finite-difference scheme, the resulting expressions can be written as follows:

$$T_{s,t} = T_{s,t-1} + \frac{k_{i,t-1}F_f\left(T_{f,t}-T_{s,t-1}\right)/d_i - \dot{q}''_{c,t}F_c}{\rho_{s,t-1}c_{s,t-1}V+\left(\rho_{i,t-1}c_{i,t-1}d_iF_f\right)/2}\Delta t \quad (3\text{-}12)$$

$$T_{s,t} = T_{s,t-1} + \frac{k_{i,t-1}F_f\left(T_{f,t}-T_{s,t-1}\right)/d_i - \dot{q}''_{c,t}F_c}{\rho_{s,t-1}c_{s,t-1}V+\left(\rho_{i,t-1}c_{i,t-1}d_iF_f\right)/3}\Delta t - \left[exp\left(\frac{\rho_{i,t-1}c_{i,t-1}d_iF_f}{10\rho_{s,t-1}c_{s,t-1}V}\right)-1\right]\left(T_{f,t}-T_{f,t-1}\right) \quad (3\text{-}13)$$

In the subsequent analyses presented in the following sections, the protective material is assumed to be sprayed fire-resistive material (SFRM), and its thermal properties are kept consistent with those used in SAFIR [42]. A time step $\Delta t = 5$ sec is recommended for lumped mass thermal calculations of steel sections [37,38]. Its thermal properties are updated at each time step using a weighted average temperature to account for the non-linear thermal gradient through the protection thickness: $0.4T_{f,t} + 0.6T_{s,t-1}$. For a slower heating rate than those considered in this study (which are based on hydrocarbon fire exposures), a different ratio may be more appropriate. For example, Drury and Quiel [43] recommended $0.1T_{f,t} + 0.9T_{s,t-1}$ for SFRM-protected steel beams that are subjected to a building fire exposure similar to ASTM E119[9] [44] which has a slower rate of heating than those considered in this study.

3.3 Material properties

When heated by fire, structural materials like steel and concrete will experience a temperature increase accompanied by a loss of strength and stiffness as well as thermal expansion. The stress-strain relationships of these materials will also become increasingly nonlinear. Guidance for calculating the thermal and structural performance of structures under fire includes the following:

- Steel and steel-concrete composite structures: AISC 360-22[6] Appendix 4 [38], Eurocode 3[5] Part 1-2 [37], and Eurocode 4[8] Part 1-2 [40]
- Cast-in-place and precast concrete structures: American Concrete Institute (ACI) 216-14(19)[10] [45], Precast Concrete Institute (PCI) 124-23[11] [46], and Eurocode 2[12] Part 1-2 [47]
- General guidance for various structural systems: American Society of Civil Engineers (ASCE) Manuals of Practice 78 [48] and 138 [49], and Society of Fire Protection Engineers (SFPE) Handbook of Fire Protection Engineering [50]

Representative reduction factors for the stiffness and strength of structural steel and reinforced concrete materials are plotted in Figure 3-2. Some key observations can be made:

- The stiffnesses of hot-rolled steel and concrete begin to decrease just before 100 °C (212 °F) and degrade at lower temperatures than their corresponding strengths.

[9] Use of ASTM E119, Test Methods for Fire Tests of Building Construction and Materials, is not a Federal requirement.
[10] Use of ACI 216-14(19), Code Requirements for Determining Fire Resistance of Concrete and Masonry Construction Assemblies, is not a Federal requirement.
[11] Use of PCI 124-23, Specification for Fire Resistance of Precast and Prestressed Concrete, is not a Federal requirement.
[12] Use of Eurocode 2, Design of concrete structures - Part 1-2: General rules - Structural fire design, is not a Federal requirement.

- The reductions of yield strength for hot-rolled steel and mild rebar are similar and begin to rapidly decrease at 400 °C (752 °F). Both have only ~25% remaining yield strength once the steel temperature reaches 700 °C (1,292 °F).
- The decrease in compressive strength for NWC has a similar rate as LWC but initiates at a lower temperature. It should be noted that LWC also has a lower thermal conductivity than NWC [40] and is therefore more resistant to thermal transmission through its thickness.
- Cold-drawn prestressing steel initiates its reduction in ultimate strength at a much lower temperature than yield strength for mild rebar. Prestressing strands will also begin to experience relaxation, thermal creep, and permanent losses of strength once their temperature exceeds 300 °C (572 °F) [51–55], though hot-rolled rebar will respond similarly to hot-rolled steel plate and experience much less permanent residual degradation [56] or thermal creep [57] at steel temperatures below 649 °C (1,200 °F).

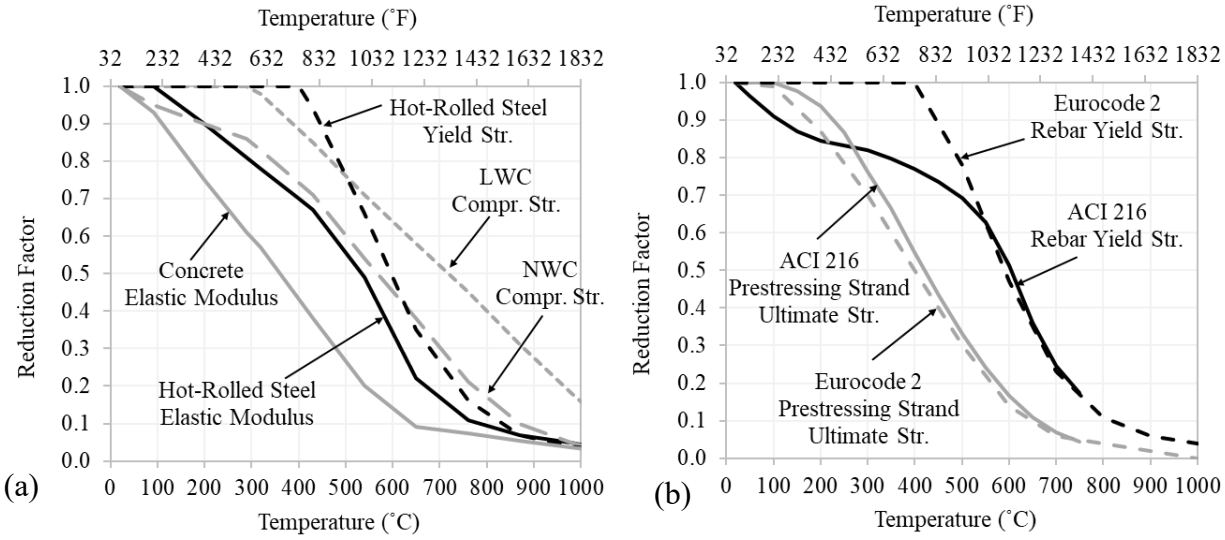

Source: S. Quiel, S. Ma, Lehigh University

Figure 3-2: Graphs. Structural material property reduction factors at high temperature: (a) steel and concrete strength and stiffness per AISC 360-22[6] Appendix 4, and (b) mild rebar and cold-drawn prestressing strand reinforcement per ACI 216-14(19)[10] and Eurocode 2[12] Part 1-2.

4 EVALUATING ANALYSIS RESULTS

Chapter 3 introduced select numerical methodologies that can be used to simulate the bridge response under fire scenarios, including approaches for thermal analysis and structural analysis. These methods provide the foundation for predicting temperature distributions, stress redistribution, and deformation development in fire-exposed bridge components. In practical engineering decision-making, it is necessary to interpret the numerical results through critical response parameters and associated threshold values in order to determine whether the bridge remains open to traffic, the level of structural damage, and whether post-fire repair remains feasible. To effectively translate simulation results into engineering decisions, it is essential to summarize commonly adopted quantitative performance metrics and establish a clear relationship between analysis results and structural condition assessment. This chapter therefore focuses on summarizing a set of metrics for evaluating the structural performance of bridges subjected to vehicle fire exposure. These metrics are used to interpret thermal and thermo-structural analysis results in terms of structural functionality, residual capacity, and failure potential.

4.1 Thermal damage criteria

Temperature is a direct and intuitive indicator of fire-induced damage, as it explicitly reflects the degradation of material mechanical properties with elevated temperature. According to ASTM E1529[13] [58], a structural steel member is considered to have failed when its average temperature exceeds 538 °C (1,000 °F) or its maximum temperature exceeds 649 °C (1,200 °F). Similarly, ASTM E119[9] [44] provides comparable failure temperature limits for flexural members, with an average temperature limit of 593 °C (1,100 °F) and a maximum temperature limit of 704 °C (1,300 °F). As shown previously in Figure 3-2(a), both Eurocode 3[5] Part 1-2 [37] and AISC 360-22[6] Appendix 4 [38] indicate that the yield strength of low-carbon structural steel begins to significantly deteriorate once the temperature exceeds 400 °C (752 °F).

Studies on the critical temperature thresholds for fire-induced damage of concrete bridge girders are relatively limited. Existing research mainly focuses on two aspects: (1) using concrete surface temperature and reinforcing steel temperature to reflect the degradation of material properties; and (2) the spalling of concrete under fire exposure. When spalling occurs, it damages the integrity of structural members and may expose the reinforcing steel directly to the fire, thereby accelerating the degradation of the overall structural load-carrying capacity. However, for the prediction of concrete spalling, especially temperature-based spalling prediction, there is currently no generally accepted method. Table 4-1 summarizes several temperature thresholds for normal-weight concrete (NWC), some temperature-based concrete spalling prediction methods proposed in the literature, prestressing steel, and mild reinforcement.

[13] Use of ASTM E1529, Test Methods for Determining Effects of Large Hydrocarbon Pool Fires on Structural Members and Assemblies, is not a Federal requirement.

Table 4-1: Summary of temperature indicators for thermal damage to NWC, prestressing steel, and mild reinforcement.

Damage Description	Indicator	Critical Temperature	Source References
Generic onset of thermally induced damage	Concrete Surface Temperature	300 °C (572 °F)	Garlock et al. [4], Khoury [59], Tenchev & Purnell [60]
Generic onset of thermally induced damage	Concrete Surface Temperature	380 °C (716 °F)	NFPA 502[1] Chapter 7 [1]
50% loss of compressive strength	Concrete Temperature	550 to 650 °C (1,022 to 1,202 °F)	Eurocode 2[12] Part 1-2 [47]
Total loss of tensile strength	Concrete Temperature	600 °C (1,112 °F)	Eurocode 2[12] Part 1-2 [47]
Onset of spalling	Concrete Surface Temperature	450 °C (842 °F)	Carlton et al. [30]
Onset of spalling	Concrete Surface Temperature	250 to 420 °C (482 to 788°F)	Khoury [59]
Onset of spalling	Concrete Surface Temperature	600 °C (1,112 °F)	Qiao et al. [61]
Degradation for mild reinforcing steel	Steel Temperature	250 °C (482 °F)	NFPA 502[1] Chapter 7 [1]
Degradation for mild reinforcing steel	Steel Temperature	593 °C (1,100 °F)	ASTM E119[9] [44]
Significant strength degradation of cold-drawn prestressing steel	Steel Temperature	427 °C (800 °F)	ASTM E119[9] [44]

4.1.1 Implications for visual post-fire inspection

For post-fire visual inspection of structural steel bridge girders, two recent experimental studies [62,63] have recommended the following guidelines to determine the maximum temperature that the steel members experienced during the fire:

- For maximum steel temperatures below 427 °C (800 °F), steel surfaces that are uncoated, weathered, or coated with paint or other treatments would be expected to show only slight discoloration or soot/smoke marks, thus indicating relatively low impact on the residual condition of the material.
- For maximum steel temperatures between 427 °C (800 °F) and 649 °C (1,200 °F), paint and other coatings would bubble, blister, and begin to crack. Uncoated fire-exposed surfaces may begin to exhibit a reddish patina.
- For maximum steel temperatures beyond 649 °C (1,200 °F), paint and other coatings would severely crack and fall off. Uncoated fire-exposed surfaces may begin to exhibit a lighter color as well as a coarser, eroded-looking finish [64].

It should be noted that hot-rolled steel members would be expected to experience little permanent material degradation (i.e., loss of strength, stiffness, or hardness, etc. due to heat-induced metallurgical changes) at maximum steel temperatures below 649 °C (1,200 °F) [64,65].

For post-fire visual inspection of concrete bridge members, guidelines to determine the maximum concrete surface temperature are dependent on the aggregate type and constitutive composition. For example,

concretes with siliceous or other iron-bearing aggregates can develop a pink/red hue after having reached a temperature of 250–350 °C (482–662 °F); however, concretes with calcareous and lightweight aggregates may only exhibit a whitish-grey hue at this temperature range [66]. Most concretes can develop cracking at the paste-aggregate interfaces due to differential thermal properties around 380 °C (716 °F) [4], which coincides with the critical concrete surface temperature prescribed by NFPA 502[1] Chapter 7 [1]. Per experimental testing by Carlton et al. [30], spalling is possible soon thereafter once the surface temperature reaches 450 °C (842 °F), and the newly exposed spalled surface would then be subjected to direct heating. Nondestructive evaluation methods (such as a rebound hammer, ground penetrating radar, etc.) or other destructive evaluation techniques (such as coring, drilling, or scratch testing) would be recommended rather than visual inspection to determine the residual properties of spalled surfaces.

Spalled surfaces can also expose embedded reinforcement to direct heating, thus reducing their material strength/stiffness and potentially reducing their bond to the concrete. A recent experimental testing program on fire-exposure precast prestressed bulb-T girders [67] showed that although spalling was significant, the spalled areas and depths were somewhat dispersed over the fire-exposed areas. Prestressing strands and mild reinforcement were partially exposed to direct heating, but most of the reinforcement remained engaged in tension through burnout, most likely since there was adequate development length at portions of the girder that were only partially spalled or unspalled. Post-fire evaluation of prestressed concrete bridge elements should examine the potential for permanent losses of prestressing force in addition to examining the post-fire condition and structural properties of the concrete.

4.2 Structural damage criteria

Although temperature is a fundamental indicator of thermal exposure, it is not sufficient by itself to characterize fire-induced failure. Consider a simple case: a bridge girder fully exposed to severe fire may develop similar cross-sectional temperature distributions as a girder subjected to localized heating only at specific locations. Despite the comparable critical temperature at certain sections, the structural responses, like internal force redistribution, and deflection, can be markedly different. In addition to temperature-based criteria, incorporating structural response-based criteria is essential. Four more failure criteria are briefly listed here [68].

4.2.1 Limits on maximum deflection or deflection rate

Maximum total deflection and deflection rate are often used in combination to determine structural failure (see Table 4-2). For example, ASTM E119[9] [44] states that once the maximum allowable deflection is reached, the criterion transitions to a limit on the deflection rate to assess whether failure has occurred. A similar procedure is adopted in British Standard (BS) 476-10[14] [69], where the deflection-rate criterion becomes active after the maximum deflection exceeds $L/30$. Because both deflection and deflection rate can be directly and accurately measured during testing, these indicators have been widely used as failure criteria in several studies [70–74]. These deflection-based limits were originally developed for beams in building applications, rather than for bridge structures. In the context of bridges, deflection-based limits do

[14] Use of BS 476-10:2009, Fire tests on building materials and structures, Part 10: Guide to the principles, selection, role, and application of fire testing and their outputs, is not a Federal requirement.

exist but typically fall under serviceability provisions rather than fire-specific criteria. For instance, AASHTO[2] [8] suggests a serviceability limit of $L/800$ for steel girders under service loads, and several studies have adopted this value as a threshold for superficial residual damage in fire-exposed bridge girders [15,16,19]. For concrete girders, a more stringent serviceability limit such as $L/1000$ is often used to represent minor damage. L refers to the clear span of the beam, and d is the distance between the extreme compression fiber and the extreme tension fiber of the critical section.

Table 4-2: Deflection-based failure criteria for fire-exposed beam members

Structural critical damage	Criteria	Source References
Maximum total deflection	$L/20$	BS 476-10[14] [69]
Maximum total deflection	$L/30$	BS 476-10[14] [69]
Maximum total deflection	$L^2/400d$	ISO 834[15] [75], ASTM E119[9] [44]
Deflection rates	$L^2/9000d$ (unit: mm/min)	BS 476-10[14] [69], ISO 834[15] [75], ASTM E119[9] [44]

4.2.2 Buckling behavior or rapid out-of-plane displacement of webs

Local flange buckling and web shear buckling [74,76–78] can also cause damage and reduce the stiffness of steel elements when exposed to fire. In fiber-beam FE models, local buckling can be considered through specialized steel material models (such as STEELSL in SAFIR [79]) that reduce the effective width of affected plates. Shell and solid elements can provide a more robust prediction of local instability if initial imperfections are accounted for, but are computationally intensive [80].

4.2.3 Other limits

A limit strain of 0.2 can be used to represent the ultimate state of steel bridge elements under fire exposure [81–83]. It should be noted that this value pertains to an extreme load case and may be greater than that used for ambient design. An inward movement at the roller end for simply supported bridges [65,81,82] can also signify the potential for a loss of bearing support. Studies by Aziz et al. [74] and Alos-Moya et al. [82] indicated that girder bridges may exhibit different failure modes depending on their structural configuration and boundary conditions.

[15] Use of ISO 834, Fire resistance tests: Elements of building construction, Part 11: Specific requirements for the assessment of fire protection to structural steel elements, is not a Federal requirement.

5 MITIGATION STRATEGIES

Compared with fire protection in buildings, fire protection for bridges is still in a fledgling state. Chapter 6 of NFPA 502[1] suggests that primary structural members of bridges be provided with fire protection; however, these provisions are not applicable for bridges with lengths less than 1,000 ft (300 m). The fire performance of a bridge depends largely on the material response of its structural components.

5.1 Passive fire protection methods for steel members

Due to their high thermal conductivity and relatively low specific heat, steel members heat up rapidly when exposed to fire, leading to a sharp reduction in both strength and stiffness. Thus, limiting the temperature rise of steel sections during fire exposure is critical for maintaining structural integrity and preventing collapse. Given these characteristics of steel bridges, an ideal passive fire protection (PFP) material must be able to withstand rapid temperature escalation to levels exceeding 1,100 °C (2,012 °F) [58], while effectively insulating the underlying structural steel so that its temperature remains below the temperature limit. Considering the large span/height ratio and cross-sections of bridge girders, such protection systems need also to be economical and practical to apply. Among the feasible passive fire protection materials for steel bridges, several primary options are commonly considered, including spray-applied fire-resistive materials (SFRM) and intumescent coatings (ICs). In addition to conventional passive fire protection materials, shotcrete or gunite applied to weather-exposed steel members have also been used in practice, providing additional thermal mass but increasing dead load and potentially complicating in-service inspection.

This section focuses on the application of passive fire protection materials, of which SFRM is widely used in modern steel building construction practice. SFRM is essentially a lightweight, porous, and low-thermal-conductivity inorganic or semi-inorganic material. Its insulating mechanism relies on forming a low-conductivity, porous thermal barrier that significantly slows the heating rate of steel, thereby delaying the reduction in steel strength and stiffness. In the building industry, SFRM systems are supported by well-established standard test methods, including material performance criteria and standardized fire testing procedures. Many studies have also evaluated SFRM performance in conjunction with structural response analyses [84–86]. SFRM has several limitations, such as susceptibility to moisture absorption, relatively poor impact resistance and durability, and rough surface finish. These characteristics may be undesirable for exposed bridge components. In addition, SFRMs can mask steel elements during in-service visual inspection, and certainly more so for hands-on nonredundant steel tension member inspections.

ICs are often considered a promising alternative because they can potentially overcome several inherent limitations of SFRM. ICs are a polymer-based system composed of various organic and inorganic materials, typically including an acid source, a carbonizing agent, a blowing agent, a binder, and additives [87]. Based on the composition of organic intumescent coatings, waterborne and solvent-based ICs have a dry film thickness (DFT) of only a few millimeters, making them suitable for protection against cellulosic fires common in building structures [88]. ICs can achieve thicknesses that are 10-25 times their DFT and are more appropriate for hydrocarbon fire conditions [89,90]. While thicker coatings improve fire protection performance, they may also complicate in-service inspection by masking underlying defects such as corrosion or cracking. When exposed to fire, ICs undergo a series of physical and chemical reactions, as shown in Figure 5-1. Initially heated, the acid source thermally decomposes, triggering the softening and melting of ICs into a viscous fluid (step B) [91]. This initiates dehydration and carbonization of the

carbonizing agent. Subsequently, the blowing agent absorbs heat and releases non-flammable gases, which are trapped within the viscous matrix, leading to a substantial expansion in thickness (step C). The resulting porous structure has low thermal conductivity and density. As heating continues, the expanded material gradually stabilizes into a black carbonaceous char layer (steps D and E). At higher temperature, the outermost char undergoes oxidation, gradually turning white and forming a fragile powdery foam (step F) [88,92]. These stages typically occur sequentially with increasing temperature but may also overlap. The activation temperature is generally from 100 °C (212 °F) to 250 °C (482 °F), depending on the formulation.

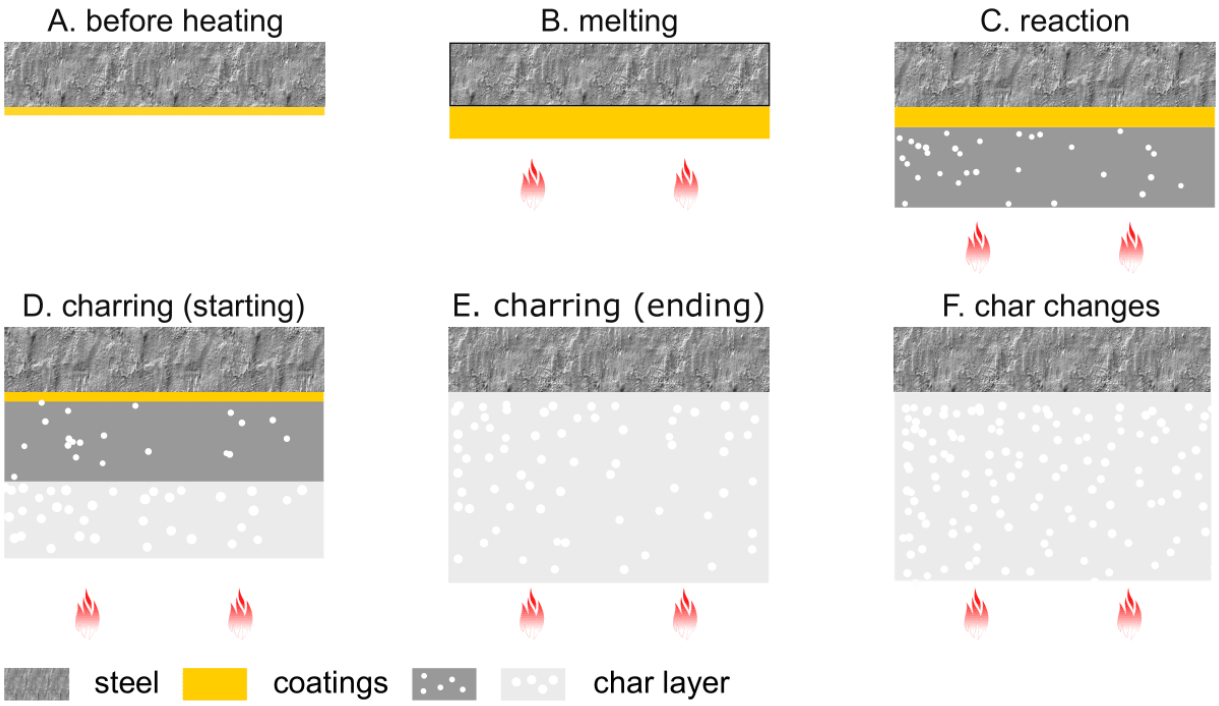

Source: S. Quiel, S. Ma, Lehigh University

Figure 5-1: Illustrations. Stages of intumescent coating transformation during fire exposure

At present, the fire performance of most intumescent coatings is certified based on standard fire curves such as International Organization for Standardization (ISO) 834[15] or ASTM E119[9], which are primarily intended for building fires. As mentioned in previous chapter, bridge fires often involve higher heat fluxes and more rapid heating rates and are commonly characterized by localized fire exposure in vehicle fire scenarios. Such non-uniform fire exposure may result in spatially discontinuous expansion of the coating, potentially compromising the overall fire protection of steel bridge components. In addition, ICs undergo significant physical structural evolution accompanied by complex chemical reactions during fire exposure, leading to highly nonlinear thermal and mechanical responses. These characteristics introduce considerable uncertainty in performance prediction, making it difficult to reliably assess fire protection effectiveness using simplified numerical approaches alone [93]. Systematic experimental data are generally required to support engineering evaluation and application, and the generation of reliable thermal response data for ICs is highlighted as a significant research need.

Despite its overall suitability for this application, the use of ICs for bridge structures still requires careful engineering consideration. Bridge structures are continuously exposed to outdoor environmental conditions, including precipitation, ultraviolet radiation, freeze–thaw cycles, and variations in temperature and humidity. These environmental actions may lead to cracking, aging, and degradation of adhesion of intumescent coatings, thereby reducing their fire protection effectiveness. Previous studies [94–96] have conducted evaluations of the performance of ICs considering aging effects; however, practical applications typically require periodic inspection, maintenance, and, when necessary, reapplication to ensure long-term protective performance. Other uncertainties remain regarding the applicability of existing fire-resistance certification of intumescent coatings to bridge fire scenarios.

It should be noted that thick fire-resistive coatings applied to steel bridge elements have the potential to impede routine in-service inspections of the substrate underneath, including welds, splices, connections, cavities, etc. There is also a need to address "special" inspection of any applied coatings. Though IC applications are generally durable, weather-resistant, and corrosion resistant, they also require periodic inspection to identify cracking, flaking, or other deterioration that would degrade their thermo-reactive response to provide full coverage to the bridge member in the event of a fire. Key components of an intumescent coating inspection for bridges include:

- Thickness Verification: Using gauges to verify dry film thickness complies with the required fire rating and manufacturer specifications.
- Visual Assessment: Checking for damage such as cracking, peeling, blistering, or delamination.
- Structural Integrity: Ensuring the coating has not experienced mechanical damage or corrosion, particularly in high-humidity or high-traffic areas.
- Environmental Exposure: Verifying those topcoats are intact to protect the intumescent layer from moisture and ultraviolet light damage, as required for outdoor applications.
- Repair Protocols: Promptly repairing damaged areas by cleaning and reapplying the paint to maintain the required fire resistance.

To enable more widespread implementation of ICs for bridges, more research is needed to determine not only the fatigue resistance of the ICs to weathering and repetitive mechanical loading but also to demonstrate the tools and procedures needed to conduct routine in-service inspections on the substrate surfaces.

5.2 Passive fire protection methods for concrete members

Concrete generally shows good fire resistance due to its favorable thermal properties, including low thermal conductivity and high heat capacity. For building structures, existing design codes provide minimum member dimensions and concrete cover thicknesses to the reinforcement in order to achieve the required fire-resistance ratings [45,46]. However, concrete is susceptible to spalling when exposed to fire, which can adversely affect structural performance in two major ways. It may lead to a reduction in the effective cross-sectional area, thereby compromising structural integrity. In addition, prestressing tendons or conventional reinforcing steel may be directly exposed to fire due to the loss of concrete cover, which accelerates their temperature rise and significantly reduces structural safety.

A primary focus of protection for concrete sections is the mitigation of thermal spalling mechanisms. Carlton et al. [97] investigated the use of passive protection materials like SFRM and ICs on concrete

members and reported that they can effectively reduce surface temperatures, thereby decreasing the likelihood of spalling via the buildup of pore pressure within the concrete during fire exposure. Mitigation of thermal spalling mechanisms requires measures that facilitate the release of internal vapor pressure. One effective approach is the incorporation of polypropylene (PP) fibers or other fibers in the concrete mix [98,99]. Due to their low melting temperature, these fibers melt during fire exposure and form small, interconnected pathways within the concrete, allowing vapor pressure to dissipate and thereby reducing the risk of spalling. Numerous experimental studies have demonstrated the effectiveness of PP fiber inclusion for mitigating thermal spalling in fire-exposed concrete structures [100–102]. However, it should be noted that after a significant fire exposure, concrete with PP fibers will have increased permeability and lower strength due to the removal of the fibers and the dehydration of the cement paste [103–105].

For bridge structures, the application of concrete overlays or sprayed concrete layers incorporating PP fibers may be explored as a potential fire mitigation measure. However, the incorporation of PP fibers can introduce additional cost while also impacting the performance and workability of a concrete mix design (particularly regarding slump and curing). Some of those impacts on the concrete performance may be beneficial, such as enhanced strength, durability, crack control, or shrinkage control [106,107]. More research is needed to determine the practical and holistic implications for the consideration of PP fibers for concrete bridge construction practice.

6 EXAMPLES OF STRUCTURAL-FIRE ANALYSIS

The examples presented in this chapter focus on a single main girder of a simply supported bridge. The results demonstrate how the fire performance of bridge structures can be evaluated using a two-dimensional thermo-structural coupled analysis. Two representative bridge types are considered as illustrative case studies:

- Example 1: I-type steel composite girder bridge
- Example 2: Bulb-T precast prestressed concrete girder bridge

As summarized in the Phase I report [2], most major bridge fire incidents in the United States over the past 20 years occurred beneath steel girder overpass bridges, where the main girders were directly exposed to fire. Unlike concrete, the high thermal conductivity of steel leads to a rapid increase in cross-section temperature during the early stage of fire exposure. Then a significant reduction in stiffness and strength may cause large increases in deformation, loss of load-carrying capacity, and possible buckling. Therefore, the primary focus is on the evolution of deflection and the time to reach failure, as governed by excessive deformation and instability.

For prestressed concrete bridges, particular attention should be paid to the temperature of the prestressing strands [7]. Owing to the relatively high heat capacity and low thermal conductivity of concrete, large temperature gradients may develop in the fire-exposed regions, while the temperature in the interior of the cross-section remains comparatively low. When no concrete spalling occurs and the concrete cover surrounding the prestressing strands remains intact, the primary concerns are the residual deflection, to assess whether post-fire serviceability requirements can still be satisfied. However, when spalling happens, the maximum temperature of the prestressing strands and the corresponding midspan deflection during the fire become the critical parameters, as they are indicative of rapid prestress degradation.

6.1 Fire scenarios and thermal boundary conditions

This subsection presents the first component of a structural-fire analysis and involves the following aspects:

- Fire scenarios
- Exposed boundary conditions

The selection of fire scenarios may follow two general approaches. A fire scenario can be considered by applying identical heating conditions along the entire bridge length, assuming that the fire acts uniformly in the longitudinal direction. In this case, the same gas temperature–time curve or equivalent heat flux history is applied on the exposed surfaces of all cross-sections. Such a case is commonly adopted for fire resistance design, comparison with furnace tests, and the evaluation of conservative envelope conditions. In contrast, a localized fire representation accounts for a fire source with a specific position, in which the thermal exposure is non-uniform along the bridge length. The resulting heat flux and gas temperature may vary with position due to factors such as wind effects, fire size, and the relative location of the burning vehicle. In the thermal analysis, this results in different cross-sections being subjected to different thermal boundary conditions. The corresponding fire modeling approaches and computational methods for deriving these non-uniform thermal inputs can be found in Chapters 2 and 3 of the Phase I report [2].

The assignment of exposed surface is also required (i.e., the identification of the external boundaries of the girder that are affected by fire), to which different thermal boundary conditions are prescribed in the numerical model. Figure 6-1 shows typical thermal boundary conditions for a girder section. In Figure 6-1(a), the entire bottom surface is subjected to fire exposure, the top surface is assigned the ambient temperature, and the two lateral surfaces are assumed to be adiabatic. This idealization is representative of fires caused by combustible materials stored beneath the bridge or by vehicles located directly under the girder, for which the primary thermal attack occurs from below. In Figure 6-1(b), only two sides of the cross-section are assumed to be exposed to fire, while the opposite side is assigned the ambient temperature. This configuration is applicable to scenarios in which the fire occurs in the vicinity of two sides of the bridge, such as a vehicle fire located near the edge of the bridge deck or in the adjacent roadside area. For fires occurring on the bridge or for more complex scenarios, the thermal boundary conditions should be defined according to the actual fire location and exposure configuration. A time–temperature curve or a time-dependent heat flux history should be prescribed for each heated boundary surface. Besides, appropriate values of parameters, like coefficient of convection on heated and unheated surfaces, and emissivity, which control the convective and radiative heat exchange between the girder and the surrounding environment, should be specified as input for the subsequent heat transfer analysis.

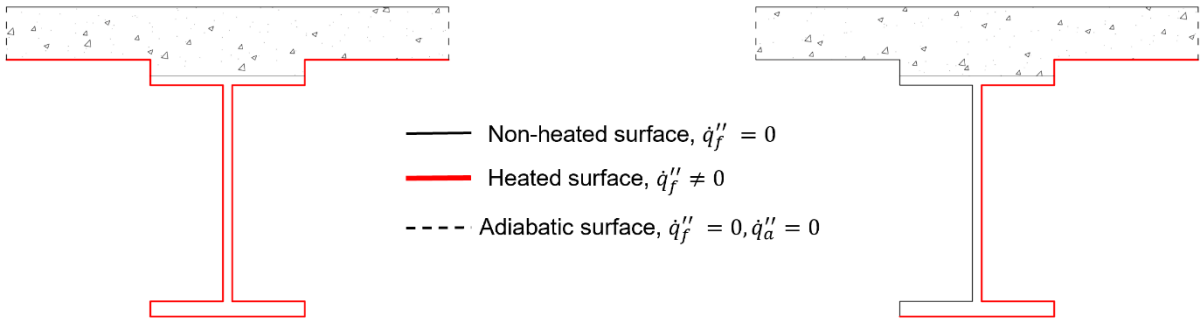

(a) Three-sided heating (b) Two-sided heating

Source: S. Quiel, S. Ma, Lehigh University

Figure 6-1: Illustrations. Representative thermal boundary conditions for steel composite girders under (a) three-sided (engulfed) and (b) two-sided (aside) fire exposure

By assuming uniform fire exposure along the entire bridge length, a single representative cross-section is sufficient to characterize the global thermal response of the girder. In the present example, the thermal input follows the ASTM E1529[13] [58] fire exposure curve, which represents the maximum thermal severity that structural members may experience when subjected to an open hydrocarbon pool fire. A surface temperature of 1,095 °C ± 85 °C (2,000 °F ± 185 °F) or an equivalent heat flux of 158 kW/m² ± 8 kW/m² is applied to the structural surface, and the specified temperature or heat flux level is reached within the first 5 minutes of fire exposure. In this example, the applied thermal load is assumed to remain constant at 158 kW/m² after the first 5 minutes of fire exposure. The time history of the prescribed heat flux acting on the surface of the bridge girder is shown in Figure 6-2(a). Per Eurocode 1[7] Part 1-2 [39], for hydrocarbon fire exposure, the convective heat transfer coefficients for the fire-exposed and unexposed surfaces are taken as 50 W/m²·K and 9 W/m²·K, respectively. The surface emissivity of both steel and concrete (ε_r) is assumed to be 0.7, while the emissivity of the hot gases (ε_e) is taken as 0.67 [108]. A Stefan-Boltzmann

constant of 5.67×10^{-8} W/(m²·K⁴) is adopted. The resultant emissivity, ε, calculated using the following equation [108], is equal to 0.52 for both the exposed and unexposed surfaces of the cross-section.

$$\varepsilon = \frac{1}{1/\varepsilon_e + 1/\varepsilon_r - 1} \tag{6-1}$$

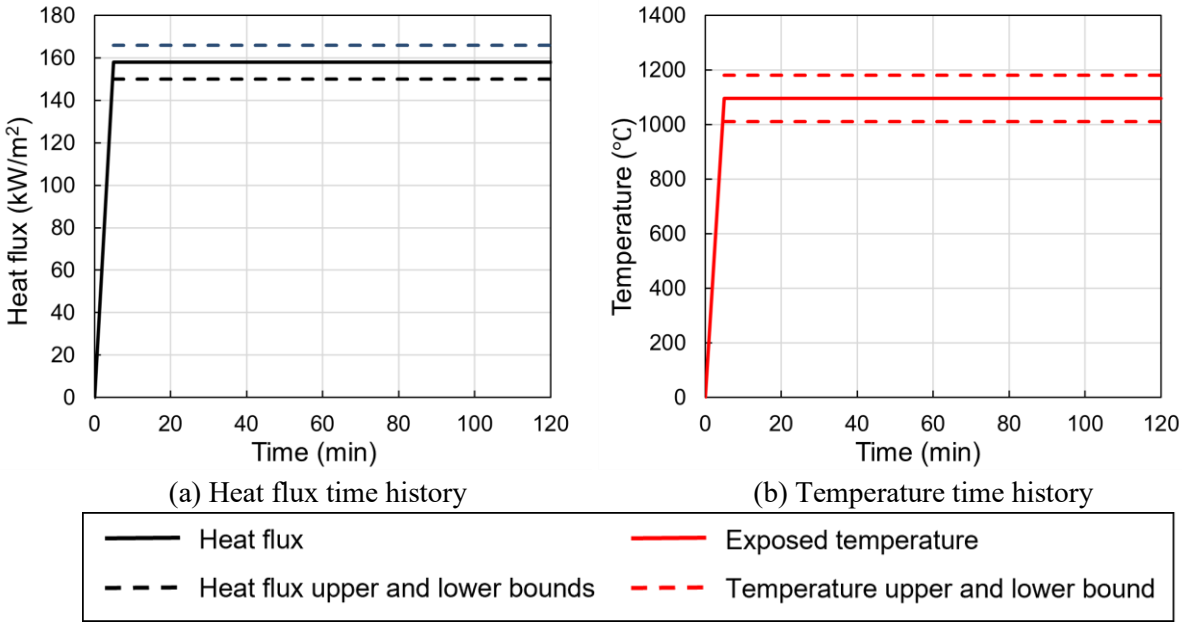

(a) Heat flux time history (b) Temperature time history

Source: Based on ASTM E1529[13]

Figure 6-2: Graphs. ASTM E1529[13] standard fire exposure time history: (a) heat flux, and (b) temperature

6.2 Example 1: I-type steel composite plate girder bridge

Due to the relative sensitivity of unprotected steel girders to fire, flexural failure or excessive deformation is likely to occur within a very short period of time. The application of fire protection materials to steel girders is often considered necessary in engineering practice. The fire performance of protective materials is typically evaluated in standardized furnaces, where classification is commonly based on the time required for the member cross-section to reach a specified average temperature or maximum temperature. This direct method provides a practical surrogate for fire-induced loss of load-carrying capacity, enabling standardized ratings and preliminary damage screening without requiring fully coupled thermo-structural analysis.

ASTM E119[9] [44] provides a standard time–temperature exposure for building construction assemblies, and associated acceptance criteria for assemblies incorporating steel beams/joists include limits on maximum and average steel temperature. For unrestrained assemblies with steel members spaced more than 1.2 m (4 ft) on center, the steel temperature is limited to a maximum of 704 °C (1,300 °F) at any location, and an average of 593 °C (1,100 °F) at any instrumented section (four thermocouples). For members spaced 1.2 m (4 ft) or less on center, only the average temperature recorded by all beam/joist thermocouples needs to be checked and is limited to 593 °C (1,100 °F).

ASTM E1529[13] [58] addresses structural members subjected to large hydrocarbon pool fires, which develop high heat fluxes and temperatures more rapidly than the ASTM E119[9] exposure and are therefore relevant to severe outdoor fire scenarios. In ASTM E1529[13], temperature-based acceptance criteria are also used in specific procedures (e.g., unloaded steel member configurations), including limits on average steel temperature (538 ℃ [1,000 ℉]) and on the maximum temperature recorded by any individual thermocouple (649 ℃ [1,200 ℉]) for the classification period.

Temperature limits of this type are attractive for screening because they are straightforward to apply once member temperatures are estimated (from analysis or instrumentation), and the criteria themselves are not parameterized by member length or span. However, the structural implications of a given peak steel temperature depend on system behavior (restraint conditions, redundancy, composite action, connections/bearings) and on temperature-dependent degradation of steel stiffness and strength, which becomes significant at elevated temperatures (commonly beyond approximately 400 °C [792 °F]) and can be severe by approximately 600 to 700 °C (1,112 to 1,292 °F). Consequently, temperature thresholds adopted for bridge applications should be explicitly linked to bridge performance measures and damage states.

In the final report from Phase I of this study [2], peak girder temperatures of 649 °C (1,200 °F) and 400 °C (752 °F) were used to delineate bridge fire response zones; however, the physical interpretation of these thresholds in terms of bridge performance and damage state was not explicitly established. This study first conducts deterministic thermo-structural analyses of a representative steel girder bridge section to illustrate the modeling and analysis procedures and to examine bridge response under fire exposure. Comparisons are performed between unprotected girders and girders with fire protection materials to quantify changes in the critical steel temperatures associated with bridge damage level. Building on the deterministic framework, the study then extends the analysis to account for uncertainties in applied loads, fire exposure conditions (heating boundary conditions), and temperature-dependent thermal and mechanical material properties. These uncertainties are propagated through the thermo-structural response to evaluate the reliability of temperature-based damage indicators and their linkage to bridge performance metrics and damage states.

For conservatism and for consistency with standardized furnace-type acceptance concepts, the baseline analyses neglect fire localization and apply a uniform heating intensity along the full bridge length. While this assumption likely overestimates global thermal demand relative to localized fire scenarios, it provides an upper-bound assessment and supports direct interpretation of results within a temperature-threshold framework. The resulting calibrated thresholds can be used to produce defensible temperature-based indicators for steel girder damage states to support post-fire evaluation and decision-making.

The prototype highway steel girder bridge used for the design fire load fragility analysis is considered to carry three lanes and consists of five simply supported steel girders. Three bridge spans are selected as the representatives: 24.4 m (80 ft), 30.5 m (100 ft) and 36.6 m (120 ft). The size of the girder is designed using eSPAN140 [109], a free web-based tool developed by Short Span Steel Bridge Alliance for the preliminary design of simple-span and modular steel girder bridges, based on the principle of cost-effectiveness. The detailed sizes of the girders are summarized in Table 6-1. A typical cross-section is shown in Figure 6-3. The deck thickness is taken as 203 mm (8 in.), with #6 reinforcing bars spaced at 457 mm (18 in.). The haunch is not considered in the present analysis. The concrete deck has a nominal strength of 39.4 MPa

(5.7 ksi), and tensile capacity is conservatively neglected. The steel girder meets ASTM A709[16] Grade 50W [110], and reinforcement complies with ASTM A615[17] Grade 60 [111].

The dead load (*DL*) accounts for the self-weight of the composite girder and deck. Live load (*LL*) is conservatively represented using the 9.3 kN/m (640 plf) uniform longitudinal load for each 3.050-m (10-ft) lane width in accordance with the AASHTO Bridge Design Specification[2] [8], resulting in a total of 5.6 kN/m (384 plf) for each girder.

Table 6-1: Plate girder designs for the simply supported prototype bridge per eSPAN140 as a function of span

Span length	24.4 m (80 ft)	30.5 m (100 ft)	36.6 m (120 ft)
Web (mm [in.])	813 × 12.7 (32 × 0.5)	1016 × 12.7 (40 × 0.5)	1245 × 12.7 (49 × 0.5)
Top flange (mm [in.])	406 × 25.4 (16 × 1.0)	457 × 19.1 (18 × 0.75)	457 × 25.4 (18 × 1.0)
Bottom flange (mm [in.])	406 × 38.1 (16 × 1.5)	457 × 50.8 (18 × 2.0)	508 × 50.8 (20 × 2.0)
Depth/Span ratio	0.0360	0.0356	0.0361
Total dead load (kN/m [klf])	25.08 (1.72)	25.81 (1.77)	26.44 (1.81)
Live load (kN/m [klf])	5.6 (0.38)	5.6 (0.38)	5.6 (0.38)

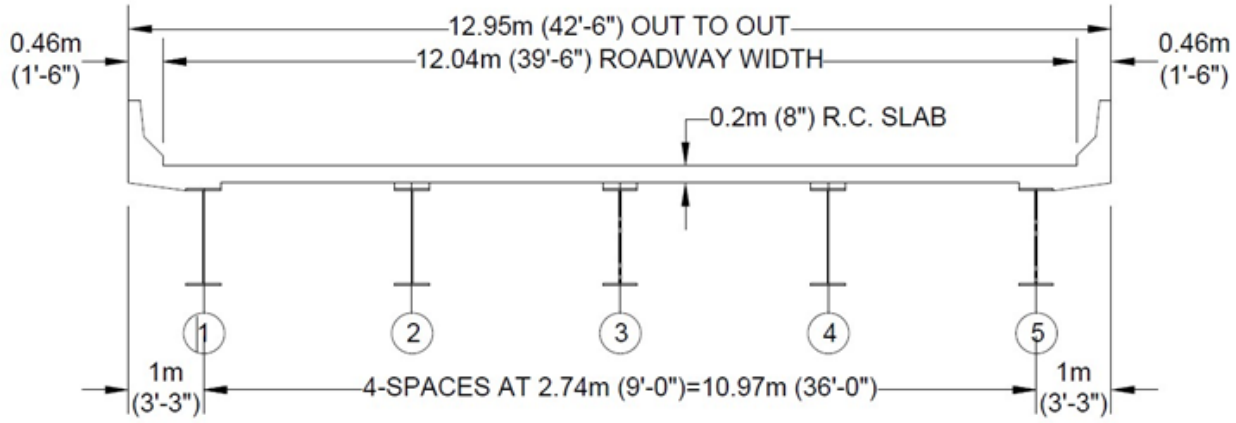

Source: eSPAN 140

Figure 6-3: Typical cross section of steel composite bridge girder

Fire is considered an extreme load scenario, and a load combination with reduced live load is therefore utilized for this evaluation. Though there is no prescribed load combination for the structural-fire analysis of bridges in US practice, several previous studies [65,81] have established $DL + 0.3LL$ as a combination that is consistent with the guidelines in Eurocode 1[7] Part 1-2 [39] for structural-fire analysis. For analysis of the steel girders in this study, a load combination of $1.05DL + 0.3LL$ is used to account for additional

[16] Use of ASTM A709, Standard Specification for Structural Steel for Bridges, is not a Federal requirement.
[17] Use of ASTM A615, Standard Specification for Deformed and Plain Carbon-Steel Bars for Concrete Reinforcement, is not a Federal requirement.

dead load of bracing, stiffeners, etc. These loads are applied as a constant distributed force along the length of the girders during the structural-fire evaluation, during which the full effects of fire exposure are also applied to the structural elements as a time history from ignition to burnout. Other load combinations that include wind, seismic, snow, rain, etc., are not considered to be likely during a severe fire event, and these loads are, therefore, not considered for this study.

6.2.1 Deterministic FE analysis

A deterministic thermo-structural analysis is first conducted for a 30.5-m (100-ft) steel girder. Table 6-2 summarizes the analysis cases considered in this part. Four fire protection configurations are considered: unprotected, and SFRM thicknesses of 12.7 mm (0.5 in.), 25.4 mm (1 in.), and 38.1 mm (1.5 in.). Two heating boundary conditions are examined, three-sided heating and two-sided heating. The girder is subjected to the ASTM E1529[13] fire curve and heated until failure, determined as a midspan deflection limit of $L/20$ (extracted from the analysis at the bottom flange centroid).

In SAFIR, the thermal properties of SFRM are implemented using the material model SFRM_PROBA, while the mechanical properties are neglected in the structural analysis due to the low strength of the material. The probabilistic thermal properties implemented in SFRM_PROBA are adopted from the material model proposed by Khorasani et al. [112], which was calibrated using experimental data from a NIST study on three SFRMs. For this example, the standard normal parameter ε is set to zero to represent the mean value of properties of a generic SFRM material. Table 6-3 shows material model names used in SAFIR analysis and their reference.

Table 6-2: Summary of deterministic analysis cases

Case Name	Heating boundary	SFRM thickness (in.)
Three-0	Three sides	0
Two-0	Two sides	0
Three -0.5	Three sides	0.5
Two-0.5	Two sides	0.5
Three -1	Three sides	1
Two-1	Two sides	1
Three -1.5	Three sides	1.5
Two-1.5	Two sides	1.5

Table 6-3: Material models and references

Analysis type	Model name in SAFIR	Reference
Concrete	SILCON_ETC	Eurocode 2[12] Part 1-2 [47]
Rebar	STEELEC2EN	Eurocode 2[12] Part 1-2 [47]
Girder steel (thermal analysis)	STEELEC3	Eurocode 3[5] Part 1-2 [37]
Girder steel (structural analysis)	STEELSL	Franssen et al. [113]

Figure 6-4 shows the temperature distributions for the steel girder cross section with and without SFRM protection after one hour of fire exposure. For the unprotected case, the maximum steel temperature reaches approximately 1,000 °C (1,832 °F) under both three-sided heating and two-sided heating conditions. When

a 25.4-mm (1-in.) thick SFRM layer is applied, the temperatures in the web are significantly reduced, to approximately 650 °C (1,202 °F) for three-sided heating and about 400 °C (752 °F) for two-sided heating. Without SFRM, two-sided heating shows in pronounced temperature gradients within the steel section, particularly in the top flange. By contrast, the application of SFRM substantially mitigates these temperature gradients across the cross section, which may help mitigate thermally induced bending effects and promote a more uniform degradation of sectional stiffness and strength.

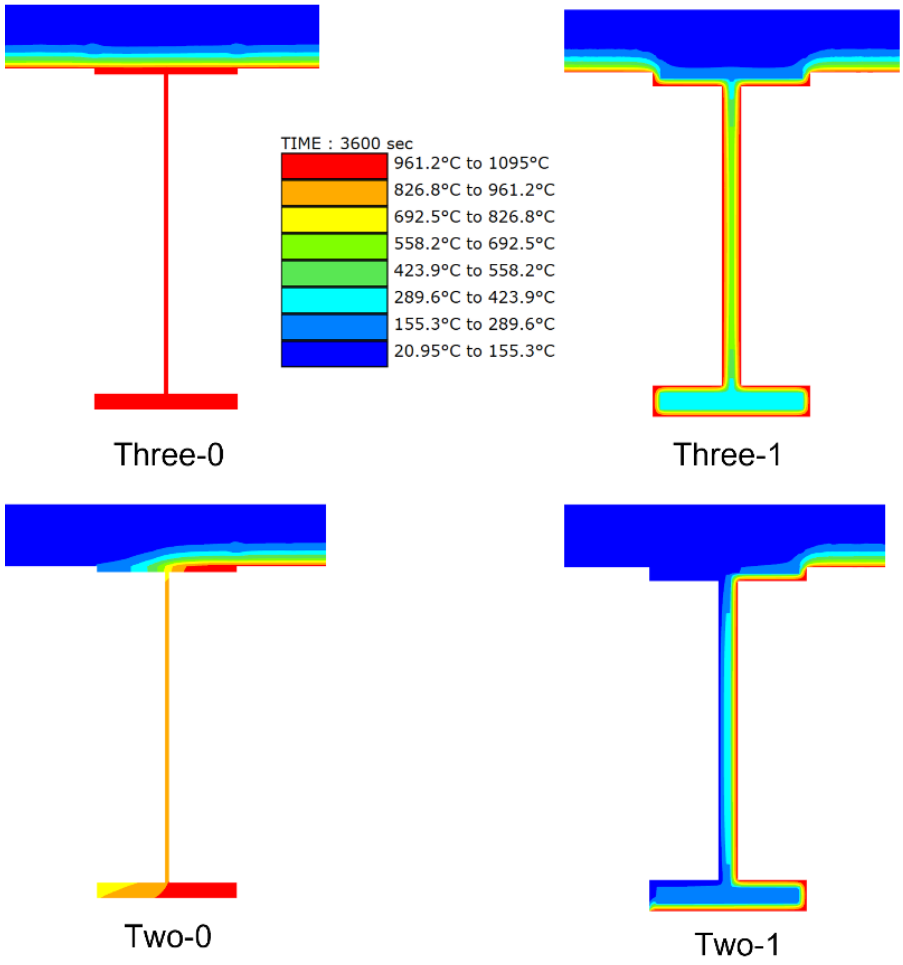

Source: S. Quiel, S. Ma, Lehigh University

Figure 6-4: Illustrations. Thermal analysis results demonstrating SFRM effectiveness for mitigating the cross-sectional temperature increase of a composite steel girder

Based on the results presented in Table 6-4 and Figure 6-5, the failure temperatures corresponding to different SFRM thicknesses under three-sided heating conditions are relatively close and exhibit a consistent trend. The failure temperature of the steel cross section decreases slightly as the SFRM thickness increases. This indicates that the resulting temperature-based failure thresholds become increasingly conservative and safety-oriented with thicker fire protection. Nevertheless, to ensure the robustness of these observations, it is still necessary to account for various sources of uncertainty and to repeat the analysis within a probabilistic framework.

Table 6-4: Summary of failure times and steel temperatures for deterministic fire analysis cases

Case Name	Time to reach *L/20* deflection (minutes)	Maximum steel temperature, °C (°F)	Average steel temperature, °C (°F)
Three-0	11	1,067 (1,952)	755 (1,391)
Two-0	18	909 (1,668)	690 (1,275)
Three-0.5	83	1,032 (1,890)	701 (1,294)
Two-0.5	140	752 (1,385)	617 (1,142)
Three-1	158	1,010 (1,850)	682 (1,259)
Two-1	265	734 (1,353)	602 (1,116)
Three-1.5	235	981 (1,797)	666 (1,232)
Two-1.5	399	726 (1,338)	594 (1,102)

Note: The average steel temperature is computed as an area-weighted average over all discretized steel finite elements in the cross-section. The temperature of each element is taken as the average of its nodal temperatures.

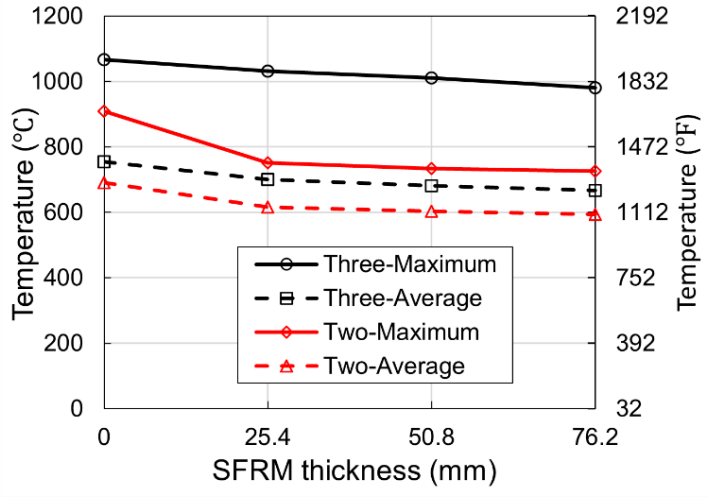

Source: S. Quiel, S. Ma, Lehigh University

Figure 6-5: Graph. Relationship between steel temperature at flexural failure and SFRM thickness under different heating cases

6.2.2 Stochastic FE analysis

The uncertainties of inputs considered in the stochastic analysis include the thermal and mechanical properties of the steel material; gravity load; and thermal input in terms of heat flux applied to the structure. The distribution, mean and standard deviation of the input parameters used in the following sampling process are summarized in Table 6-5. The total load for each analysis iteration is calculated per Eq. (6-2):

$$P = E(A \cdot 1.05DL + B \cdot 0.3LL) \tag{6-2}$$

where A and B reflect the uncertainties in the translation of load into the load effects, and E represents the uncertainties in the structure analysis [114]. The probabilistic temperature-dependent reduction factor of the yield strength of hot rolled steel adopts the model proposed by Khorasani et al. [112]:

$$k_{y,T} = \frac{1.7 \times exp\,[r_{logit} + 0.412 - 0.81 \times 10^{-3} \times T + 0.58 \times 10^{-6} \times T^{1.9} + 0.43 \times \varepsilon_k]}{1 + exp\,[r_{logit} + 0.412 - 0.81 \times 10^{-3} \times T + 0.58 \times 10^{-6} \times T^{1.9} + 0.43 \times \varepsilon_k]} \quad (6\text{-}3)$$

$$r_{logit} = \ln \frac{(k_{y,EN,T} + 10^{-6})/1.7}{1 - (k_{y,EN,T} + 10^{-6})/1.7} \quad (6\text{-}4)$$

where $k_{y,EN,T}$ is the reduction factor of nominal yield strength at temperature T(°(C) according to Eurocode 3[5] Part 1-2 [37]. The concrete strength is sampled from a lognormal distribution per Holicky and Sykora [115]. The stress-strain relationships and material reduction factors for concrete and the steel reinforcement at elevated temperature are considered to be deterministic per Eurocode 2[12] Part 1-2 [47].

Table 6-5: Input parameters for stochastic analysis

Variable category	Variable Type	Description	Unit	Distribution	Mean Value	COV
Thermal load	Independent	Heat flux	kW/m^2	Uniform	85	-
Thermal load	Independent	Exposure Duration	min	Deterministic	90	-
Gravity load	Independent	DL	kN/m	Normal	specific to section type	0.1
Gravity load	Independent	LL	kN/m	Gamma[a]	9.34	0.6[b]
Gravity load	Independent	E in Eq. (6-2)	-	Normal	1.00	0.04
Gravity load	Independent	A in Eq. (6-2)	-	Normal	1.00	0.20
Gravity load	Independent	B in Eq. (6-2)	-	Normal	1.00	0.05
Steel material properties	Independent	ε_k in Eq. (6-3)	-	Normal	0.00	1.00
Ambient concrete strength	Independent	f_c'	MPa	Lognormal	39.40	0.15

Notes:
a: The live load (LL) is modeled using a gamma distribution with a coefficient of variation (COV) of 0.6 per Zhu et al. [116]*, based on a previous study by Gernay et al.* [117].
b: The relatively large COV is intentionally adopted to induce a wider range of load effects and corresponding M/M_n ratios in the stochastic structural-fire analysis, rather than to represent typical traffic load statistics.

The stochastic input parameters for the fire model and thermo-structural analysis are sampled via Monte Carlo simulation (MCS), with Latin hypercube sampling (LHS) [118] utilized for increased efficiency. The LHS technique reduces the number of simulations that are needed for stochastic analysis of multidimensional problems while maintaining the probabilistic quality of the results versus purely random sampling via traditional MCS [119]. For bridge models of each span length and each heating condition (i.e., three-sided heating vs. two-sided heating), 500 cases are generated with inputs listed in Table 6-5. For each specific case, the thermal structure analysis is performed with SAFIR 2022.

The damage of a bridge subjected to fire hazard is categorized into three classes corresponds to the post-fire actions, per the experience from the author's past work sponsored by PennDOT: The damage of a bridge subjected to fire hazard is categorized into three classes corresponds to the post-fire actions, which have been adapted from recent bridge fire projects for PennDOT [15,19]:

- **SUPERFICIAL**: Maximum residual deflection increment is less than L/800, which equals to the vehicular load induced deflection per AASHTO[2] [8]. A small amount of permanent deformation

has occurred, potentially requiring small amounts of repair, such as heat straightening, with the entire bridge remaining reusable.

- **MODERATE**: Maximum residual deflection increment is over *L*/800, while the maximum deflection during the fire is less than *L*/20 (i.e., the critical deflection limit per BS 476-10[12] [69]). The bridge has suffered permanent deformation but collapse has not occurred during or after the fire hazard.
- **HAZARDOUS**: Maximum deflection during the fire is over *L/20* or thermal structure analysis cannot converge due to large deflections or the development of large strains that cause critical material failure. This damage state indicates that the bridge is at or near the onset of flexural collapse and does not achieve a stable residual state.

The outcomes of all simulated cases are plotted in Figure 6-6 as a function of (i) the midspan moment capacity ratio, calculated as the applied midspan moment divided by the room-temperature composite girder moment capacity ($M_{mid}/M_{n,20°C}$), which represents the state of flexural loading, and (ii) the peak steel temperature attained during the heating history. The results are classified according to the damage-state definitions and show distinct transition regions between each state. In general, increasing load demand shifts the transition to a slightly lower temperature, indicating that higher utilization slightly reduces the thermal margin to a given damage state. Because this shift is modest over the range examined, a single (load-independent) temperature threshold provides an adequate and practical basis for damage classification.

In Figure 6-6, the green and red dashed lines denote 95% confidence classification boundaries, i.e., thresholds chosen such that only 5% of cases exhibiting a higher damage state would be misclassified into a lower damage state. Based on Figure 6-6(a), using average steel girder temperature as the indicator, the mean thresholds corresponding to the onset of moderate and hazardous damage are 451 °C (844 °F) and 589 °C (1,092 °F), respectively. When maximum steel temperature is used per Figure 6-6(b), the corresponding thresholds increase to 572 °C (1,062 °F) and 743 °C (1,369 °F).

These thresholds are compared with the temperature-based acceptance criteria in ASTM E1529[13] and ASTM E119[9] in Table 6-6. The thermo-structural analyses indicate that the average-temperature threshold associated with hazardous damage is close to the ASTM E119[9] limit, and higher than the ASTM E1529[13] limit. Therefore, adopting the ASTM E1529[13] average-temperature criterion as the critical threshold for bridge damage classification would be conservative (i.e., it would tend to classify damage at lower temperatures than those associated with hazardous response in the simulations). For the maximum-temperature indicator, the limits provided in both ASTM E119[9] and ASTM E1529[13] fall below the simulated hazardous-damage threshold and are therefore conservative.

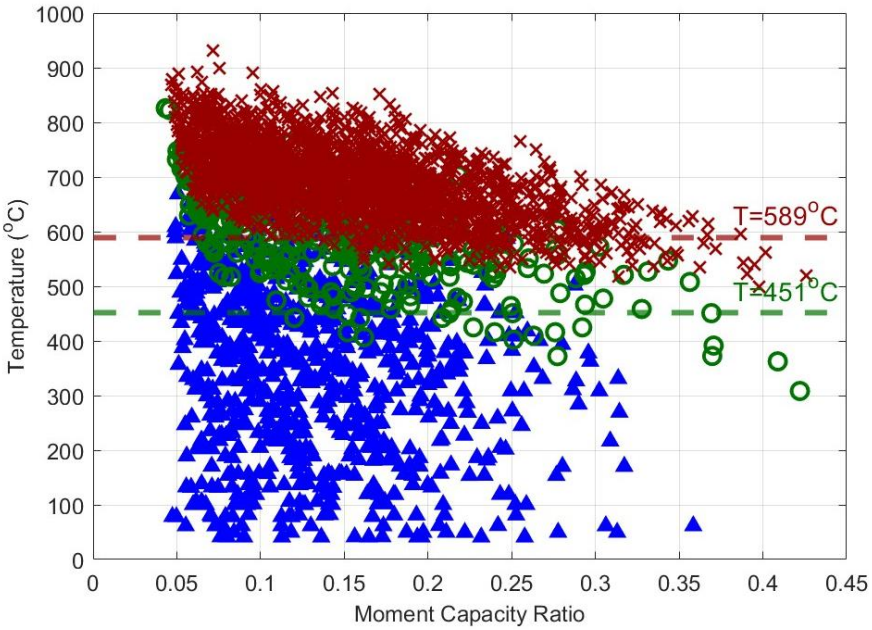

(a) Average temperature

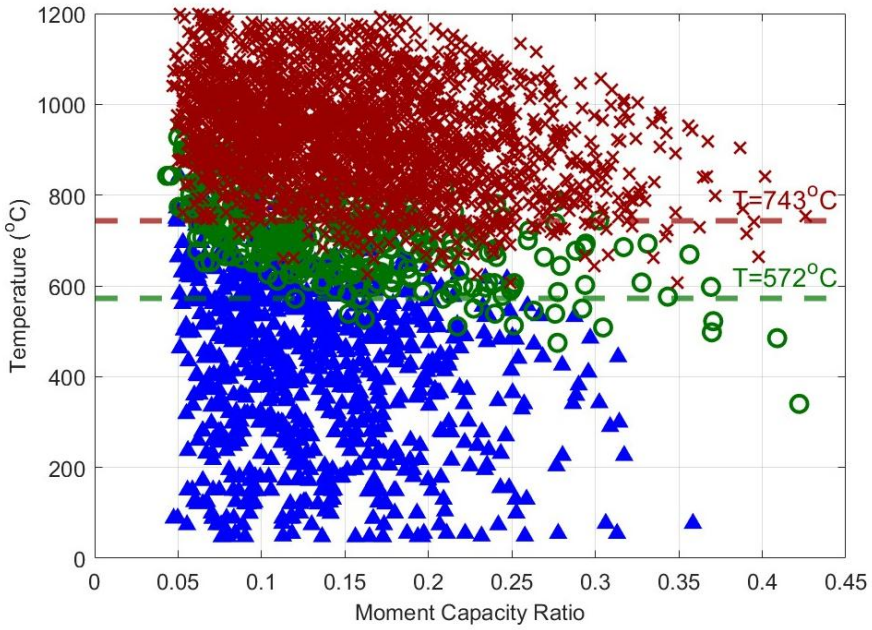

(b) Maximum temperature

Source: S. Quiel, S. Ma, Z. Zhu, Lehigh University

Figure 6-6: Graphs. Damage levels reached during stochastic FE analyses as a function of either (a) average or (b) maximum steel temperature for the steel composite girder

Table 6-6: Comparison of critical temperature thresholds to evaluate flexural performance

Source	Parameter	Average Temp., °C (°F)	Maximum Temp., °C (°F)
Thermo-structural analysis	Superficial–Moderate	451 (844)	572 (1,062)
Thermo-structural analysis	Moderate–Hazardous	589 (1,092)	743 (1,369)
ASTM E119[9]	Temperature Increase Limit	593 (1,100)	704 (1,300)
ASTM E1529[13]	Temperature Increase Limit	538 (1,000)	649 (1,200)

6.2.3 Lumped mass analysis for critical temperatures

In the preceding sections, detailed thermo-structural analyses were conducted to establish critical temperature thresholds corresponding to various levels of structural damage. However, the determination of steel temperatures under fire exposure generally requires cross-sectional thermal analysis, typically performed using 2D or 3D finite element methods. Although these methods provide detailed temperature distributions, they rely on specialized software and are computationally intensive. For I-shaped steel bridge girders, structural response can often be adequately characterized by a representative steel temperature, without explicitly resolving full temperature gradients. Therefore, a simplified thermal analysis framework based on lumped mass assumptions is adopted in this study.

In the heat-transfer analysis, the temperature at the fire-exposed surface of the insulation layer is conservatively assumed to be equal to the fire (gas) temperature [37]. In Section 3.1, the equations required for the lumped mass calculation have already been presented. For the calculation of steel sections with insulation, when the incident heat flux is known, it must first be converted into an equivalent exposure temperature using the following equation:

$$T_{f,t} = \left(\frac{\dot{q}''_{f,t}}{\sigma \varepsilon_f}\right)^{1/4} - 273 \tag{6-5}$$

where ε_f is the resultant emissivity for incoming radiation heat energy. The practical value of ε_f for this application can be determined based on the relationship between heat flux and temperature observed in standard hydrocarbon pool fire tests. Recall that according to ASTM E1529[13] [58], exposure to a hydrocarbon pool fire can be represented by either an average total heat flux of 158 kW/m² ± 8 kW/m² or an equivalent exposure temperature of 1,095 °C ± 85 °C. Here, ε_f is taken as 0.8, so that an equivalent exposure temperature of 1,093 °C (2,000 °F) is acquired. Figure 6-7 compares the steel temperatures predicted using the incident heat flux input and the gas temperature input for the ASTM E1529[13] fire exposure. The temperatures predicted using the incident heat flux input are close to those obtained using the gas temperature input for both lumped mass method and SAFIR analysis.

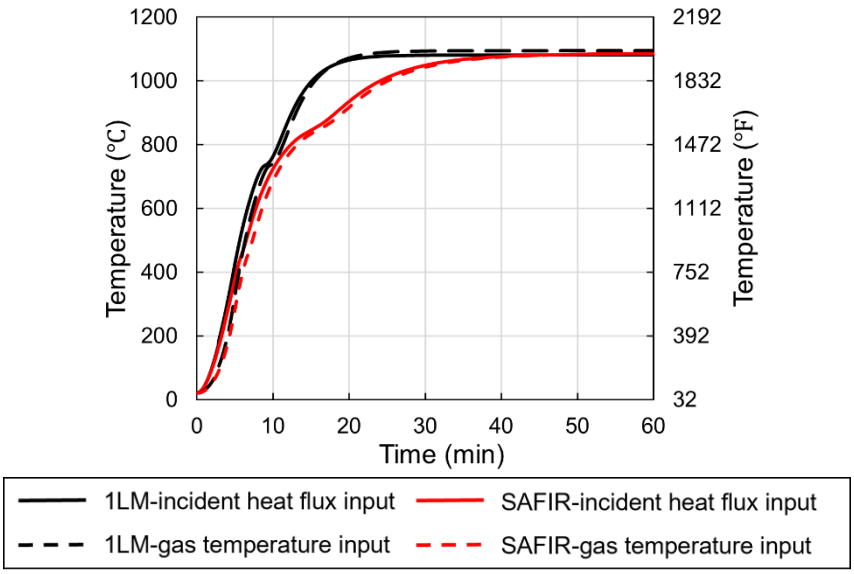

Source: S. Quiel, S. Ma, Lehigh University

Figure 6-7: Graphs. Comparison of steel temperature predictions with incident heat flux input and gas temperature input for ASTM E1529[13] fire exposure (unprotected section, three-sided heating).

Figure 6-8 compares the one-lumped-mass (1LM) predictions with the SAFIR results under the ASTM E1529[13] fire and the simplified design fire curve from Section 5.5 of the Phase I report [2] (the case with an incident heat flux of 170 kW/m² is adopted here). Since both scenarios represent severe fire exposures, it is reasonable to assume that the girder is engulfed by the fire, i.e., three-sided heating. For the unprotected case, the 1LM and SAFIR results agree well below 800 °C (1,472 °F). The discrepancy observed between 800 °C and 1,100 °C (1,472 °F and 1,832 °F) is attributed to the phase transformation of steel near 735 °C (1,355 °F). In the SAFIR, the phase transformation occurs progressively across the section due to the temperature gradient, whereas in the lumped-mass model the transformation is assumed to occur instantaneously throughout the cross-section. The times corresponding to the two threshold temperatures are predicted consistently by the 1LM method and SAFIR. The presence of the concrete slab in the SAFIR model has a minor influence on the results for these severe fire scenarios. Thus, for severe fire exposure, neglecting the concrete slab and considering only the steel girder is acceptable.

When passive fire protection is applied, the results from the 1LM method and SAFIR still show good agreement. A 25.4-mm (1-inch) SFRM layer approximately corresponds to a 2-hour fire rating under the ASTM E1529[13] fire when the concrete slab is considered, which is associated with the “Hazardous damage” performance level. Due to the presence of the protection layer, the steel temperature increases more slowly and the overall heating process becomes longer. During heating, the presence of the concrete slab begins to influence the analysis, since there is more time for heat transfer between the steel and the slab. For protected sections under three-sided heating, the primary temperature gradient occurs from the bottom flange to the web and then to the top flange.

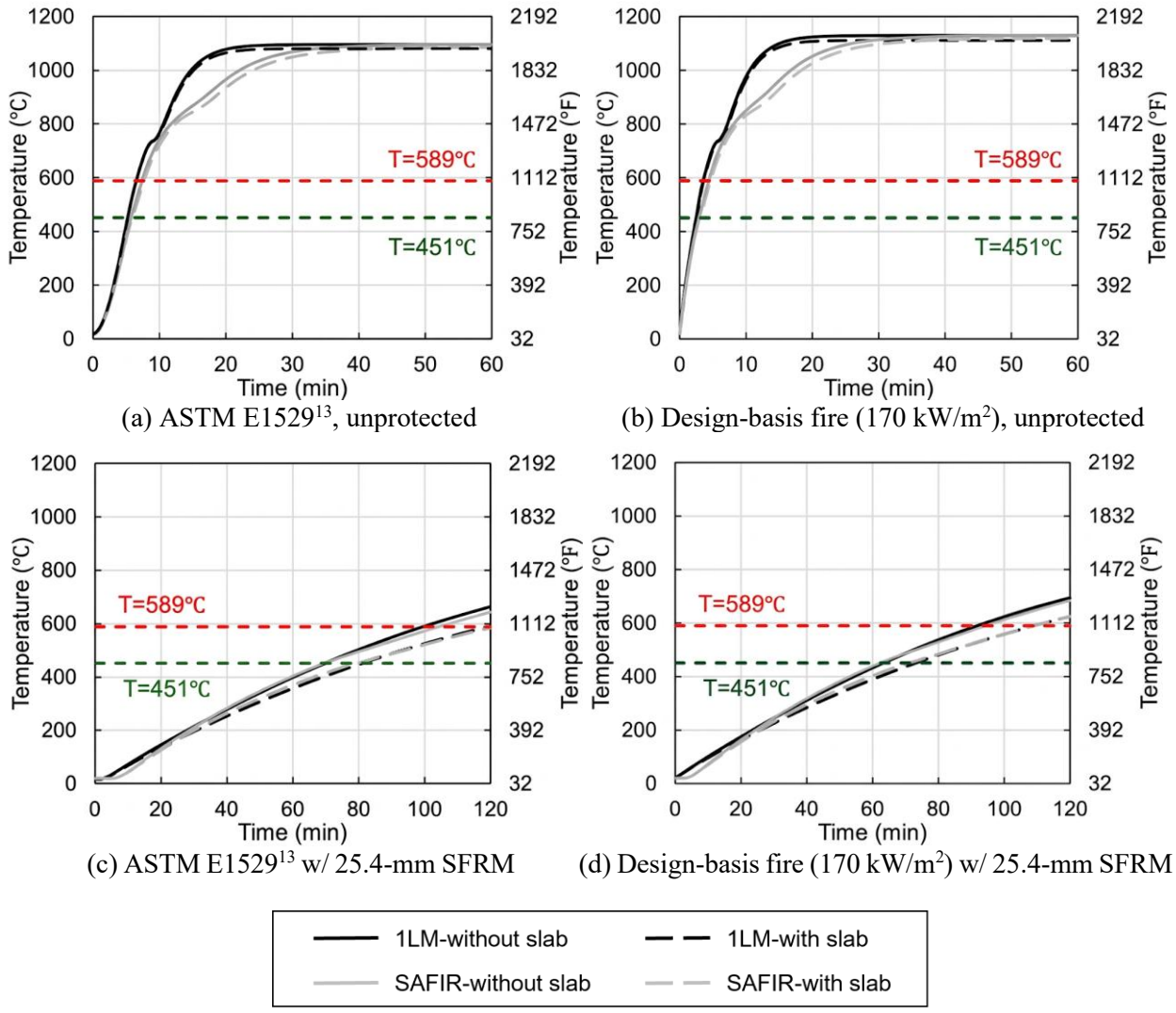

Source: S. Quiel, S. Ma, Lehigh University

Figure 6-8: Graphs. Comparison of steel girder average temperature predicted by the 1LM method and SAFIR under severe fire exposure with three-sided heating

Using the design-basis fire equation provided in Section 5.5 of the Phase I report [2], together with the method described earlier in this section, a simplified calculation was performed to estimate the time required for the this 30.5-m (100-ft) bridge to reach the two temperature thresholds at different standoff distances. A vertical clearance of 4.57 m (15 ft) was assumed. For this clearance, when the standoff distance is less than 2 m (6.5 ft), the incident heat flux is taken as 170 kW/m². The standoff distance is then increased from 0 m (0 ft) onward until the incident heat flux becomes sufficiently small such that even superficial damage to the bridge would not occur. For a standoff distance of 0 m (0 ft), the steel girder is assumed to be subjected to three-sided heating. When the standoff distance exceeds 2 m (6.5 ft), a two-sided heating condition is assumed. For consistency in the comparison, the convective heat transfer coefficient is assumed to be 25 W/m²·K for the exposed surfaces and 9 W/m²·K for the unexposed surfaces. The results are summarized in Table 6-7. When the standoff distance exceeds approximately 6.5 m (21.3 ft), the heat flux

estimated using the simplified design fire equations in Section 5.5 of the Phase I report [2] does not cause significant damage to the bridge.

Table 6-7: Time to reach damage thresholds at different standoff distances

Standoff (m)	Incident heat flux (kW/m^2)	Superficial–Moderate transition time (min)	Moderate–Hazardous transition time (min)
0.0	170	2.4	3.6
2.0	170	4.5	6.7
2.5	134	5.8	8.8
3.0	125	6.3	9.7
3.5	115	6.9	10.8
4.0	104	7.8	12.3
4.5	93	9.0	14.4
5.0	81	10.7	17.9
5.5	68	13.4	24.4
6.0	55	18.4	45.6
6.5	41	31.4	Does not reach threshold

The calculations presented here can be considered conservative, as the fire is assumed to be at its peak intensity from the beginning, without considering the fire growth phase. Additionally, the incident heat flux is assumed to be uniform over the entire bridge cross-section, when in reality, it would vary spatially when exposed to a realistic localized fire [15,19]. The results of these calculations can be utilized by engineers (for design or planning purposes) or by emergency responders (during an active response) to estimate the onset time for each damage threshold for fires located at varying locations relative to the bridge's structural elements. Figure 6-9 shows the average steel girder temperature histories predicted by the 1LM method and SAFIR at standoff distances of 3 m (9.8 ft) and 6 m (19.7 ft). Relatively good agreement between the two methods can be observed in both cases. At a standoff of 3 m (9.8 ft), the steel temperature can still quickly exceed the 451 °C (844 °F) and 589 °C (1,092 °F) thresholds, However, when the standoff distance increases to 6 m (19.7 ft), the fire intensity rapidly decreases, and the temperature rise becomes much slower and only approaches the higher temperature threshold.

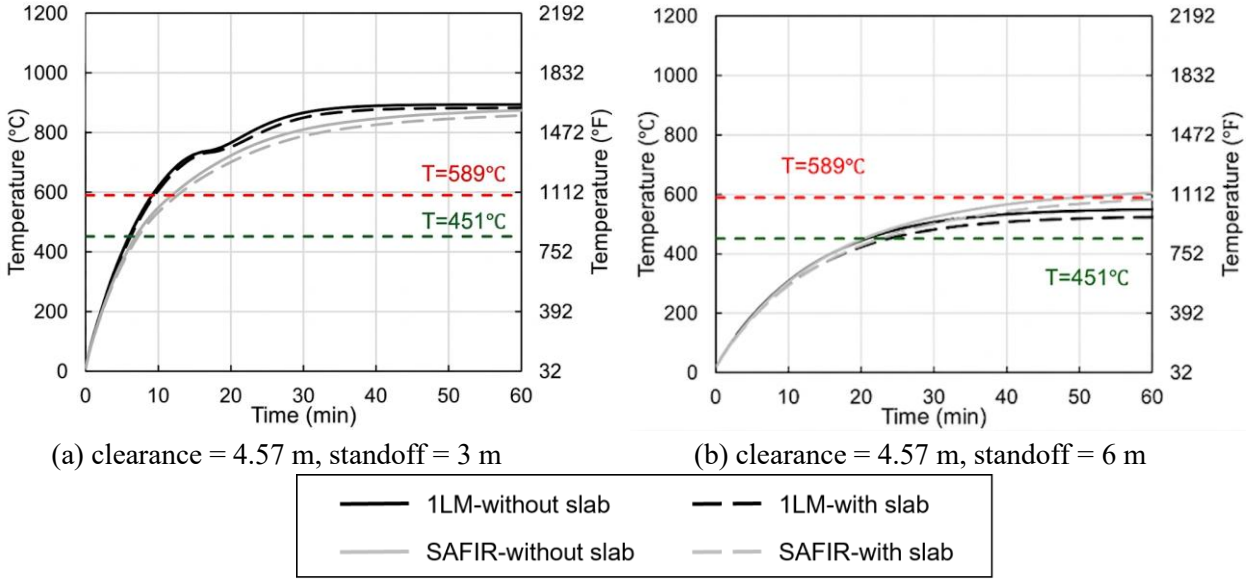

(a) clearance = 4.57 m, standoff = 3 m (b) clearance = 4.57 m, standoff = 6 m

Source: S. Quiel, S. Ma, Lehigh University

Figure 6-9: Graphs. Comparison of unprotected steel girder average temperature predicted by the 1LM method and SAFIR at different standoff with two-sided heating

6.3 Example 2: Precast prestressed concrete bulb-T girder bridge

Previous work [7] on this type of bridge has indicated that the collapse mode was governed by flexural failure, resulting from the combined effects of concrete cover spalling and heating of the prestressing strands. However, the duration of fire exposure may be reduced by emergency response and fire suppression, and concrete spalling can be mitigated by appropriate material and protective strategies. Therefore, in cases where collapse does not occur, the post-fire residual status of the bridges deserves careful evaluation.

The thermo-structural response will be evaluated for exposure to several fire scenarios. The baseline fire exposure considered for this analysis is the ASTM E1529[13] hydrocarbon curve. The exposure either continues until the girder has reached a flexural failure, or the fire is terminated at a predetermined time of burnout, at which time the temperature time history immediately returns to ambient temperature. The burnout approximation is implemented in order to evaluate the residual deflected state in the event that the girder survives the duration of the fire. The key parameters under consideration relate to bridge span and spalling. For the spalling case, the primary objective is to determine the time to structural failure under rapid temperature rise associated with hydrocarbon fires. For the non-spalling case, the residual deflection of the girder is evaluated after a specified fire duration to quantify the post-fire performance.

The example span from a recent bridge construction project consists of multiple girders with varying span lengths but similar cross-sectional configurations. The plan details, girder layout, and bridge cross section are shown in Figure 6-10. The span consists of a total of nine bulb-T girders with a uniform spacing of 2.7 m (8 feet, 10 ⅞ inches) on center. The span lengths of the nine girders vary from 13.8 m (45 feet, 4 ¾ inches) to 33.2 m (108 feet, 11 ⅝ inches). Among them, Beams 1, 5, 6, and 9 were selected for analysis. The calculation length for each beam was taken as the bearing-to-bearing distance, equal to 12.9 m (42 feet, 3

¾ inches), 22.0 m (72 feet, 0 ⅞ inches), 24.2 m (79 feet, 5 ⅞ inches), and 31.0 m (101 feet, 8 inches). Per Figure 6-11, each girder is prestressed with 30 (Beam 1 to Beam 5) or 32 (Beam 6 to Beam 9) 0.6-inch ASTM A416[18] Grade 270 [120] 7-wire strands. The strands are tensioned to approximately 75% of the ultimate tensile strength. The mild steel reinforcement conforms to ASTM A615[17] Grade 60 [111]. For the prestressed concrete girders, the nominal compressive strength is 34.4 MPa (5,000 psi), while the nominal compressive strength of the reinforced composite deck is 24.1 MPa (3,500 psi). The concrete deck has a thickness of 216 mm (8.5 inches), and its effective width is assumed to be equal to the horizontal center-to-center spacing between the two girders.

A summary of the gravity loading applied to this span is provided in Table 6-8. These loads are assumed to be distributed to the nine girders. The concrete weight assumes a density of 2400 kg/m^3 and accounts for the concrete girder, deck slab, taper in the overhangs, haunches above the beams, and parapet. A wearing surface is assumed to provide an additional 25 psf over the 76.7-ft width of the roadway surface. Live load is conservatively represented using the 640 plf uniform longitudinal load for each lane in accordance with the AASHTO[2] LRFD Bridge Design Specifications [8], and this bridge supports four lanes. This study does not include the concentrated truck live load with dynamic effects since heavy vehicles will most likely not be traveling across the bridge at full speed during the fire event. The load combination considered under fire conditions is taken as $DL + 0.3LL$ [7,16]. Note that the DL factor in Example 1 for the steel girder bridge was taken as 1.05 rather than the 1.0 used here for the bulb-T. The 5% increase was applied to the steel girder bridge to account for additional steel weight of bracing, stiffeners, etc. compared to the bulb-T.

[18] Use of ASTM A416, Specification for Low-Relaxation, Seven-Wire Steel Strand for Prestressed Concrete, is not a Federal requirement.

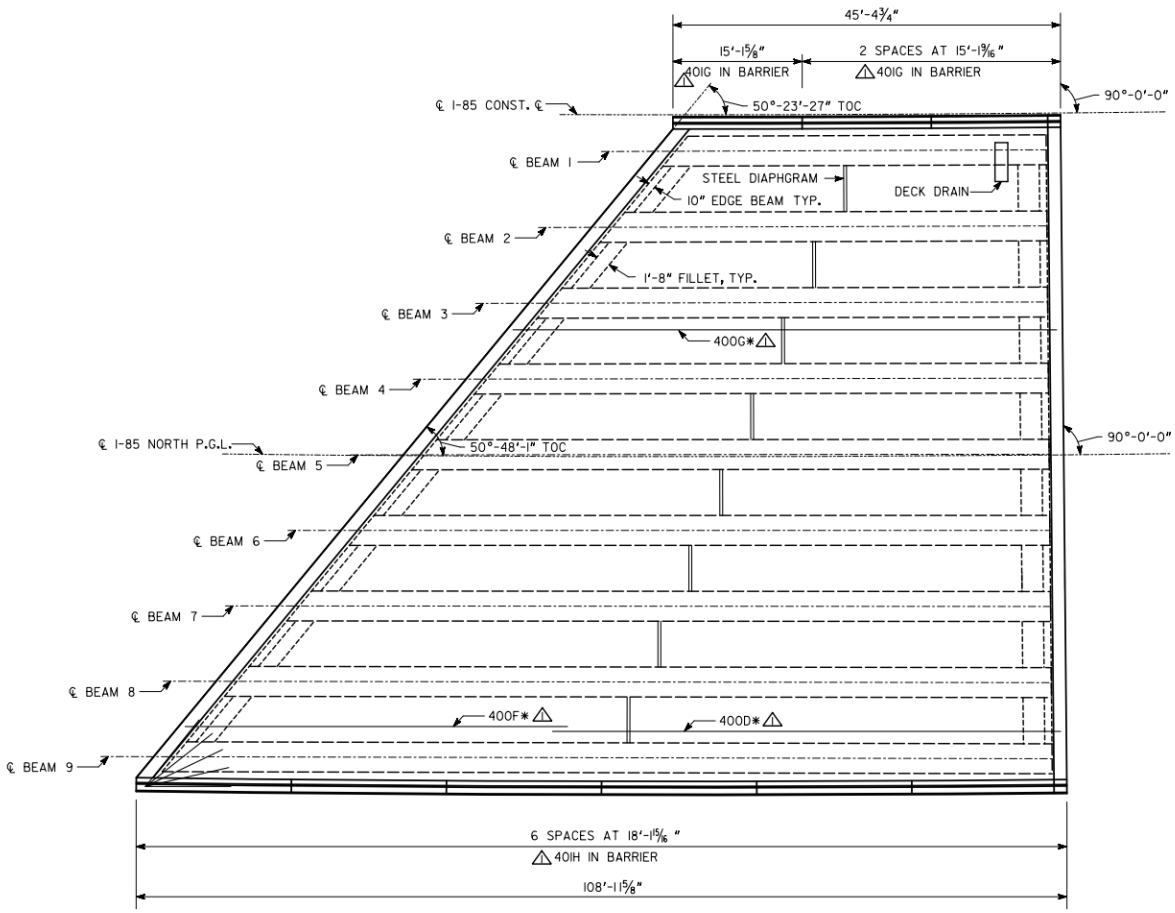

(a) Girder layout

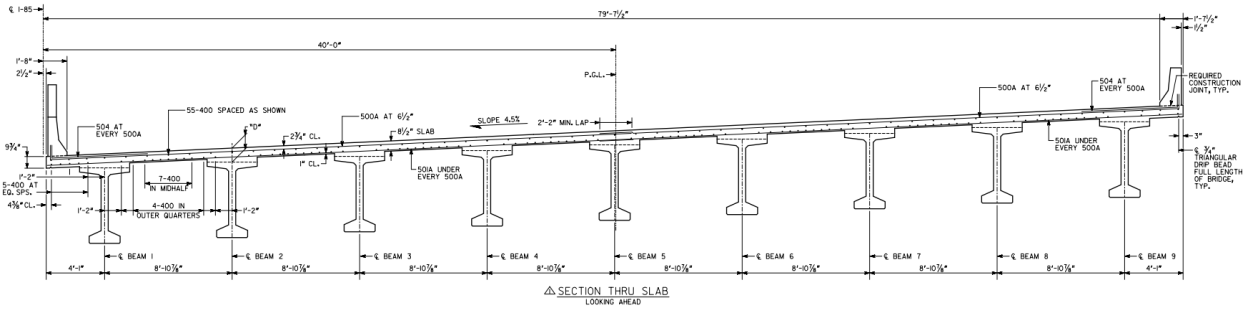

(b) Bridge section

Source: Georgia Department of Transportation (GDOT)

Figure 6-10: Illustrations. Structural configuration of example skewed bridge span with precast prestressed bulb-T girders

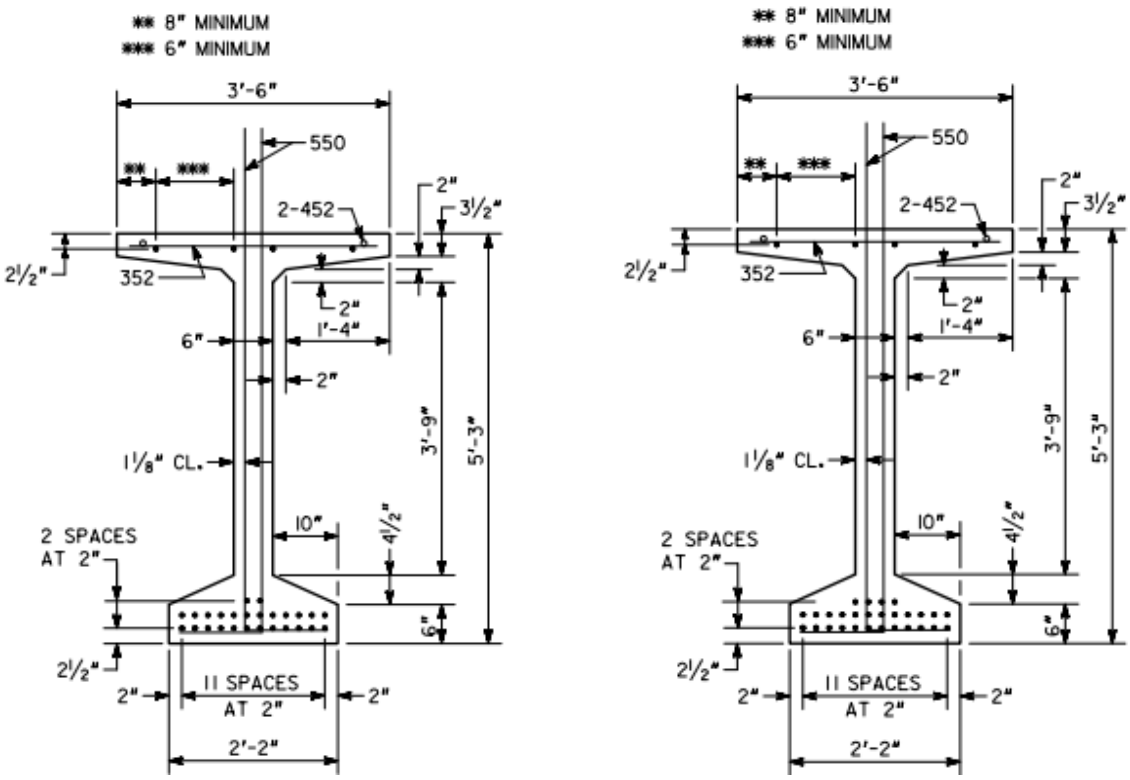

Beams 1-5 **Beams 6-9**

Source: Georgia Department of Transportation (GDOT)

Figure 6-11: Illustrations. Section details for the example precast bulb-T girders

Table 6-8: Summary of gravity loading on each example concrete girder.

Load Case	Calculation	Load Per Girder
Deck Slab	(150 pcf)×(79.6 ft)×(8.5 in.)/12/9	940 plf
Girder Self Weight	–	743 plf
Barrier	–	64 plf
Haunch weight	(0.5 in.)×(42 in.)/144×(150 pcf)	22 plf
Wearing surface	(25 psf)×(76.7 ft)/9	213 plf
Total DL per girder	–	1982 plf
Uniform Lane Load	(640plf/lane)×(4 lanes)/(9 girders)	284.4 plf
Load Combination, DL + 0.3LL	–	2266.4 plf

Note: For simplicity, the total deck width and associated superstructure dead loads are distributed equally among the nine girders (i.e., total width divided by 9), rather than distinguishing between exterior and interior girder tributary widths.

6.3.1 Parametric FE analysis

Several influential parameters for bulb-T bridge girders under fire have been identified previously in the study by Zhu et al. [7]. In this section, the focus is placed on examining the effects of span length and spalling on the fire-induced behavior of prestressed concrete bridge girders. Table 6-9 summarizes the seven cases considered in the parametric evaluation.

Table 6-9: Analysis cases for prestressed bulb-T girders

Case Name	Beam number	Fire duration	Spalling?
B(Beam number)-C-S*	1, 5, 6, 9	Continue (until failure)	Yes
B(Beam number)-C-NoS*	1, 5, 6, 9	240 minutes	No
B(Beam number)-30min-S	1, 5, 6, 9	30 minutes	Yes
B(Beam number)-60min-S	1, 5, 6, 9	60 minutes	Yes
B(Beam number)-60min-NoS	1, 5, 6, 9	90 minutes	No
B(Beam number)-120min-NoS	1, 5, 6, 9	120 minutes	No
B(Beam number)-180min-NoS	1, 5, 6, 9	180 minutes	No

**: "C" denotes continuous heating, implemented as heating until failure or up to 240 min.*

Figure 6-12(a) shows the FE mesh of the entire girder cross-section (Beam 6 and Beam 9), and the corresponding thermal model is shown in Figure 6-12(b). The whole section is meshed using quadrilateral elements. To simulate the fire-induced spalling process, the concrete cover at the fire-exposed surfaces is subdivided into multiple layers following the layered removal strategy used by Zhu et al. [7]. The potential spalling concrete thickness is taken as 51–64 mm (1.7–2.2 in.) in the bottom flange and approximately 28.6 mm (1.125 in.) in the web. At other locations, an approximate element edge length of 12.7 mm (0.5 in.) is adopted. The total number of elements in the thermal model is approximately 19,000. All prestressing strands are assumed to be straight, and harping is not considered.

The numerical implementation of the spalling process is as follows per the semi-empirical relationship developed by Carlton et al. [30]. When the temperature at the monitoring point on the exposed surface reaches 450 °C (842 °F), spalling is assumed to initiate. At that stage, the depth of the spalled region is determined based on the temperature distribution within the concrete cover, and all layers whose temperature exceeds 150 °C (302 °F) are removed from the model, i.e., this temperature is used to determine the spalling depth after initiation rather than to trigger spalling. Thermal analysis is then continued for the updated cross-section, and the same removal procedure is repeated. This heating–evaluation–removal cycle is carried out progressively until all ten cover layers have been eliminated, corresponding to the exposure of the prestressing strands or stirrups.

All reinforcement and strands are modeled using temperature-dependent thermal properties, including thermal conductivity and specific heat per Eurocode 2^{12} Part 1-2 [47]. The thermal properties of concrete, for both the deck and the girder, are taken as the mean temperature-dependent relationships for siliceous aggregate concrete provided in Eurocode 2^{12} Part 1-2 [47].

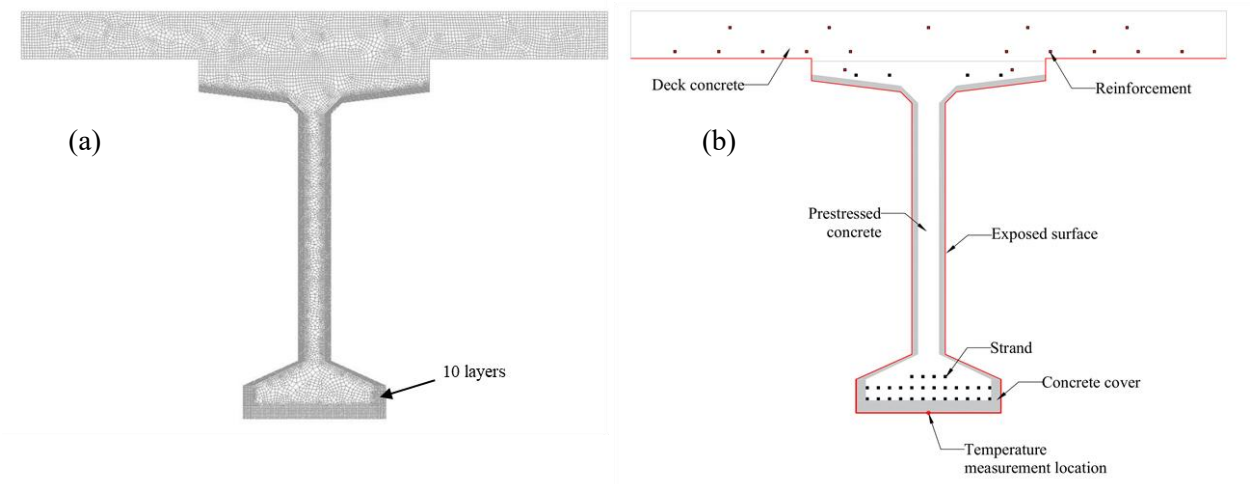

Source: S. Quiel, S. Ma, Lehigh University

Figure 6-12: Illustrations. Bulb-T cross-section: (a) mesh and (b) thermal analysis model.

In this case, the spalling process occurs in five separate events, starting at 250 sec and stopping at 530 sec. Figure 6-13 compares the cross-sectional temperature distributions after one hour of heating for cases with and without spalling for Beam 6 and 9. When spalling is considered, portions of the prestressing strands become directly exposed to the fire following the loss of concrete cover, resulting in significantly elevated strand temperatures. Here spalling is assumed to progress only up to the outermost layer of prestressing strands. However, some experimental studies [121–123] on concrete panels have reported spalling depths that substantially exceed this assumption. Therefore, the effectiveness of spalling mitigation measures for prestressed concrete structures subjected to fire warrants careful consideration. Figure 6-14 presents the temperature–time histories of two of the lowest prestressing strands. The edge strand shows a more rapid temperature rise as a result of spalling at both the bottom surface and the side face. For example, fiber 1 approaches the ASTM E1529[13] standard fire exposure temperature of 1,095 °C (2,000 °F) within a short duration after spalling.

The structural analysis is conducted using temperature-dependent mechanical properties defined in SAFIR, per Eurocode 2[12] Part 1-2 [47]. Steel reinforcement is modeled using the STEELEC2EN material model, which follows the stress–strain relationship and temperature-dependent reduction factors specified in Eurocode 2[12] Part 1-2 [47] for hot-rolled Class N steel. Prestressing steel is modeled using the PSTEELA16 material model in SAFIR, adopting the Eurocode 2[12] Part 1-2 [47] parameters for cold-worked Class B steel. A strength reduction factor of $\beta = 0.9$ is applied to the characteristic tensile strength f_{pk} to determine the yield strength of the prestressing strands. Temperature-dependent reductions in elastic modulus and strength, as well as strain-based failure limits, are automatically incorporated through the material model. At the beginning of a SAFIR structural analysis, prestressing strands are assigned their initial prestress – then during the first time step of the analysis, the cross-section achieves equilibrium at "release," with the concrete engaged in compression to equilibrate the strand prestress forces. As the strand temperature increases, their prestress force can decrease due to thermal expansion, creep, and permanent mechanical elongation (based on the material model). In spalling cases, outer strands heat up faster and lose prestress more quickly.

Concrete in both the bridge deck and prestressed girder is modeled as normal-strength concrete with siliceous aggregates, consistent with the thermal analysis. The SILCON_ETC material model in SAFIR is adopted to explicitly account for transient creep effects at elevated temperatures, including the non-reversibility of creep strain during cooling [124].

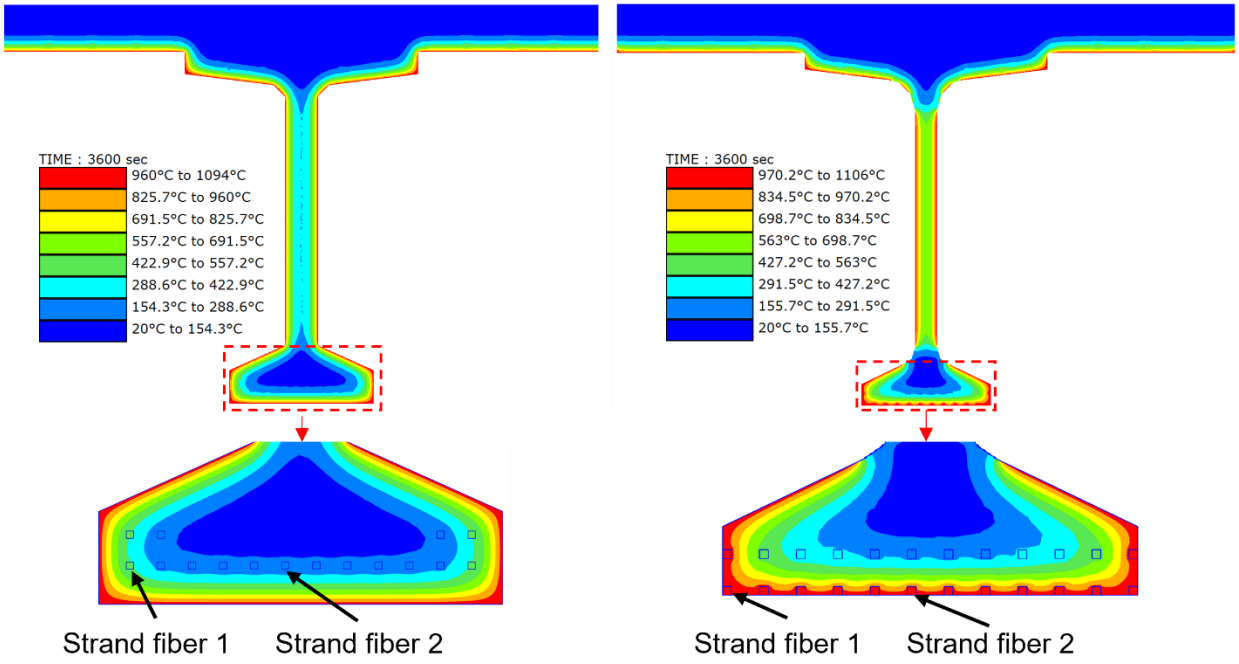

(a) Temperature distribution without spalling (b) Temperature distribution with spalling

Source: S. Quiel, S. Ma, Lehigh University

Figure 6-13: Illustrations. Cross-sectional temperature contours Beam 9 after 1 hour of fire exposure

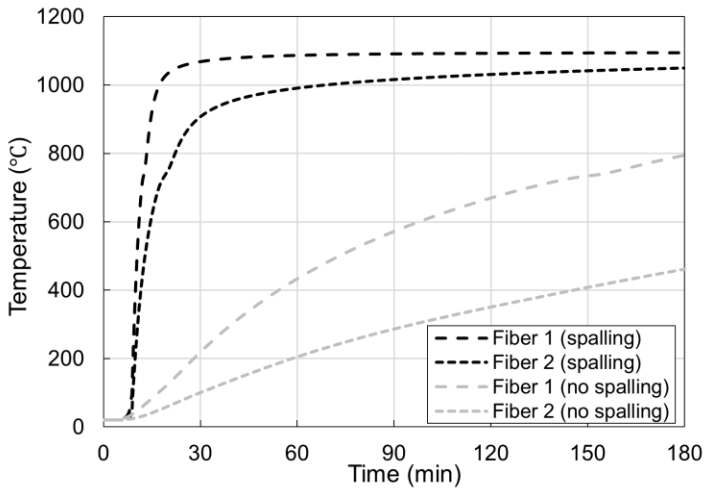

Source: S. Quiel, S. Ma, Lehigh University

Figure 6-14: Graph. Temperature time histories for selected strand fiber locations marked on Figure 6-13

Figure 6-15 presents the midspan deflections during fire exposure and residual deflections after fire for different cases. Several key observations can be drawn from the results:

(1) Concrete spalling has a pronounced negative effect on the fire performance of relatively long-span prestressed concrete girders. Preventing concrete spalling can therefore significantly enhance the fire resistance of prestressed concrete bridges.
(2) As shown in Figure 6-15(a) and (b), under otherwise similar conditions, longer-span girders are more sensitive to deformation-controlled failure modes, whereas for shorter-span girders, spalling has a comparatively limited influence on displacement-governed failure. Deflection is far more sensitive to span length than bending moment or shear force, scaling with L^4, compared with L^2 and L for bending moment and shear force, respectively. Under elevated temperatures, spalling and material degradation can lead to a rapid reduction in effective stiffness, which may trigger a sharp increase in displacement for longer-span girders. For relatively short spans, force-controlled failure mechanisms, such as shear-dominated failure, may govern the structural response. For structures with similar cross sections but varying span lengths, it is therefore necessary to further investigate the critical span at which the governing failure mode transitions.
(3) After the end of fire exposure, deflections continue to increase until the prestressing strands begin to cool. This behavior is more pronounced in non-spalling cases, as the presence of the concrete cover delays the cooling of the prestressing steel after heating ceases.

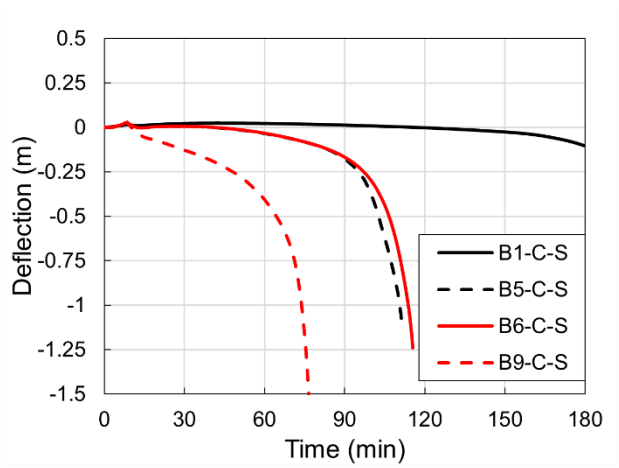

(a) Deflection with spalling

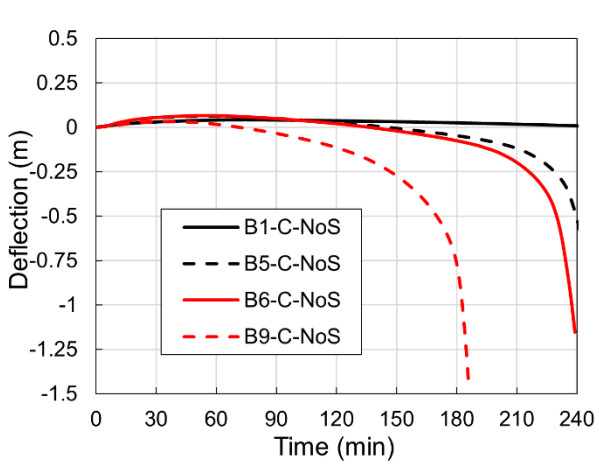

(b) Deflection without spalling

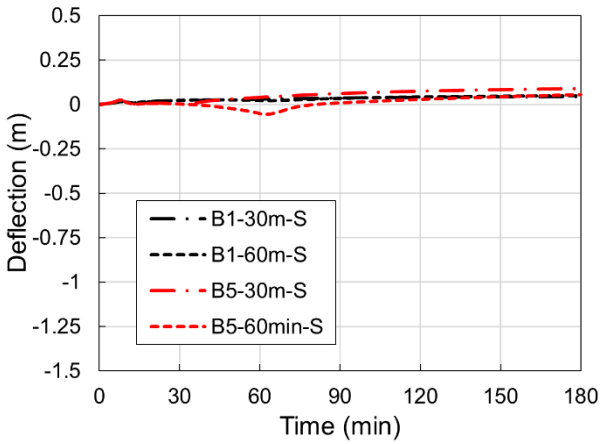

(c) Residual deflection (spalling, B1 and B5)

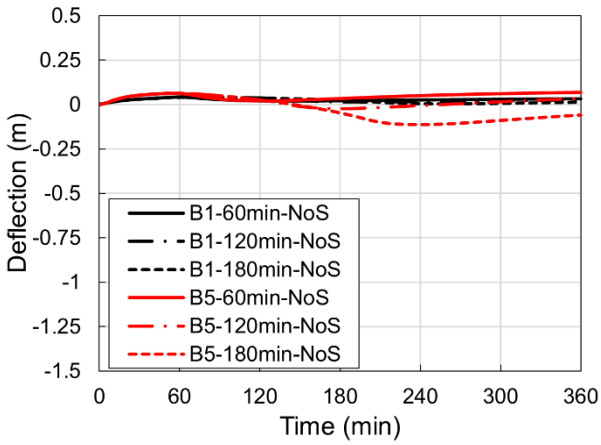

(d) Residual deflection (non-spalling, B1 and B5)

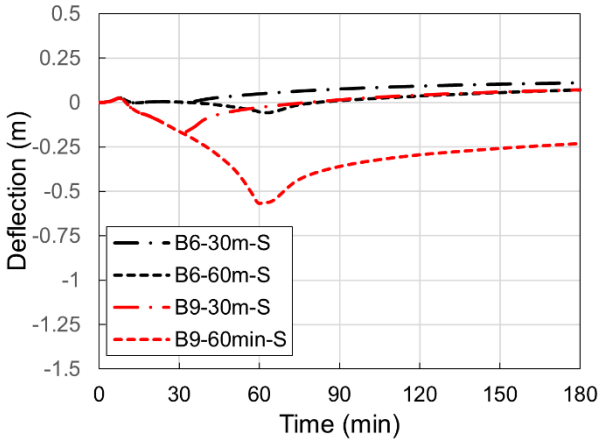

(e) Residual deflection (spalling, B6 and B9)

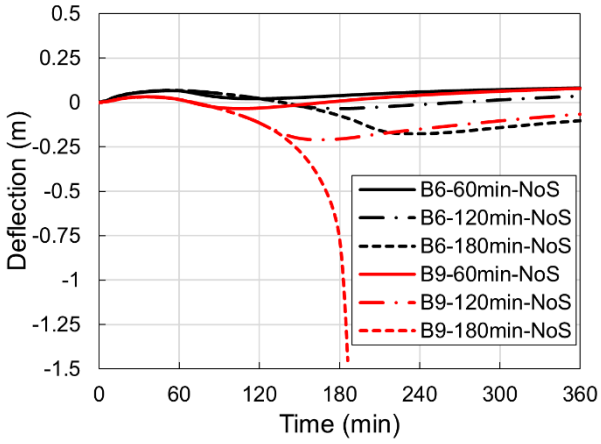

(f) Residual deflection (non-spalling, B6 and B9)

Source: S. Quiel, S. Ma, Lehigh University

Figure 6-15: Graphs. Midspan deflection of bulb-T girders subjected to the ASTM E1529[13] fire in different cases: (a-b) no burnout, and (c-f) with burnout after varying durations

6.3.2 Discussion of simplified approaches for concrete girders.

As stated earlier, lumped mass methods are not appropriate for thermal evaluation of structural concrete members due to their large thermal mass and low thermal conductivity. One option for simplified thermal evaluation of prestressed or reinforced concrete beams is to apply the isotherm diagrams from ACI 216-14(19)[10] [45] or PCI 124-23[11] [46] to determine the temperature at various depths into the concrete section. For example, a diagram such as that shown in Figure 6-16 could be used to approximately determine the temperature and associated reduced strength at each strand in a prestressed cross-section. Cross-sectional analysis as shown in Figure 6-17 could then account for the contributions of all heated strands in equilibrium with the compression block in the top flange and/or composite slab. This approach for cross-sectional capacity analysis at various timestamps of a fire exposure is referred to "rational design" in PCI 124-23[11] [46] and has been applied to precast prestressed elements such as double-tee floor elements [125].

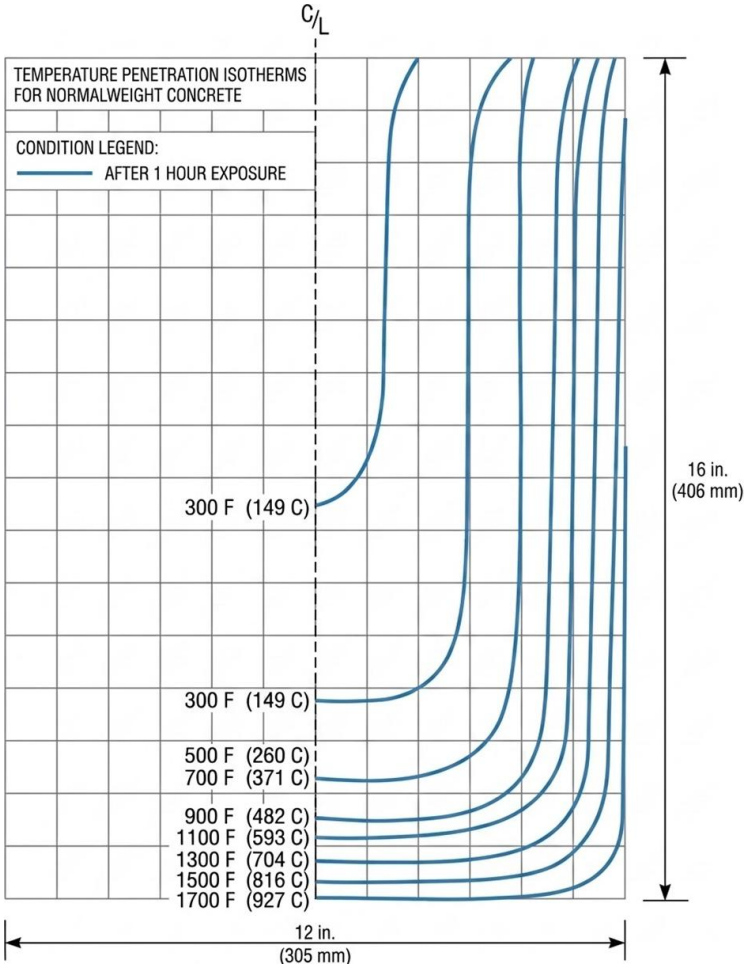

Source: S. Quiel, S. Ma, Lehigh University, based on PCI 124-23[11]

Figure 6-16: Illustration. Isotherm temperature distribution in a rectangular NWC section at 2 hrs of exposure to the ASTM E119[9] standard fire

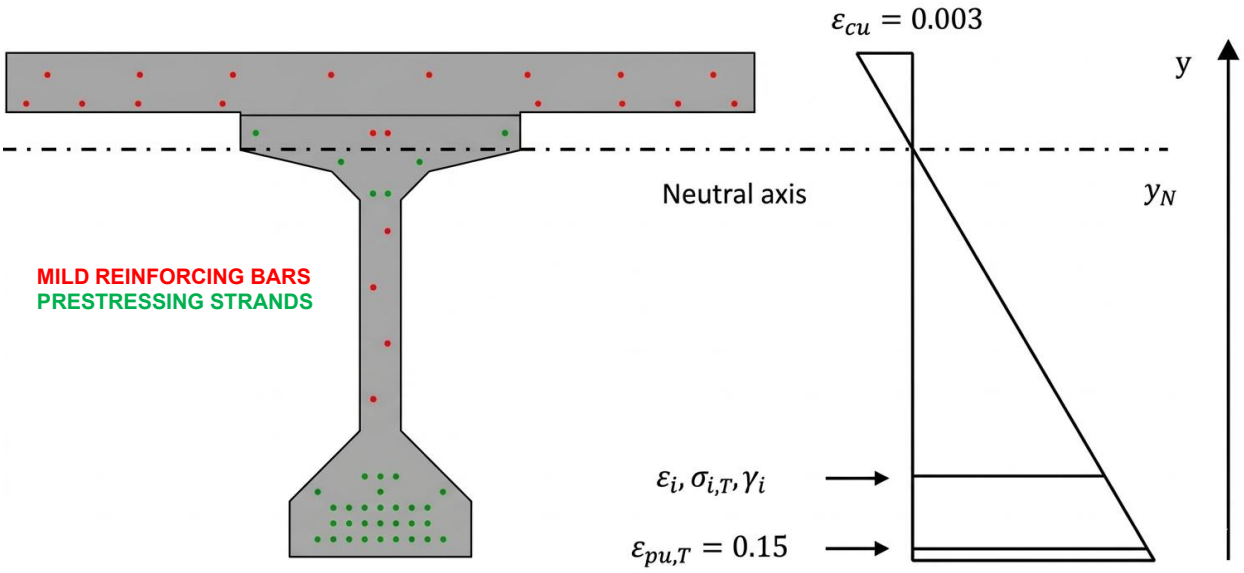

Source: S. Quiel, Z. Zhu, Lehigh University

Figure 6-17: Illustration. Strain profile of the cross-section for ultimate moment capacity calculation for a prestressed bulb-T girder (based on previous work by Zhu et al. [16])

Despite the opportunity for simplified analysis, there are several challenges to consider if a rational design method were to be pursued for a precast prestressed bulb-T bridge girder cross-section:

- Isotherm charts that are currently available in published standards are usually formulated for the ASTM E119[9] standard fire exposure, which is used for building applications. Similar charts for ASTM E1529[13] standard hydrocarbon fire exposure would be more pertinent for bridge applications and would need to be generated in future research. Charts that are tailored to more complicated cross-sectional geometries like the bulb-T rather than generic rectangular sections would also improve their applicability for bridge girders.
- Isotherm charts do not account for spalling during fire exposure; however, a worst-case assumption corresponding to the full instantaneous loss of cover to the outer layer of reinforcement could deliver a conservative estimate of thermal response.
- Cross-sectional capacity analysis for rational design neglects the impact of progressive relaxation of prestressing forces during the time history of fire exposure. Loss of prestressing can potentially impact the flexural behavior (as well as the shear capacity) of the section during fire exposure.
- Cross-sectional capacity analysis as a snapshot during the fire time history also neglects the effects of thermal creep, which may increase the permanent strains in the strand before reaching ultimate strength.

As an alternative, thermal FE analysis of the cross-section could provide the temperature data needed to conduct the cross-sectional capacity analysis per Figure 6-17. This approach was used in the previous study by Zhu et al. [7,16] on the 2017 fire-induced collapse of the I-85 overpass in Atlanta, GA and is therefore not reproduced here. Design aids such as fragility curves for fire exposure could also provide a viable solution for simpler evaluation of precast prestressed bulb-T bridge girders under fire. Zhu et al. [116] previously developed a similar tool for steel plate bridge girders, but more research is needed to develop a similar approach for prestressed concrete girders.

7 SUMMARY AND CONCLUSIONS

Recent events have demonstrated that the consideration of vehicular or stationary fire hazards may be justifiable for highway bridges that are shorter than the 1,000-ft (300-m) lower-bound length prescribed by NFPA 502[1]. Rather than using the bridge length as the sole parameter in determining the importance of the bridge, the decision to address the impact of fire on a bridge structure can instead be made based on an assessment that considers the likelihood of occurrence for a structurally significant fire near a bridge, the vulnerability of the bridge's structural elements to fire-induced damage or collapse, and the resulting impacts to user life-safety and the transportation network functionality both during and after the fire. When applicable, NFPA 502[1] states that an "engineering analysis," including the consideration of design fire scenarios and their proximity to the structure, is needed to determine whether the collapse of the bridge due to fire would have adverse impacts to life safety or other unacceptable impacts to functionality. This report addresses the need to provide synthesized information to practitioners to conduct thermo-structural performance-based analysis of steel and concrete bridge structures under fire loading. Available methods of analysis were outlined, ranging from simplified lumped mass thermal analyses (which are conducive to spreadsheet solutions) to numerical finite element (FE) analyses. Temperature-dependent material properties are needed as the input for these analyses, and available sources pertaining to structures made with steel and concrete were summarized.

Thermal and structural FE analysis is an effective tool for evaluating both steel and concrete bridge elements under fire exposure. These exposures can include a "standard" fire temperature time history (which are used to develop fire resistance ratings and continue until a failure condition is reached) or a design-basis "natural" fire temperature time history (which ramps up to a peak intensity and then eventually burns out). Thermal FE analysis of steel sections can capture the impact of heating rate and magnitude, the potential presence of passive fire protection, and the cooling effects through burnout. Thermal FE analysis for reinforced or prestressed concrete cross-sections can also capture the development of large thermal gradients (due to concrete's large thermal capacity and low thermal conductivity compared to steel) as well as the impact of fire-induced spalling (which will suddenly reduce the cross-section, particularly the cover thickness, accelerate the heating of flexural and shear reinforcement). Structural FE analysis uses the results of thermal analysis as input and accounts for the onset of thermal expansion and weakening of the structural materials. The impact of applied loading in combination with the thermal loading via a time history analysis will indicate whether the structure would be able to withstand the fire until burnout, and if not, what are the limit states that would govern failure (flexural, shear, cracking, etc.).

Lumped mass methods of thermal analysis are appropriate for steel materials, which have relatively high thermal conductivity and can therefore be approximated as having a relatively uniform temperature increase over the cross-section. Calculated changes in steel temperature can then be used to calculate the corresponding decrease in the element's strength and stiffness, as well as its thermal elongation. In this study, a large suite of thermo-structural analyses for composite steel bridge girders identified steel temperature thresholds that correspond to levels of fire-induced flexural performance. Lumped mass methods could then be used to calculate the steel temperature under a given fire hazard exposure, to determine whether those thresholds would be exceeded. For concrete and other materials with lower thermal conductivity, a significant internal thermal gradient will typically develop under fire exposure, thus rendering the lumped mass method ineffective. More research is needed to develop calculation tools that are more simplified than FE analysis to evaluate concrete bridge elements under fire.

7.1 Recommendations for Future Work

After performing the research reported herein, the following are possible areas for future work:

- In Section 5.1, it was noted that intumescent coatings (ICs) are typically developed for cellulosic fires, which are much smaller than hydrocarbon fires that bridges are often subjected to. Extrapolating the required millimeters of IC thickness to resist cellulosic fires can result in centimeters of IC thickness for a bridge hydrocarbon fire. Investigating ICs to resist hydrocarbon fires for bridges is certainly an area of need.
- In Section 5.1, it was noted that there is little published research regarding the thermal properties and structural performance of most IC materials for the purposes of modeling and calculation. More work is needed to develop these resources as an accessible tool for practitioners to develop performance-based IC solutions for a given bridge structure when subjected to a design-basis fire hazard.
- In Section 5.1, it was noted that centimeters of IC thickness applied to bridge elements have the potential to impede routine in-service inspections of the substrate underneath, including welds, splices, connections, cavities, etc. There is also a need to address "special" inspection of any applied coatings to monitor their durability and continued effectiveness in the field under realistic service conditions. More research is needed to determine not only the fatigue resistance of the ICs to weathering and repetitive mechanical loading but also to demonstrate the tools and procedures needed to conduct routine inspections on the substrate surfaces.
- In Section 5.2, it was noted that the incorporation of polypropylene (PP) fibers in concrete mix designs can provide potential fire resistance enhancement for concrete bridge elements. The incorporation of PP fibers can introduce additional cost while also impacting the workability of a concrete mix design (particularly regarding slump and curing), but it may also offer some benefits such as enhanced strength, durability, crack control, or shrinkage control. More research is needed to determine the practical and holistic implications for the consideration of PP fibers for concrete bridge construction practice.
- In Section 6, the parametric study on steel composite girders was limited to just simple spans where fire would cause sag, which does result in beneficial membrane action of the deck and girders. This would not be the case for continuous spans, particularly in the negative moment regions at interior supports where the stability under fire is unknown. Extending the simple span example in this report to continuous spans would be an area of need for future research.
- In Section 6, the results of stochastic analyses for the simple-span steel composite girder cases indicated that the critical steel temperatures used in current standard fire testing practice such as ASTM E1529[13] can reasonably indicate the steel temperature at which the girder experiences flexural failure under a load combination for an extreme event (which has reduced live load). Also, the steel temperature at which the yield strength of the steel begins to decrease (400 to 450 °C [752 to 842 °F]) can reasonably indicate the onset of permanent fire-induced damage. More research is needed to further solidify these conclusions for broader application across a wider range of structural element types, boundary conditions, loading scenarios, and fire scenarios for bridges.
- In Section 6, lumped mass methods were demonstrated as a potential simplified method for thermal evaluation of thin-plated steel elements under fire exposure. However, those methods are not appropriate for concrete methods due to their lower thermal conductivity and larger thermal mass. There is a need for more research and development of simplified design aids (such as fragility curves or isotherm charts) for bridge-specific fire exposures as a viable alternative to FE modeling for evaluating concrete bridge elements under fire.

8 REFERENCES

[1] NFPA. NFPA 502: Standard for road tunnels, bridges, and other limited access highways. Quincy, MA: National Fire Protection Association; 2017.

[2] Quiel S, Zhu Z, Murphy T, Lopez M, Artmont F. Characterizing Design-Basis Fire Exposure for Highway Bridges (ATLSS Report No. 24-02). Bethlehem, PA: Lehigh University; 2024.

[3] Wardhana K, Hadipriono FC. Analysis of Recent Bridge Failures in the United States. Journal of Performance of Constructed Facilities 2003;17:144–50. https://doi.org/10.1061/(ASCE)0887-3828(2003)17:3(144).

[4] Garlock M, Paya-Zaforteza I, Kodur V, Gu L. Fire hazard in bridges: Review, assessment and repair strategies. Engineering Structures 2012;35:89–98. https://doi.org/10.1016/j.engstruct.2011.11.002.

[5] Lee GC, Mohan SB, Huang C, Fard BN. Technical Report MCEER-13-0008: A Study of U.S. Bridge Failures (1980-2012). Buffalo, NY: MCEER, University at Buffalo, State University of New York; 2013.

[6] Peris-Sayol G, Paya-Zaforteza I, Balasch-Parisi S, Alós-Moya J. Detailed Analysis of the Causes of Bridge Fires and Their Associated Damage Levels. Journal of Performance of Constructed Facilities 2017;31:04016108. https://doi.org/10.1061/(ASCE)CF.1943-5509.0000977.

[7] Zhu Z, Quiel SE, Naito CJ. Thermo-structural response of a prestressed bulb-tee girder bridge to severe fire: Case study and parametric analysis. Engineering Structures 2025;343:120994. https://doi.org/10.1016/j.engstruct.2025.120994.

[8] AASHTO. AASHTO LRFD Bridge Design Specifications, 9th Edition. Washington, D.C.: American Association of State Highway and Transportation Officials; 2020.

[9] Lee J, Choi K, Yoon J, Chung C-H. Numerical analysis-based structural behavior assessment of a cable-stayed bridge under tanker fire. Structure and Infrastructure Engineering 2023;19:1761–78. https://doi.org/10.1080/15732479.2022.2053553.

[10] Liu Z, Lou G, Hou J, Li G. Designing a Two-Level Steel Cable-stayed Bridge against Fires. Structural Engineering International 2023;33:569–75. https://doi.org/10.1080/10168664.2023.2171331.

[11] Gong X, Agrawal AK. Numerical Simulation of Fire Damage to a Long-Span Truss Bridge. Journal of Bridge Engineering 2015;20:04014109. https://doi.org/10.1061/(ASCE)BE.1943-5592.0000707.

[12] Bennetts I, Moinuddin K. Evaluation of the Impact of Potential Fire Scenarios on Structural Elements of a Cable-Stayed Bridge. Journal of Fire Protection Engineering 2009;19:85–106. https://doi.org/10.1177/1042391508095091.

[13] Kim MO, Kim K, Yun JH, Kim MK. Fire risk assessment of cable bridges for installation of firefighting facilities. Fire Safety Journal 2020;115:103146. https://doi.org/10.1016/j.firesaf.2020.103146.

[14] Quiel S, Yokoyama T, Mueller K, Bregman L, Marjanishvili S. Mitigating the effects of a tanker truck fire on a cable-stayed bridge. Proceedings of the International Conference on Performance-based and Life-cycle Structural Engineering (PLSE 2015), Brisbane, Australia: University of Queensland; 2015, p. 1002–12. https://doi.org/10.14264/uql.2016.539.

[15] Quiel SE, Zhu Z. Numerical Evaluation of a Sample Steel Girder Bridge for a Construction Trailer Fire Underneath (ATLSS Report No. 18-03). Bethlehem, PA: Lehigh University; 2019.

[16] Zhu Z, Quiel SE, Naito CJ. Resiliency of Prestressed Concrete Beams Exposed to Fire (Revision 1) (FHWA-PA-2023-006-E04005 WO 07). Bethlehem, PA: Advanced Technology for Large Structural Systems (ATLSS) Engineering Research Center; 2023.

[17] Liu Z, Li G-Q. Performance of steel cable-stayed bridges in ship fires, part I: Numerical method and baseline fire scenario study. Journal of Constructional Steel Research 2023;210:108090. https://doi.org/10.1016/j.jcsr.2023.108090.

[18] Zhu Z, Quiel SE, Carlton A, Mueller KA, Marjanishvili SM. Performance-based prioritisation of fire protection for steel girder overpasses in a complex highway interchange. Structure and Infrastructure Engineering 2020;16:394–411. https://doi.org/10.1080/15732479.2019.1666884.
[19] Zhu Z, Quiel SE. Structural-Fire Evaluation of the I-95 Cottman Ave. Overpass Collapse (ATLSS Report No. 23-03). Bethlehem, PA: Lehigh University; 2024.
[20] Zhu Z, Quiel SE, Naito CJ. Performance-Based Optimization of Passive and Active Fire Protection for the Resilience of Concrete Tunnel Liners to Vehicular Fires. Fire Technol 2025. https://doi.org/10.1007/s10694-025-01794-y.
[21] Kodur VKR, Naser MZ. Importance factor for design of bridges against fire hazard. Engineering Structures 2013;54:207–20. https://doi.org/10.1016/j.engstruct.2013.03.048.
[22] Naser MZ, Kodur VKR. A probabilistic assessment for classification of bridges against fire hazard. Fire Safety Journal 2015;76:65–73. https://doi.org/10.1016/j.firesaf.2015.06.001.
[23] Quiel SE, Yokoyama T, Bregman LS, Mueller KA, Marjanishvili SM. A streamlined framework for calculating the response of steel-supported bridges to open-air tanker truck fires. Fire Safety Journal 2015;73:63–75. https://doi.org/10.1016/j.firesaf.2015.03.004.
[24] Banerjee DK. A Review of Models for Heat Transfer in Steel and Concrete Members During Fire. J Res Natl Inst Stand Technol 2021;126:126030. https://doi.org/10.6028/jres.126.030.
[25] Franssen J-M, Gernay T. Modeling structures in fire with SAFIR®: theoretical background and capabilities. Journal of Structural Fire Engineering 2017;8:300–23. https://doi.org/10.1108/JSFE-07-2016-0010.
[26] Jiang J, Usmani A. Modeling of steel frame structures in fire using OpenSees. Computers & Structures 2013;118:90–9. https://doi.org/10.1016/j.compstruc.2012.07.013.
[27] ANSYS, Inc. ANSYS® Workbench, Products 2021 R2 2021.
[28] ABAQUS Inc. Abaqus/CAE, Release 2020 Release 2020.
[29] Hua N, Tessari A, Khorasani NE. Characterizing damage to a concrete liner during a tunnel fire. Tunnelling and Underground Space Technology 2021;109:103761.
[30] Carlton A, Guo Q, Ma S, Quiel SE, Naito CJ. Experimental assessment of explosive spalling in normal weight concrete panels under high intensity thermal exposure. Fire Safety Journal 2022;134:103677. https://doi.org/10.1016/j.firesaf.2022.103677.
[31] Choe G, Kim G, Yoon M, Hwang E, Nam J, Guncunski N. Effect of moisture migration and water vapor pressure build-up with the heating rate on concrete spalling type. Cement and Concrete Research 2019;116:1–10. https://doi.org/10.1016/j.cemconres.2018.10.021.
[32] Harmathy TZ. Effect of Moisture on the Fire Endurance of Building Elements. In: Robertson AF, editor. Moisture in Materials in Relation to Fire Tests, 100 Barr Harbor Drive, PO Box C700, West Conshohocken, PA 19428-2959: ASTM International; 1965, p. 74-74–22. https://doi.org/10.1520/STP48429S.
[33] Wickstrom U. A Very Simple Method for Estimating Temperatures in Fire Exposed Structures. New Technology to Reduce Fire Losses and Costs. Ed., Grayson. SJ and Smith, DA. UK London; 1986.
[34] Kodur VKR, Yu B, Dwaikat MMS. A simplified approach for predicting temperature in reinforced concrete members exposed to standard fire. Fire Safety Journal 2013;56:39–51. https://doi.org/10.1016/j.firesaf.2012.12.004.
[35] Ghojel JI, Wong MB. Three-sided heating of I-beams in composite construction exposed to fire. Journal of Constructional Steel Research 2005;61:834–44. https://doi.org/10.1016/j.jcsr.2004.11.006.
[36] Drury MM, Kordosky AN, Quiel SE. Structural fire resistance of partially restrained, partially composite floor beams, II: Modeling. Journal of Constructional Steel Research 2020;167:105946. https://doi.org/10.1016/j.jcsr.2020.105946.
[37] CEN. EN 1993-1-2:2005 Eurocode 3: Design of steel structures - Part 1-2: General rules - Structural fire design. Brussels, Belgium: European Committee for Standardization; 2005.

[38] AISC. Specification for Structural Steel Buildings (ANSI/AISC 360-22). Chicago, IL: American Institute of Steel Construction; 2022.
[39] CEN. EN 1991-1-2:2002 Eurocode 1: Actions on structures - Part 1-2: General actions - Actions on structures exposed to fire. Brussels, Belgium: European Committee for Standardization; 2009.
[40] CEN. EN 1994-1-2:2005 Eurocode 4: Design of composite steel and concrete structures - Part 1-2: General rules - Structural fire design. Brussels, Belgium: European Committee for Standardization; 2008.
[41] Gamble WL. Predicting protected steel member fire endurance using spread-sheet programs. Fire Technology 1989;25:256–73. https://doi.org/10.1007/BF01039782.
[42] Franssen J-M, Gernay T. User's Manual for SAFIR 2022: A Computer Program for Analysis of Structures Subjected to Fire, Part 5: Material Properties. Liege, Belgium: University of Liege; 2022.
[43] Drury M, Quiel S. Load-Dependent Critical Temperatures for Standard Fire Resistance of W-Shape Floor Beam Assemblies: Experimental Validation and Simplified Analysis. Engineering Journal 2025;62:003–26. https://doi.org/10.62913/engj.v62i1.1335.
[44] ASTM Standard E119-24. Test Methods for Fire Tests of Building Construction and Materials. West Conshocken, PA: ASTM International; 2024.
[45] ACI/TMS. Code requirements for determining fire resistance of concrete and masonry construction assemblies (ACI/TMS 216.1-14(19)). Farmington Hills, MI: American Concrete Institute; 2019.
[46] PCI. PCI 124-23: Specification for Fire Resistance of Precast and Prestressed Concrete. Chicago, IL: Precast/Prestressed Concrete Institute; 2023.
[47] CEN. EN 1992-1-2:2004 Eurocode 2: Design of concrete structures - Part 1-2: General rules - Structural fire design. Brussels, Belgium: European Committee for Standardization; 2008.
[48] Lie TT, editor. Manual of Practice 78: Structural Fire Protection. Reston, VA: American Society of Civil Engineers; 1992.
[49] LaMalva KJ, editor. Manual of Practice 138: Structural Fire Engineering. Reston, VA: American Society of Civil Engineers; 2018.
[50] Hurley MJ, Gottuk D, Hall JR, Harada K, Kuligowski E, Puchovsky M, et al., editors. SFPE Handbook of Fire Protection Engineering. New York, NY: Springer New York; 2016. https://doi.org/10.1007/978-1-4939-2565-0.
[51] Neves IC, Rodrigues JPC, Loureiro A de P. Mechanical properties of reinforcing and prestressing steels after heating. Journal of Materials in Civil Engineering 1996;8:189–94.
[52] MacLean KJN, Bisby LA, MacDougall CC. ACI SP-255-7: Post-Fire Deterioration and Prestress Loss in Steel Tendons used in Post-Tensioned Slabs. ACI SP-255: Designing Concrete Structures for Fire Safety, Farmington Hills, MI: ACI; 2008, p. 147–74.
[53] Tao Z. Mechanical properties of prestressing steel after fire exposure. Mater Struct 2015;48:3037–47. https://doi.org/10.1617/s11527-014-0377-5.
[54] Wei Y, Zhang L, Au FTK, Li J, Tsang NCM. Thermal creep and relaxation of prestressing steel. Construction and Building Materials 2016;128:118–27. https://doi.org/10.1016/j.conbuildmat.2016.10.068.
[55] Abdulridha A, Thompson C, Gonzalez B, Wang S, Bergquist S, Quiel S. Effects of load rate, heating rate, and creep on the ultimate strength and rupture of A416 7-wire strand at elevated temperature. Fire Safety Journal 2024;146:104160. https://doi.org/10.1016/j.firesaf.2024.104160.
[56] Felicetti R, Gambarova PG, Meda A. Residual behavior of steel rebars and R/C sections after a fire. Construction and Building Materials 2009;23:3546–55. https://doi.org/10.1016/j.conbuildmat.2009.06.050.
[57] Abdulridha A, Wang S, Charbal A, Cinoglu IS, Naito C, Quiel S, et al. Creep of normal and high-strength A615 carbon-steel reinforcing bars at elevated temperature. Fire Safety Journal 2023;140:103868. https://doi.org/10.1016/j.firesaf.2023.103868.

[58] ASTM Standard E1529-22. Test Methods for Determining Effects of Large Hydrocarbon Pool Fires on Structural Members and Assemblies. West Conshohocken, PA: ASTM International; 2022.
[59] Khoury GA. Effect of fire on concrete and concrete structures. Progress in Structural Engineering and Materials 2000;2:429–47.
[60] Tenchev R, Purnell P. An application of a damage constitutive model to concrete at high temperature and prediction of spalling. International Journal of Solids and Structures 2005;42:6550–65.
[61] Qiao R, Guo Y, Zhou H, Xi H. Explosive Spalling Mechanism and Modeling of Concrete Lining Exposed to Fire. Materials 2022;15:3131. https://doi.org/10.3390/ma15093131.
[62] Brandt T, Varma A, Rankin B, Marcu S, Connor R, Harries K. Effects of Fire Damage on the Structural Properties of Steel Bridge Elements. Pittsburgh, PA: University of Pittsburgh; 2011.
[63] Pessiki S, Augustyn K. Determination of Peak Fire Temperature in the 2016 Liberty Bridge Fire (ATLSS Report No. 17-04). Bethlehem, PA: Lehigh University; 2017.
[64] Tide RHR. Integrity of Structural Steel After Exposure to Fire. Engineering Journal-American Institute of Steel Construction 1998;35:26–38.
[65] Aziz E, Kodur V. An approach for evaluating the residual strength of fire exposed bridge girders. Journal of Constructional Steel Research 2013;88:34–42. https://doi.org/10.1016/j.jcsr.2013.04.007.
[66] Short NR, Purkiss JA, Guise SE. Assessment of fire damaged concrete using colour image analysis. Construction and Building Materials 2001;15:9–15. https://doi.org/10.1016/S0950-0618(00)00065-9.
[67] Tseng T-C, Varma AH. Synthesis Study: Repair and Durability of Fire-Damaged Prestressed Concrete Bridge Girders. West Lafayette, IN: Purdue University; 2022. https://doi.org/10.5703/1288284317378.
[68] Liu Z, Li G-Q, Paya-Zaforteza I, Cai CS, Huang Q. Fire hazards in bridges: state of the art, recent progress, and current research gaps. Journal of Bridge Engineering 2023;28:03123003.
[69] BS 476-10:2009. Fire tests on building materials and structures. Part 10. Guide to the principles, selection, role, and application of fire testing and their outputs. London, UK: British Standards Institute (BSI); 2008.
[70] Song C, Zhang G, Li X, Kodur V. Experimental and numerical study on failure mechanism of steel-concrete composite bridge girders under fuel fire exposure. Engineering Structures 2021;247:113230. https://doi.org/10.1016/j.engstruct.2021.113230.
[71] Zhang G, Kodur V, Song C, He S, Huang Q. A numerical model for evaluating fire performance of composite box bridge girders. Journal of Constructional Steel Research 2020;165:105823.
[72] Hu J, Usmani A, Sanad A, Carvel R. Fire resistance of composite steel & concrete highway bridges. Journal of Constructional Steel Research 2018;148:707–19.
[73] Kodur VK, Aziz EM, Naser MZ. Strategies for enhancing fire performance of steel bridges. Engineering Structures 2017;131:446–58. https://doi.org/10.1016/j.engstruct.2016.10.040.
[74] Aziz EM, Kodur VK, Glassman JD, Moreyra Garlock ME. Behavior of steel bridge girders under fire conditions. Journal of Constructional Steel Research 2015;106:11–22. https://doi.org/10.1016/j.jcsr.2014.12.001.
[75] ISO. ISO 834-11:2014 Fire resistance tests — Elements of building construction — Part 11: Specific requirements for the assessment of fire protection to structural steel elements. Geneva, Switzerland: International Organization for Standardization; 2019.
[76] Garlock MEM, Glassman JD. Elevated temperature evaluation of an existing steel web shear buckling analytical model. Journal of Constructional Steel Research 2014;101:395–406. https://doi.org/10.1016/j.jcsr.2014.05.021.
[77] Song C, Zhang G, Kodur V, Zhang Y, He S. Fire response of horizontally curved continuous composite bridge girders. Journal of Constructional Steel Research 2021;182:106671. https://doi.org/10.1016/j.jcsr.2021.106671.

[78] Zhang G, Song C, Li X, He S, Huang Q. Fire Performance of Continuous Steel-Concrete Composite Bridge Girders. KSCE Journal of Civil Engineering 2021;25:973–84. https://doi.org/10.1007/s12205-021-0985-x.
[79] Franssen J-M, Cowez B, Gernay T. Effective stress method to be used in beam finite elements to take local instabilities into account. 11th International Symposium on Fire Safety Science, 2014.
[80] Glassman JD, Moreyra Garlock ME, Aziz EM, Kodur VK. Modeling parameters for predicting the postbuckling shear strength of steel plate girders. Journal of Constructional Steel Research 2016;121:136–43. https://doi.org/10.1016/j.jcsr.2016.01.004.
[81] Payá-Zaforteza I, Garlock MEM. A numerical investigation on the fire response of a steel girder bridge. Journal of Constructional Steel Research 2012;75:93–103. https://doi.org/10.1016/j.jcsr.2012.03.012.
[82] Alos-Moya J, Paya-Zaforteza I, Garlock MEM, Loma-Ossorio E, Schiffner D, Hospitaler A. Analysis of a bridge failure due to fire using computational fluid dynamics and finite element models. Engineering Structures 2014;68:96–110. https://doi.org/10.1016/j.engstruct.2014.02.022.
[83] Peris-Sayol G, Paya-Zaforteza I, Alos-Moya J, Hospitaler A. Analysis of the influence of geometric, modeling and environmental parameters on the fire response of steel bridges subjected to realistic fire scenarios. Computers & Structures 2015;158:333–45. https://doi.org/10.1016/j.compstruc.2015.06.003.
[84] Kordosky AN, Drury MM, Quiel SE. Structural fire resistance of partially restrained, partially composite floor beams, I: Experiments. Journal of Constructional Steel Research 2020;167:105945. https://doi.org/10.1016/j.jcsr.2020.105945.
[85] Drury MM, Quiel SE. Standard versus natural fire resistance for partially restrained composite floor beams: 1-Testing. Journal of Constructional Steel Research 2022;under review.
[86] Braxtan NL, Pessiki SP. Postearthquake fire performance of sprayed fire-resistive material on steel moment frames. Journal of Structural Engineering 2011;137:946–53.
[87] Horacek H, Pieh S. The importance of intumescent systems for fire protection of plastic materials. Polymer International 2000;49:1106–14.
[88] Lucherini A, Maluk C. Intumescent coatings used for the fire-safe design of steel structures: A review. Journal of Constructional Steel Research 2019;162:105712. https://doi.org/10.1016/j.jcsr.2019.105712.
[89] Gardelle B, Duquesne S, Vandereecken P, Bourbigot S. Resistance to fire of silicone-based coatings: Fire protection of steel against cellulosic fire. Journal of Fire Sciences 2014;32:374–87. https://doi.org/10.1177/0734904114522390.
[90] Mariappan T. Recent developments of intumescent fire protection coatings for structural steel: A review. Journal of Fire Sciences 2016;34:120–63.
[91] Jimenez M, Duquesne S, Bourbigot S. Intumescent fire protective coating: Toward a better understanding of their mechanism of action. Thermochimica Acta 2006;449:16–26. https://doi.org/10.1016/j.tca.2006.07.008.
[92] Ghiji M, Joseph P, Guerrieri M. Some recent developments and testing strategies relating to the passive fire protection of concrete using intumescent coatings: a review. JSFE 2022. https://doi.org/10.1108/JSFE-11-2021-0069.
[93] Lucherini A, de Silva D. Modelling intumescent coatings for the fire protection of structural systems: a review. Journal of Structural Fire Engineering 2024;15:483–507.
[94] Häßler D, Mund M, Daus L-H, Hothan S, Schaumann P, Schartel B. Durability of intumescent coatings and recommendations for test concepts for a working life of more than 10 years. Fire Safety Journal 2024;146:104173. https://doi.org/10.1016/j.firesaf.2024.104173.
[95] Maciulaitis R, Grigonis M, Malaiskiene J. The impact of the aging of intumescent fire protective coatings on fire resistance. Fire Safety Journal 2018;98:15–23. https://doi.org/10.1016/j.firesaf.2018.03.007.

[96] Wang J, Zhao M. Study on the effects of aging by accelerated weathering on the intumescent fire retardant coating for steel elements. Engineering Failure Analysis 2020;118:104920. https://doi.org/10.1016/j.engfailanal.2020.104920.
[97] Carlton A, Ma S, Quiel SE, Naito CJ. Comparative response of tiled finishes and bonded fire resistive coatings for normal weight concrete tunnel liners under high-intensity one-sided heating. Tunnelling and Underground Space Technology 2023;139:105225. https://doi.org/10.1016/j.tust.2023.105225.
[98] Bilodeau A, Kodur VKR, Hoff GC. Optimization of the type and amount of polypropylene fibres for preventing the spalling of lightweight concrete subjected to hydrocarbon fire. Cement and Concrete Composites 2004;26:163–74. https://doi.org/10.1016/S0958-9465(03)00085-4.
[99] Song C, Zhang G, Lu Z, Li X, Zhao X. Fire resistance tests on polypropylene-fiber-reinforced prestressed concrete box bridge girders. Engineering Structures 2023;282:115800. https://doi.org/10.1016/j.engstruct.2023.115800.
[100] Hager I, Mróz K. Role of Polypropylene Fibres in Concrete Spalling Risk Mitigation in Fire and Test Methods of Fibres Effectiveness Evaluation. Materials 2019;12:3869. https://doi.org/10.3390/ma12233869.
[101] McNamee R, Sjöström J, Boström L. Reduction of fire spalling of concrete with small doses of polypropylene fibres. Fire and Materials 2021;45:943–51. https://doi.org/10.1002/fam.3005.
[102] Zeiml M, Leithner D, Lackner R, Mang HA. How do polypropylene fibers improve the spalling behavior of in-situ concrete? Cement and Concrete Research 2006;36:929–42. https://doi.org/10.1016/j.cemconres.2005.12.018.
[103] Behnood A, Ghandehari M. Comparison of compressive and splitting tensile strength of high-strength concrete with and without polypropylene fibers heated to high temperatures. Fire Safety Journal 2009;44:1015–22. https://doi.org/10.1016/j.firesaf.2009.07.001.
[104] Eidan J, Rasoolan I, Rezaeian A, Poorveis D. Residual mechanical properties of polypropylene fiber-reinforced concrete after heating. Construction and Building Materials 2019;198:195–206. https://doi.org/10.1016/j.conbuildmat.2018.11.209.
[105] Bošnjak J, Ožbolt J, Hahn R. Permeability measurement on high strength concrete without and with polypropylene fibers at elevated temperatures using a new test setup. Cement and Concrete Research 2013;53:104–11. https://doi.org/10.1016/j.cemconres.2013.06.005.
[106] Li P, Huang M, Shang Y, Kuang Y, Xiong G, Tang X. Study on Mechanical Properties of Coarse-Fine Polypropylene Fiber Blended Concrete. Buildings 2025;15. https://doi.org/10.3390/buildings15162971.
[107] Tan CT, Yew MK, Yew MC, Lee FW, Lim SK, Beh JH, et al. Mechanical property enhancement in concrete composites with hybrid polypropylene fibre reinforcement. Sci Rep 2025;15:24986. https://doi.org/10.1038/s41598-025-04219-6.
[108] Buchanan AH, Abu A. Structural design for fire safety. Second edition. Chichester, West Sussex, United Kingdom: John Wiley & Sons Inc; 2017.
[109] SSSBA. eSPAN140. Washington, D.C.: Short Span Steel Bridge Alliance; 2017.
[110] ASTM Standard A709-17. Standard Specification for Structural Steel for Bridges. West Conshohocken, PA: ASTM International; 2017.
[111] ASTM Standard A615-18. Specification for Deformed and Plain Carbon-Steel Bars for Concrete Reinforcement. West Conshohocken, PA: ASTM International; 2018. https://doi.org/10.1520/A0615_A0615M-18E01.
[112] Khorasani NE, Gardoni P, Garlock M. Probabilistic Fire Analysis: Material Models and Evaluation of Steel Structural Members. J Struct Eng 2015;141:04015050. https://doi.org/10.1061/(ASCE)ST.1943-541X.0001285.
[113] Franssen J-M, Cowez B, Gernay T. Effective stress method to be used in beam finite elements to take local instabilities into account. Fire Safety Science 2014;11:544–57. https://doi.org/DOI: 10.3801/IAFSS.FSS.11-544.

[114] Iqbal S, Harichandran RS. Capacity Reduction and Fire Load Factors for Design of Steel Members Exposed to Fire. Journal of Structural Engineering 2010;136:1554–62. https://doi.org/10.1061/(asce)st.1943-541x.0000256.
[115] Holicky M, Sykora M. Stochastic models in analysis of structural reliability. Proc. of the Int. Sypmosium on Stochastic Models in Reliability Engineering, Life Sciences, and Operations Management, Beer Sheva, Israel: Sami Shamoon College of Engineering; 2010.
[116] Zhu Z, Quiel SE, Khorasani NE. Bivariate structural-fire fragility curves for simple-span overpass bridges with composite steel plate girders. Structural Safety 2023;100:102294. https://doi.org/10.1016/j.strusafe.2022.102294.
[117] Gernay T, Khorasani NE, Garlock M. Fire fragility curves for steel buildings in a community context: A methodology. Engineering Structures 2016;113:259–76. https://doi.org/10.1016/j.engstruct.2016.01.043.
[118] Olsson AMJ, Sandberg GE. Latin Hypercube Sampling for Stochastic Finite Element Analysis. Journal of Engineering Mechanics 2002;128:121–5. https://doi.org/10.1061/(ASCE)0733-9399(2002)128:1(121).
[119] Helton JC, Davis FJ. Latin hypercube sampling and the propagation of uncertainty in analyses of complex systems. Reliability Engineering & System Safety 2003;81:23–69. https://doi.org/10.1016/S0951-8320(03)00058-9.
[120] ASTM Standard A416-18. Specification for Low-Relaxation, Seven-Wire Steel Strand for Prestressed Concrete. West Conshohocken, PA: ASTM International; 2021. https://doi.org/10.1520/A0416_A0416M-18.
[121] Lo Monte F, Felicetti R, Meda A, Bortolussi A. Assessment of concrete sensitivity to fire spalling: A multi-scale experimental approach. Construction and Building Materials 2019;212:476–85. https://doi.org/10.1016/j.conbuildmat.2019.03.332.
[122] Guerrieri M, Fragomeni S. Spalling of Large-Scale Walls Exposed to a Hydrocarbon Fire. Journal of Materials in Civil Engineering 2019;31:04019249. https://doi.org/10.1061/(ASCE)MT.1943-5533.0002828.
[123] Boström L, Wickström U, Adl-Zarrabi B. Effect of specimen size and loading conditions on spalling of concrete. Fire and Materials 2007;31:173–86. https://doi.org/10.1002/fam.931.
[124] Gernay T, Franssen J-M. A formulation of the Eurocode 2 concrete model at elevated temperature that includes an explicit term for transient creep. Fire Safety Journal 2012;51:1–9. https://doi.org/10.1016/j.firesaf.2012.02.001.
[125] Kumar P, Kodur VKR. A Rational Approach for Fire-Resistance Evaluation of Double-Tee, Prestressed Concrete Slabs in Parking Structures. PCI Journal 2020;65. https://doi.org/10.15554/pcij65.2-01.